SAPIENZA
UNIVERSITÀ DI ROMA

SYNTHESIS AND CHARACTERIZATION OF NOVEL METHACRYLATES BEARING A 2-(HYDROXYIMINO)ALDEHYDE GROUP AND THEIR COPOLYMERS

Martina Nardi

Matricola: 1317560

Supervisori: Prof. P. Gentili, Dr. F. D'Acunzo

Coordinatore: Prof. O. Lanzalunga

DOTTORATO DI RICERCA IN SCIENZE CHIMICHE

XXXI CICLO

Dipartimento di Chimica

Facoltà di Scienze Matematiche, Fisiche e Naturali

Università di Roma La Sapienza

Anno Accademico: 2017/2018

Keywords

Multi-stimuli responsive polymers, polymethacrylates, 2-(hydroxyimino)aldehydes, photoisomerism, thermal response.

Table of Contents

List of Figures

List of Tables

List of Schemes

List of Abbreviations

ADMET	Acyclic diene metathesis
AIBN	Azobisisobutyronitrile.
ARGET-ATRP	Activator regenerated by electron transfer-ATRP
ATRP	Atom transfer radical polymerization
BAIB	Bis(acetoxy)iodobenzene
BPO	Benzoyl peroxide
CBO	Cyclobutanol oxime
COSY	Correlation spectroscopy
CPDB	2-Cyanopropan-2-yl dithiobenzoate
CRP	Controlled radical polymerization
CTA	Chain transfer agent
DCM	Dichloromethane
Đ	Dispersity
DEGMA	Di(ethylene glycol) methyl ether methacrylate
DEPT	Distortionless enhancement by polarization transfer
DFT	Density functional theory
DLS	Dynamic light scattering
DMAP	4-(Dimethylamino)pyridine
DMF	*N*,*N*-Dimethylformamide
DMSO	Dimethyl sulfoxide
DP	Degree of polymerization
FTIR	Fourier-transform infrared spectroscopy
GC	Gas chromatography
GPC	Gel permeation chromatography
HIA	2-(Hydroxyimino)aldehyde
HIABMA	4-[(Hydroxyimino)aldehyde]butyl methacrylate
HIHMA	6-(Hydroxyimino)hexyl methacrylate
HMBC	Heteronuclear multiple-bond correlation spectroscopy
HPLC	High performance liquid chromatography
HSQC	Heteronuclear single-quantum correlation spectroscopy
ICAR-ATRP	Initiators for continuous activator regeneration-ATRP
LCSC	Lower critical solution concentration
LCST	Lower critical solution temperature
M_n	Number-average molecular weight
NHE	Normal hydrogen electrode
NMP	Nitroxide-mediated polymerization
NOESY	Nuclear overhauser effect spectroscopy
OEGMA	Oligo(ethylene glycol) monomethylether methacrylate
OHMA	6-Oxohexyl methacrylate
ORP	Organic radical polymer
PCC	Pyridinium chlorochromate
PCM	Polarizable continuum model
PET-RAFT	Photoinduced electron transfer-RAFT
PISA	Polymerization induced self-assembly
PNIPAM	Poly(*N*-isopropyl acrylamide)
PRE	Persistent radical effect

RAFT	Reversible addition-fragmentation chain-transfer polymerization
RI	Refractive index
ROMP	Ring-opening metathesis polymerization
SARA-ATRP	Supplemental activation reducing agent-ATRP
SET-LRP	Single-electron transfer living radical polymerization
TBAF	Tetrabutylammonium fluoride
TBDMS	*tert*-Butyldimethylsilyl ether
TEA	Triethylamine
TEMPO	2,2,6,6-Tetramethylpiperidine 1-oxyl
THF	Tetrahydrofuran
UCST	Upper critical solution temperature

Statement of Original Authorship

The work contained in this thesis has not been previously submitted to meet requirements for an award at this or any other higher education institution. To the best of my knowledge and belief, the thesis contains no material previously published or written by another person except where due reference is made.

Signature: _____

Date: _____

Chapter 1: Background

1.1 MULTI-STIMULI RESPONSIVE POLYMERS

It's been only a hundred years since Wolfgang Otswald referred to compounds with size between molecular and macroscopic as *the world of neglected dimensions.*[1] Not long after, the Nobel Prize Hermann Staudinger coined the term "*macromolecules*", stating, for the first time, that high molecular weight molecules are formed by a large number of small molecules linked together.[2] Even though the science of polymers is relatively young, over the past century considerable progresses and discoveries have allowed them to be an essential part of our daily life.

When the human being had not comprehended yet the meaning and the relevance of polymers, Nature was already using macromolecules to allow the development of life. In fact, the natural world gives us innumerable examples of polymers-based systems with tunable properties in response to changes in their surrounding environment. To date, natural polymers such as proteins, carbohydrates and DNA remain the most attractive and efficient in terms of specificity, complexity and structure. Inspired by their characteristics, few decades ago the scientific community began to focus on "*smart*" materials. The idea was the development of polymers able to change their structure or behavior, or give specific signals in response to different chemical and physical stimuli, such as temperature, light, pH, host-guest interaction and electron transfer.[3,4,5] In recent years, an unprecedented increase in *smart* materials (multi-stimuli responsive gels, smart surface,[6] particles and films,[7] shape memory polymer nanocomposites[8]) finds applications in drug delivery,[9–12] chemical and biological sensors,[13] separation techniques,[14] catalysts and electrochemical energy storage.[15] In this contest, hydrophilic multi-stimuli-responsive polymers assume particular interest for their potential employments in aqueous solutions[5] and will be taken in particular consideration in this introduction.

1.1.1 Stimuli

Smart polymers are usually equipped with one or more functionalities which respond to different stimuli. In this section the most important stimuli and the groups associated with them are described.

Temperature

Temperature variations can induce a reversible phase separation of a solution of thermo-responsive polymer. This is one of the most extensively studied phenomenon both in its fundamental physical-chemical aspects, and in view of its applicative fallout. In a water-polymer binary mixture two different transition temperature can arise. If the temperature increase leads to phase separation, the water-polymer system is said to exhibit a LCST (Lower Critical Solution Temperature). LCST is the minimum temperature of the coexistence curve of the mixture and it is associated with a Lower Critical Solution Concentration (LCSC). Otherwise, if the polymer solution separates upon temperature decrease, the system exhibits a UCST (Upper Critical Solution Temperature).[16]

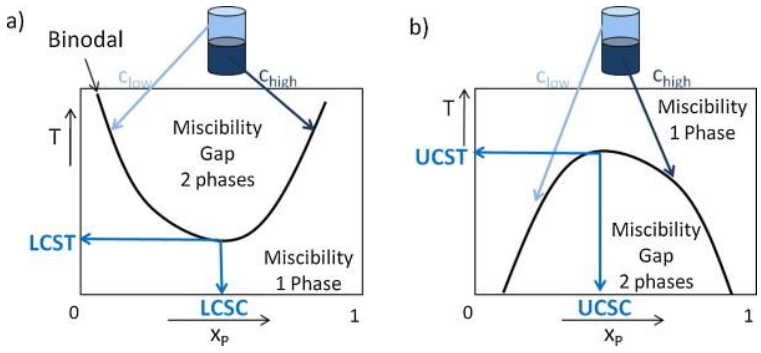

Figure 1.1. Phase diagram of a water-polymer mixture exhibiting an LCST (left) and UCST (right). Reproduced with permission from Ref.[17]

Specifically, the coil-to-globule transition occurring at temperature above LCST is governed by a re-organization of hydrogen bonds in the polymer-water mixture. At low temperature the polymer chains are well solvated by water molecules resulting in one phase system. Hence, the mixing enthalpy is favourable, but the ordered system governed by hydrogen bonds leads to an unfavourable entropy ($\Delta H_{mix} > T\Delta S$). When the temperature is increased above the LCST, the hydrogen bond between polymer chains and water are weakened; the entropy term becomes higher than the mixing enthalpy and the polymer chains start to collapse and aggregate ($\Delta H_{mix} < T\Delta S$).[16]

Many examples of polymers exhibiting a LCST in aqueous solution are described in the literature. The main thermo-responsive functionalities are polyacrylamides, polyvinylethers, polyoxazolines and poly(oligo(ethylene glycol) methacrylate)s.[5] (Figure 1.3). On the other hand, zwitterionic polymers are a good example of macromolecules that exhibit a UCST.[18]

Light

Upon irradiation, organic chromophores are able to isomerize, dissociate, tautomerize, produce radicals, and so forth.[19] The richness of photochemical reactions can be used to create responsive polymers with tunable behavior. Furthermore, the development of laser and LED systems has allowed spatial control, modulable intensity and monochromatic excitation wavelength, thus giving great advantages in the use of light.

Three common light responsive moieties used in multi-stimuli responsive polymers are shown in Figure 1.3. Azobenzene provides an excellent example of reversible *cis-trans* isomerization, while spiropyran can switch to merocyanine form under the effect of the light. The last one, fulgide group, offers a photochromic behavior through an electrocyclic reaction (Figure 1.2).[20]

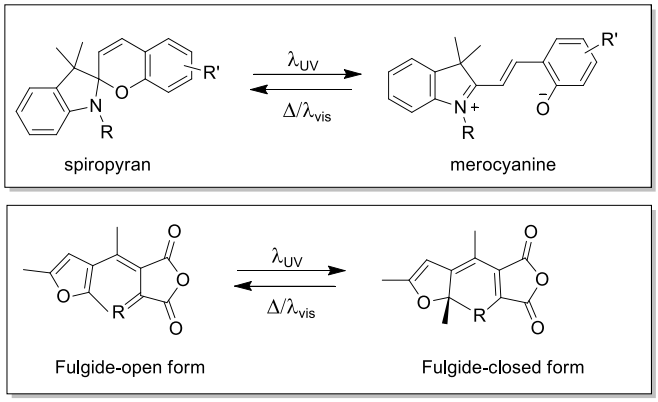

Figure 1.2. Photoisomerization of spiropyran and fulgide.

Besides the reaction of isomerization and photochromism, another intriguing use of light in polymer science is the formation of block copolymers.[21,22] Specifically, photo induced cycloaddition forms covalent bonds between two terminal photoreactive group belonging to different chains.

pH

pH-responsive polymers have gained an increasing attention especially in the field of cancer therapy.[9] Macromolecules that can modify their structure in middle-acidic environment result very attractive, since tumour cells usually have lower pH (6.5) than that of normal cells (7.4).

More generally, polymers bearing base or weak acid functionalities can collapse or extend their chains in different pH environments.[23] Groups such as carboxylic acids,

phosphates acid and amines are the most used pH-responsive moieties, since they can cause a change in the secondary structure of polymer chains in a range of pH between 2 and 12. (Figure 1.3)

Electron-transfer

Although the majority of redox-sensitive systems are inorganic, there are some organic molecules such as ferrocene, disulphide and tetramethylpiperidine-1-oxyl (TEMPO) derivatives that can change reversibly their oxidation state.[5] When these groups are integrated in a polymer chain, a change in their redox state results in a build up of or a drop of hydrophilicity of the whole polymer. For example, the reduction of TEMPO moieties leads to more hydrophilic polymers due to formation of a hydroxyl group, similarly the oxidation of ferrocene units increases the solubility of the chains. (Figure 1.3).

Furthermore, the development of Stable Organic Radical Polymers (ORPs) has gained increasing attention towards replacing heavy metals in application as catalysts and electrochemical active materials.[15]

Chemical-responsive

A wide range of examples is found in literature, in which a reversible change is caused by the addition or removal of reagents such as gases, hydrophobic molecules or alcohols. CO_2 responsive groups are usually amines, amidines or guanidines.[24] These moieties can accept proton from carbonic acid formed through dissolution of CO_2 in water, leading to an increase of polymer hydrophilicity. Polymers bearing boronic acid functionalities have been shown to be sugar[25] or fluoride ion responsive.[26] Moreover, polymers encompassing cyclodextrin groups are responsive to host-guest interactions. In fact, they are able to increase the solubility of low polarity molecules through their uptake in their hydrophobic cavity.[27]

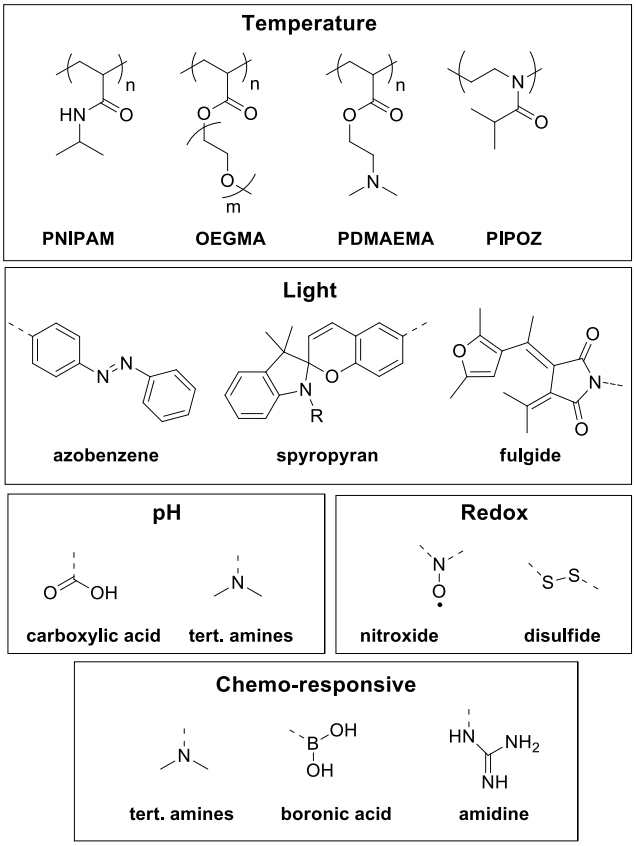

Figure 1.3. Stimuli-responsive groups.

1.1.2 Parallel, serial and casual responses.

As pointed out by P. Theato and coworkers in his review[5], smart polymers bearing two or more responsive groups show three different types of combined response.

The parallel interplay between two or more groups takes place when the response to different stimuli is orthogonal, i.e. it is indipendent. For example, Jochum *et al.* [28] prepared a thermo-responsive PNIPAM (Poly(N-isopropylacrylamide)) bearing the photoresponsive fulgide moiety. The photocyclization of the fulgide group does not affect the LCST of the polymer, and the system is considered as a "LOGIC NOT A" gate.

Serial response occurs if the responses of two or more groups in the same polymer are dependent. Fu *et al.* synthetized a PNIPAM containing the TEMPO moiety.[29] After reduction of nitroxyl radical to nitroxide anion the solubility in water of PNIPAM is increased resulting in a more hydrophilic polymer, having a higher LCST. Thus, the LCST behavior of PNIPAM is influenced by the redox stimulus.

The last type of combined response is maybe the most intriguing. Causal interplay takes place if one responsive group produces structural or environmental change after stimulus application and these changes, in turn, produce a new stimulus for the second group in the same polymer. Iwai *et al*. prepared a copolymer bearing N,N-dimethylaminopropylacrylamide, N-*t*-butylacrylamide and a benzofurane derivative in the side chain. When the temperature is increased above LCST, the whole polymer becomes more hydrophobic. As a result, benzofurane polarity sensitive fluorophore, changes its emission wavelength.[30]

In recent years, research on smart material has been focused both on the design of new multi-stimuli responsive polymers bearing two or more functionalities and on the development of new responsive group. Moreover, the use of complex architectures has allowed to create materials with specific properties suitable for complex applications such as drug delivery, tissue engineering and bioimaging .[31,32]

1.2 LIVING POLYMERIZATIONS

Chain growth polymerizations (namely anionic, cationic or radical) usually comprise four mechanistic steps: initiation, propagation, chain transfer and termination. Deviations from the ideal polymer architectures and Đ broadening, caused by chain transfer and termination, should be avoided in order to obtain polymers with well-defined properties. In a living polymerization,[33] termination and chain transfer steps are not present[34] and the rate of initiation step is much larger than the rate of chain propagation. The absence of termination and chain transfer steps during the polymerization can be accomplished in a variety of ways and leads to a constant chain growth throughout the reaction. These features allow a control on composition, molecular weight and architectures of the polymer. Moreover, the propagation should continue after further addition of monomer at the end of reaction. The requirements of a "living polymerization" are:[33]

- Linear first-order plot of logarithmic monomer consumption versus time (x axis). If this relation deviates from linearity, the number of growing chains is not constant. Termination reactions result in negative deviation, while an inefficient initiation process leads to an increase of the slope. For this reason, initiation step should be quantitative and fast ($k_i > k_p >> k_t$)

- Constant number of propagating chains ends. As a consequence, the number-average molecular weight grows linearly with monomer conversion.
- The dispersity ($Đ=M_w/M_n$) in accordance with the Poisson distribution.[35]

The concept of "living polymerization" was first introduced by Szwarc in 1956 when he prepared polystyrene in THF at -78°C using sodium napthalenide as initiator.[36] In an anionic living polymerization the addition of radical anions, Lewis bases or carbanions, to a vinyl monomer initiates the reaction and the growing chain has a negatively charge at the end (Scheme 1.1). Monomers with an electron withdrawing substituent are preferred, since they stabilize the resulting carbanion. Clearly, acidic protons originating from solvents, monomers and impurities as well as electrophilic centres quench the reaction. Temperature is kept low to avoid termination process. The choice of the solvent and of the counterion of the negative charge are also of fundamental importance because separated ion pairs increase the rate of polymerization. At the end of polymerization, suitable chain-end functionalization, such as hydroxylation and carbonation could be done if the process is truly living.

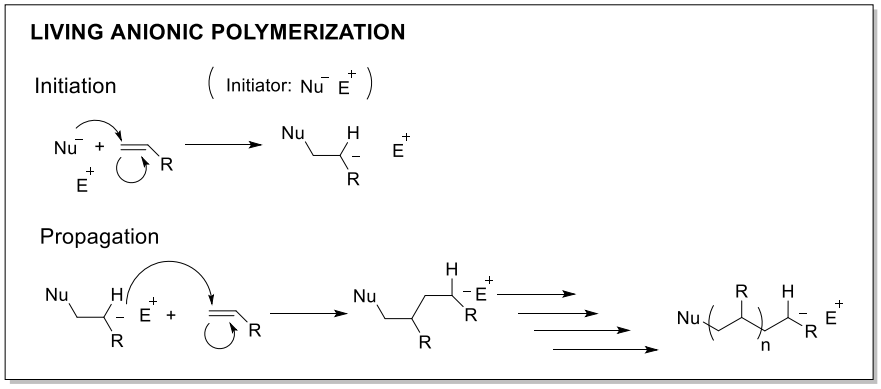

Scheme 1.1. Mechanistic steps of living anionic polymerization.

Living cationic polymerizations are analogous to anionic reactions. Initiators are usually protic acids, Lewis acids or carbenium salts. When carbenium ion is generated, addition to vinyl monomers continues during the propagation process. Differently from anionic, cationic polymerization works well with monomers bearing an electron donating group that could stabilize positive charge (Scheme 1.2). Electrophilic solvents favour the polymerization and the reaction is carried out a low temperature (-90°C, -30°C) to avoid termination and irreversible chain transfer process. In fact, one

of the main problems of cationic polymerization is rearrangement to more stable carbocation, and, as consequence, the formation of irregular chains.

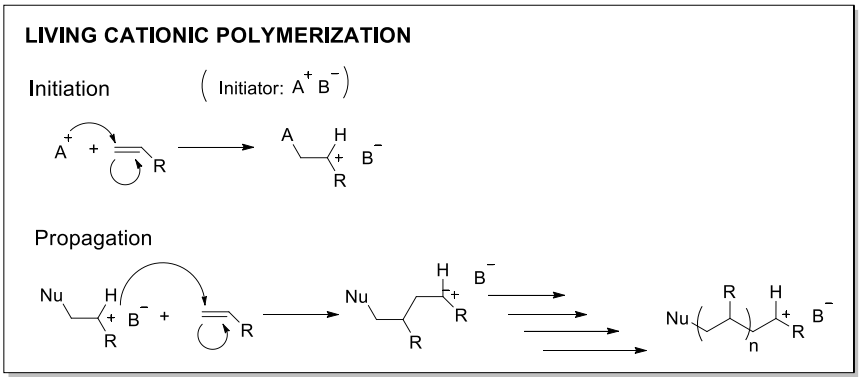

Scheme 1.2. Mechanistic steps of living cationic polymerization.

Other common living polymerizations are Ring-Opening Metathesis Polymerization (ROMP) and Acyclic Diene Metathesis (ADMET) (Scheme 1.3). Both of them use molybdenum and ruthenium complex as initiators/ complex and are based on Chauvin mechanism of olefin metathesis.[37] Cyclic alkenes are typical monomers for ROMP polymerization; in general the rate of reaction increases with ring strain and steric hindrance of monomers.[38] ADMET polymerization works with terminal olefines and the process is driven by the loss of volatile ethylene. The tolerance on functional groups depends on catalysts used. More detailed description on catalyst synthesis and new developments of these polymerization techniques are reported by R.T. Mathers[38] and Numara.[39]

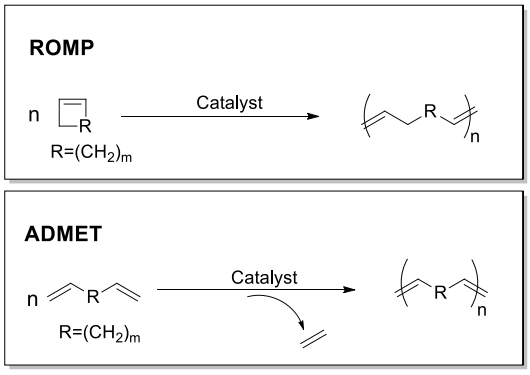

Scheme 1.3. Ring-opening metathesis polymerization (ROMP) and acyclic diene metathesis (ADMET).

In wider terms, the concept of "living polymerization" is not strictly associated to a polymerization technique. In fact, anionic or cationic polymerizations may not proceed as living polymerization if the reaction conditions are not optimal. The choice

of solvent, monomers and temperature play a fundamental role in the success of the process. Similarly, polymerization techniques that do not show at first glance living character may be controlled with appropriate conditions.

For completeness, other living polymerization methods and emerging progress are briefly discussed. Group Transfer Organocatalytic Polymerization proceeds using silyl ketene acetals as initiators and nucleophiles or Lewis acid as catalyst. The resulting silyl enolate activated by catalyst is able to add double bond of monomer relocating the silyl group at the chain terminal group. Temperature is usually higher and more accessible with respect to that of anionic living polymerization.[40,41] Recently, the concepts of living polymerization have invested the realm of noncovalent bonds. Significant progress has been made in the field of supramolecular polymerizations, and the first controlled architectures and functions have been explored.[42]

1.3 CONTROLLED RADICAL POLYMERIZATIONS (CRPs)

Radical polymerizations are widely used in industrial and technological applications, especially photoiniziated processes.[43]

In a free radical polymerization (Scheme 1.4) initiation is usually generated by thermal or photochemical decomposition of molecules such as organic peroxides, azo and diazo molecules. The most common initiators are benzoyl peroxide (BPO) and azobisisobutyronitrile (AIBN). After decomposition of the initiator, the resulting radical adds to a double bond of a vinyl monomer and generates a radical adduct. In the propagation step, a further monomer adds to the new radical centre, thus relocating the active centre to the new chain end. Propagation of the active chain can be terminated by coupling with another radical centre (another growing chain or initiator) or by disproportionation via β-hydrogen abstraction. Chain transfer occurs when a radical species reacts with a nonradical species (monomer, polymer, solvent, Chain Transfer Agent). So, a new radical centre is formed, and the old growing chain is terminated. If the chain transfer occurs with another polymer chain undesired branch points may be formed, leading to ill-defined chain architecture.

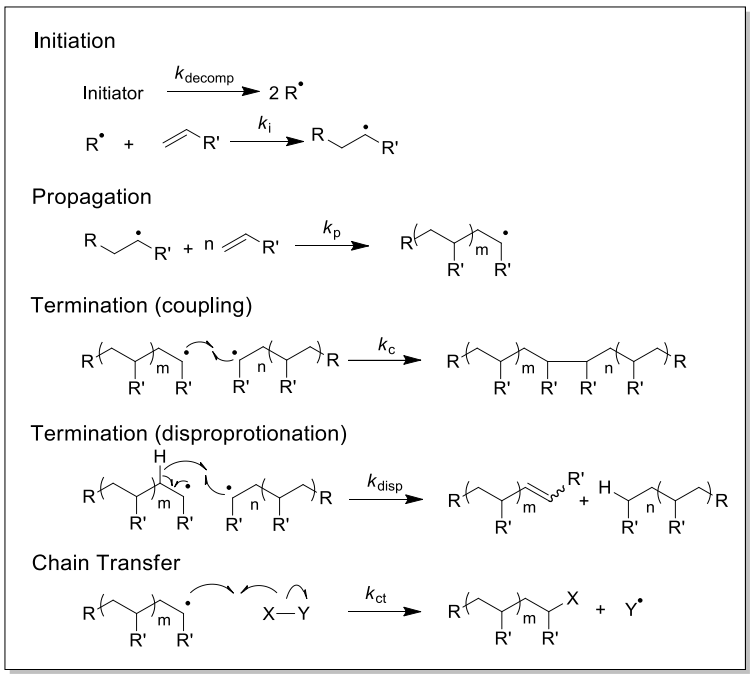

Scheme 1.4. Mechanistic steps of free radical polymerization.

Free radical polymerizations are uncontrolled processes, since termination and chain transfer reactions occur extensively, leading to high dispersity Đ and ill-defined architectures. Furthermore, the reaction usually lasts few seconds. In this time frame, synthetic manipulations, such as chain extension, end group modification and variation of monomer feed are impossible to perform.[44]

Indeed, one of the most important advances in the field of polymer chemistry over the last decades is the development of Controlled Radical Polymerizations (CRP). In the CRP approach, terminal and chain transfer step are not suppressed as in an ideal living polymerization. Termination and irreversible chain transfer reactions are kept to a minimum thanks to a fast dynamic equilibration between the active growing chain and dormant species. The time of polymerization becomes longer and synthetic manipulations become possible. The most common CRPs are Nitroxide-Mediated Polymerization (NMP), Atom-Transfer Radical Polymerization (ATRP) and Reversible Addition-Fragmentation Chain Transfer (RAFT). These polymerization methods will be described in detail in the next section.

Two relevant variants of CRPs are Polymerization Induced Self-Assembly (PISA) and photomediated CRPs. Controlled induced self-assembly polymerization allows synthesis of amphiphilic block copolymers in water forming self-stabilized nano-objects of different morphologies.[45] Photomediated CRPs offer several advantages with respect to controlled radical polymerizations including more

environmentally friendly conditions, reaction at room temperature and spatial and temporal control.[46]

1.3.1 Controlled Radical Polymerization (CRP)

As mentioned in the precedent section, Controlled Radical Polymerization have revolutionized the field of multi-stimuli responsive polymers thanks to the large number of accessible architectures and wide versatility towards different monomers and functional groups.[47]

Generally, all CRPs involve a dynamic equilibration between active (propagating chains) and dormant species. During the reaction, growing chains are activated/deactivated reversibly from/to the dormant species with rate constants k_a/k_d. When the active species are formed, they can add monomers with propagating rate constant k_p and terminate with termination rate constant k_t. Matyjaszewski grouped CRPs in four different types according to their reaction mechanism (Scheme 1.5).[44]

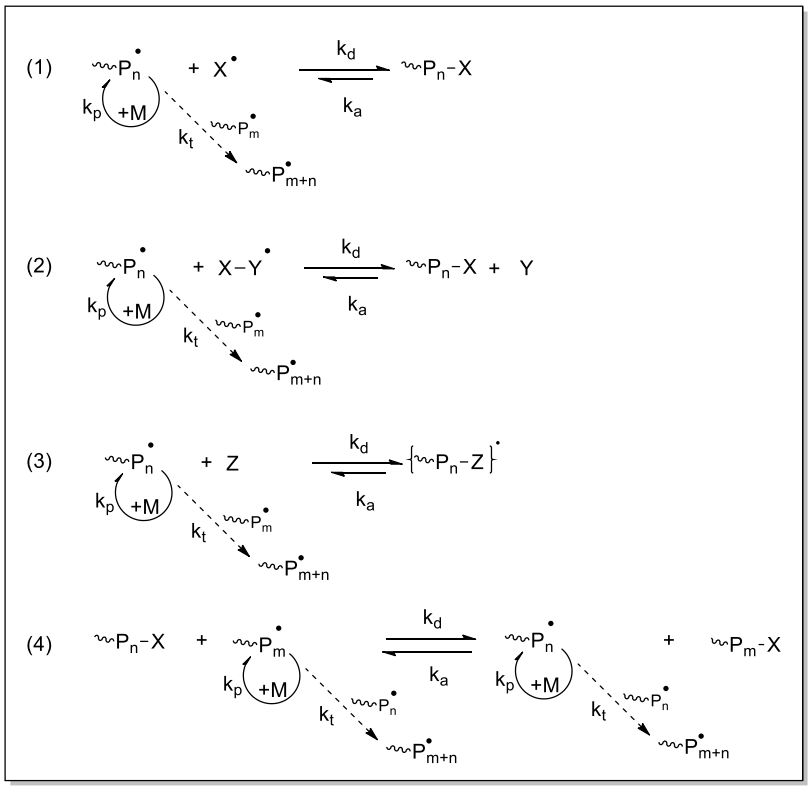

Scheme 1.5.Mechanism-based classification of CRPs.[44]

Cases 1,2,3 are characterized by Persistent Radical Effect (PRE),[48] where the formation of dormant species is promoted by the reaction of persistent radicals with transient radicals (growing chains). For example, in Case 1 transient radical P_n• can

react with persistent radical X• or self-terminate, while X• can only disappear by cross-reaction with P_n•. Over time, concentration of P_n• decrease because of termination reactions, whereas X• remains constant. Thus, the increasing excess of persistent radicals shifts the equilibrium towards the formation of dormant species. As a consequence, dynamic equilibrium between active and dormant species is favoured over termination reactions and the concentration of growing radicals remains low during the polymerization. NMP is an example of Case 1. If the process involves species with an even number of electrons (for examples phosphites or reactive but non-polymerizable alkenes) as radical trap, the CRP is described by Case 3. Case 2 is similar to 1, but the dormant species are converted to active species in a bimolecular process. Catalyst as Ru, Cu and Fe derivatives promotes cleavage of the reversible covalent bond of the dormant species through a redox process. This reaction is better known as Atom Transfer Radical Polymerization (ATRP). The last case is completely different from 1,2,3 since does not involve PRE. The control over polymerization is promoted by a degenerative transfer process in which a propagating radical, present at low concentration, is in a reversible equilibrium with the dormant species, present at higher concentration. RAFT polymerizations follow mechanism 4.

In the case 1, 2, 3 the rate of polymerization is much less than that of conventional radical polymerization, since the reversible equilibrium promoted by persistent radicals decreases the concentration of active chains during the reaction. Conversely, case 4 should have approximately the same rate of conventional polymerization, but the formation of stable intermediates during the exchange of two propagating chains can also decrease the rate of reaction.

Three common requirements are essential for a good control of the polymerizations. First, exchange between dormant and active species must be fast and shifted towards non-propagating chains. Second, termination should be reduced to minimum (CRPs usually give 10% of termination reaction) and, finally, initiation process should be quantitative, fast and efficient.

Below the three most used CRPs are described in detail.

Nitroxide-Mediated Polymerization

In NMP, the reversible equilibrium between active and dormant species is promoted by nitroxide derivatives. The propagating chains react with nitroxide to yield (macro)alkoxyamine as dormant species (Scheme 1.6).[49]

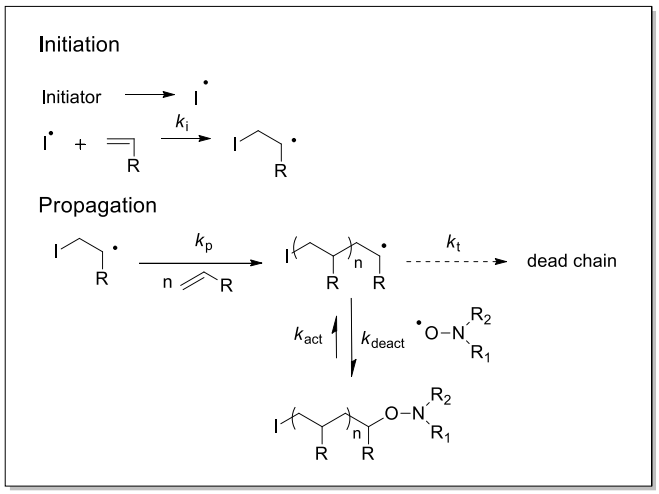

Scheme 1.6. Mechanism of NMP.

As a result, the temperature dependent activation-deactivation equilibrium is established. Examples of nitroxide agents are reported in Figure 1.4. Initiation is usually a bimolecular process, where common initiators as AIBN or BPO are employed. The optimised ratio between nitroxide and initiator is 1.3 and the reactions are carried out at high temperatures (~120 °C) because they are slow processes. A further strategy is the use of alkoxyamines that act as unimolecular initiators by decomposing into an initiator fragment and the nitroxide agent in 1:1 ratio. This approach can be useful to design the end-group of the resulting polymers and for post-modification reactions. NMP works well with styrene and its derivatives, acrylamides, dienes, acrylates but it is less effective with methacrylates because of undesired side reactions that affect control over the polymerization.[50] Recently, some strategies have been developed to control NMP with these monomers, while new NMP process such as emulsion, surface-mediated and photoinitiated polymerizations have been gaining increasing attention.[49]

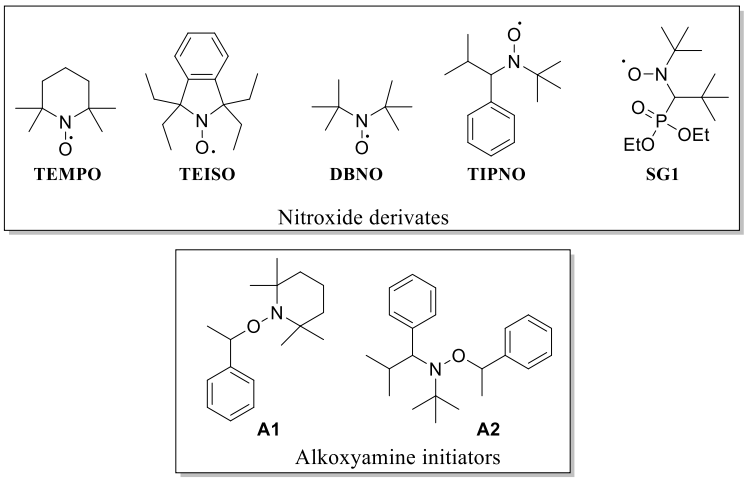

Figure 1.4. Examples of nitroxides (above): [2,2,6,6-Tetramethy l piperidine 1-oxyl (TEMPO); 1,1,3,3-tetraethyl-1,3-dihydroisoindol-2-yloxyl (TEISO); di-tert-butyl nitroxide (DBNO); N-(tert-butyl)-N-(2-methyl-1-phenylpropyl)-N-oxyl (TIPNO); N-tert-butyl-N-[1-diethylphosphono-(2,2-dimethylpropyl)] nitroxide (SG1)] and alkoxyamines initiators (below): [1-phenyl-1-(2',2',6',6'-tetramethyl-1'-piperidinyloxy)ethane (A1); N-tert-butyl-N-(2-methyl-1-phenyl-propyl)-O-(1-phenyl-ethyl)-hydroxylamine (A2)].

Atom Transfer Radical Polymerization

ATRP is one of the most versatile living polymerizations thanks to the wide range of polymerizable monomers, developed catalysts and initiators.[33] In this polymerization method the equilibrium between active and dormant species is promoted by transition metal complexes via redox processes (Scheme 1.7). Although Cu complexes are the most widely used catalysts, Ru, Fe, Ni, Ti, Mo are also employed in ATRP.

During the initiation process, a halogen atom is transferred from an alkyl halide to Cu(I) complex to obtain an alkyl radical able to add vinyl monomers. When this active species reacts with Cu(II) complex, a dormant chain bearing a halogen atom in at chain-end is formed, while Cu(II) complex is reduced to Cu(I). Unavoidable termination reactions increase the amount of Cu(II) complex at the expense of Cu(I) complex. For this reason the catalyst should be 1% (mol/mol). The use of chemical additives or electrodes[51] to regenerate Cu(I) complex can reduce the quantity of catalyst to ppm amounts. Specifically, ARGET-ATRP uses reducing agent as sulphites and ascorbic acid, while ICAR-ATRP employs general radical initiators as AIBN to recycle the catalyst.[52] The addition of Cu(0) in SARA-ATRP and SET-LRP ensures the regeneration of catalyst through comproportionation with $Cu(II)L_2$.[53,54] Furthermore, constant research on ATRP has allowed the development of metal-free

polymerizations based on photocatalysts able to establish a reversible activation/deactivation equilibrium between active and dormant species.[55,56]

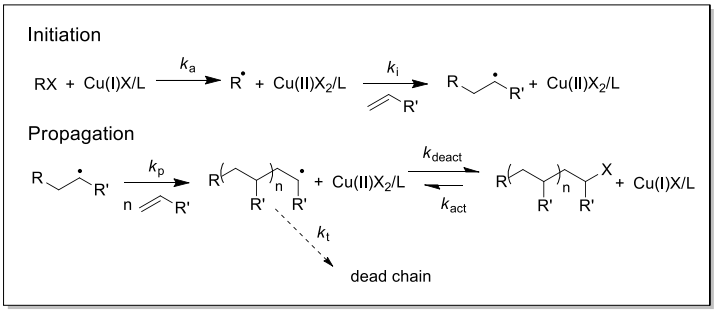

Scheme 1.7. Mechanism of ATRP.

Reversible Addition-Fragmentation Chain Transfer

Despite RAFT polymerization is the youngest among the most popular CRPs, it has been widely applied both in the academic and industrial fields.[57] In contrast with NPM and ATRP, the mechanism of RAFT does not imply Persistent Radical Effect, but it is based on degenerative transfer (Case 4 in Matyjaszewski classification).[44] A radical initiator is required to begin the polymerization and the concentration of radical species remains thereby constant (Scheme 1.8). After initiation, propagating chains add to RAFT agents (typically thiocarbonylthio compounds) that release a new radical R• similar to classical initiator fragments, able to start a new chain. The process of re-initiation is followed by the main equilibrium, where a reversible transfer between dormant and active chains is established. For a good outcome, the rate of addition-fragmentation process should be higher than that of chain propagation so that less than one monomer is added per activation cycle and all chains have approximately the same degree of polymerization. A small percentage of termination reactions is usually unavoidable in RAFT polymerization and depends only on the number of radicals produced by decomposition of initiators. At the end of the process, all "living chains" bear Z-C(C=S)S-Group and R at the extremities of the polymer chains, while dead chains encompass R groups at both α- and ω-ends. The presence of a dithiocarbonyl group at the chain end allows the synthesis of block copolymers and several end-group modifications.

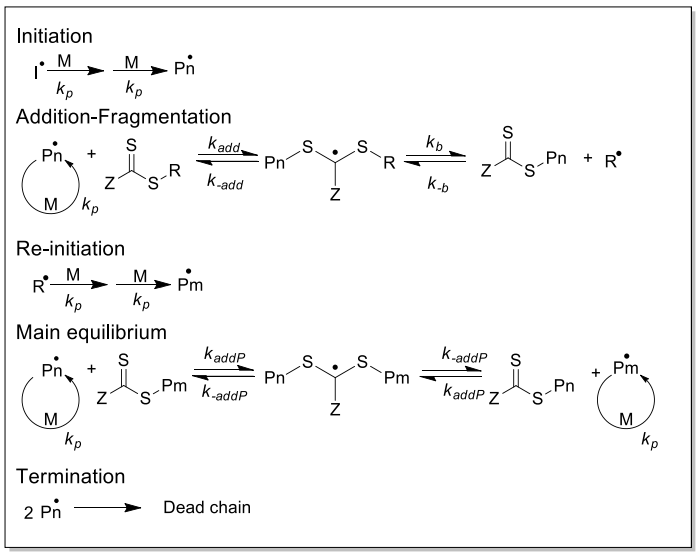

Scheme 1.8. Mechanism of RAFT.

The greatest merit of RAFT is its versatility towards a wide range of monomers and its tolerance of many functional groups that allow it to be a powerful technique for the synthesis of multi-stimuli responsive polymers.[58] The nature of Z and R groups of RAFT agent can be tuned in order to control the polymerization of a great number of monomers. Generally, "more activated" monomers (MAMs), characterized by a vinyl group conjugated to an aromatic ring, double bond, carbonyl or nitrile group such as in styryl derivatives, (meth)acrylates, dienes, (meth)acrylamides, acrylonitrile, are controlled using dithioesters/dithiobenzoates or trithiocarbonate. Otherwise, "less activated" monomers (LAMs), bearing a double bond adjacent to oxygen, nitrogen, halogen or saturated carbon such as in vinyl acetate, vinyl chloride, 1-alkene, react with a high transfer constant using N-alkyl-N-aryldithiocarbamates and the O-alkyl xanthates.[59] (Figure 1.5). Switchable RAFT agents such as *N*-methyl-*N*-(4-pyridinium) dithiocarbamates can provide a good control in polymerization of both MAMs and LAMs by simply interconverting the deprotonated and protonated forms. Specifically, neutral agents are effective in controlling polymerization of LAMs while the protonated form, obtained with addition of a strong protic or Lewis acid, is more active with MAMs. In this way a direct synthesis of low dispersity polyMAM-*block*-polyLAM copolymers is feasible.[60]

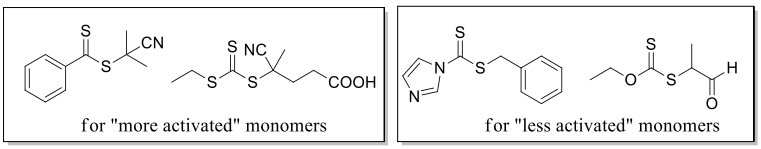

Figure 1.5. Examples of RAFT agents for MAMs and LAMs.

Recently, several variants of RAFT polymerization have been developed in order to improve conditions and success of reaction.[61] RAFT-mediated Polymerization-Induced Self-Assemblies (PISA-RAFT) is an efficient process to produce nano-objects of controlled size and morphology[62] based on block copolymers, while flow polymerization has been used for synthesis of block-gradient-block copolymer[63] and end-group modification.[64] Photo Electron Transfer RAFT (PET-RAFT) is a O_2-tolerant technique that uses a photoredox catalyst (transition metal complexes, organic dyes or biologically derived chromophores) to reduce chain transfer agent and produce radicals to initiate the polymerization.[65]

1.4 2-(HYDROXYIMINO)ALDEHYDES (HIAs)

As mentioned in the previous section, the employment and the development of CRPs have allowed polymerization of highly functionalized monomers and design of complex architectures. Currently, the research on multi-stimuli responsive polymers is geared towards both the integration of several functionalities in new tunable structures and the study of novel responsive groups.

In this context, oximes are molecules that have already demonstrated a versatile use in several fields and applications. In fact they are building blocks for the synthesis of heterocyclic compounds,[66] they can show biological activity[67] and they are used as ligands in metal coordination complexes,[68] while oximate ions are employed in decontamination of organophosphorus compounds.[69] Furthermore, the existence of two configurations, *E* and *Z*, due to the presence of double bond C=N has allowed their employment in the field of light-driven molecular machines.[70]

In the field of macromolecules, the research on oximes has taken different directions. Oxime esters are widely known as photoinitiators for radical polymerization,[71,72] and, in a recent work, H. Pu and coworkers have prepared three different novel thiophene-containing oxime sulfonates as photoacid generators for cationic polymerization.[73] Several crosslinked polymers can be obtained through reversible oxime bond formation. In particular, the presence of this reversible covalent

bond in hydrogel[74] or cross-linked polymer networks[75] generates materials with self-healing ability. Oxime bonds can also be viewed as an alternative for click reaction[76] or bioconjugation[77] thanks to their metal-free formation conditions. Moreover, oxime is a pH-sensitive linkage that can provide a controlled release of drugs in cancer therapy.[78,79] Recently, Liu *et al.*[80] reported a new class of polyurethanes based on oxime-carbamate bonds that show healable/recyclable properties while maintaining similar mechanical properties of traditional polyurethanes.

Besides its role as reversible linker in several applications in polymer chemistry and drug delivery, the oxime group has been occasionally investigated as stimulus-responsive moiety. In 2007, P. Theato and co-workers prepared acetone oxime acrylate as a new reactive ester monomer.[81] Copolymer poly(*N*-isopropylacrylamide-*co*-acetone oxime acrylate) 8:2 shows a LCST 61°C, while, after complete reaction with ammonia, the resulting copolymer poly(*N*-isopropylacrylamide-*co*-acrylamide) does not possess a LCST. Cai and co-workers prepared random copolymers of oligo(ethylene glycol) methacrylate (OEGMA) bearing an oxime moiety in the side chain that switch their pre-organization and thermal behavior in water solution via light-tunable H-bonding.[82] In fact, *E*-isomer led to "dimerization", in which an oxime group forms *two* H-bonds with *another* oxime, whereas *Z*-isomer produce an extensively "polymerization" where an oxime group can form *two* H-bonds with *other two* oximes. (Figure 1.6). The same light-tunable H-bonding behavior has been exploited for the formation of long range ordered nanopatterns starting from block copolymer micelles.[83]

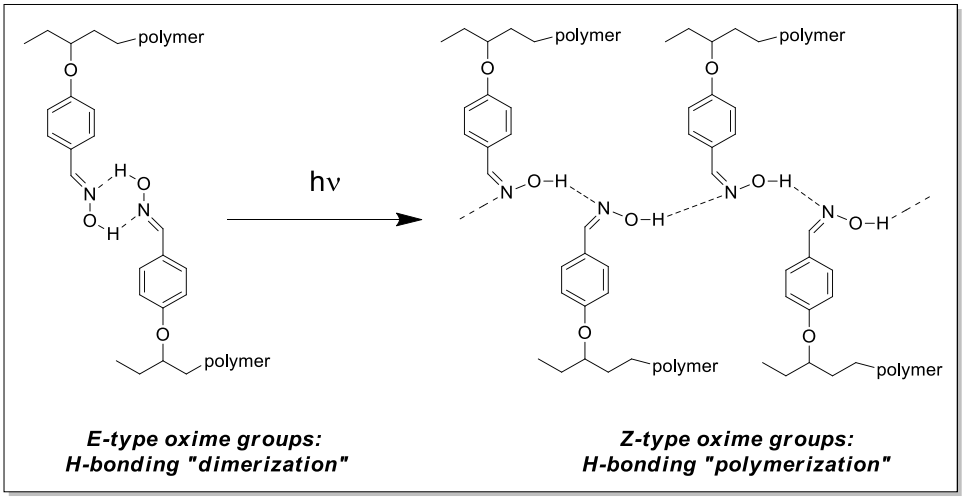

Figure 1.6. Switch of H-bonding pattern upon photoisomerization.[82]

Copolymers encompassing aldoxime azobenzene derivatives and dimethyl acrylamide groups have demonstrated to be a multiple analyte sensor for selective and consecutive detection of Hg^{+}, Ag^{+}, ClO^{-} and cysteine in water solution.[84]

The versatility of oximes, especially in the field of multi-stimuli responsive polymers, has prompted us to carry out further investigations in this area of research. Specifically, our team has developed a suitable α-oximation of aldehydes via organo-somo catalysis,[85] affording good to excellent yield of 2-(hydroxyimino)aldehydes (HIA) compounds. (Scheme 1.9)

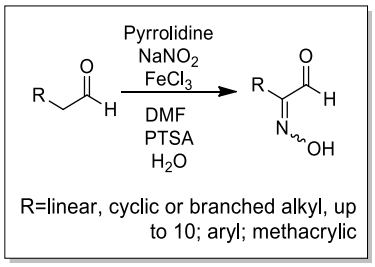

Scheme 1.9. Synthesis of HIA.

These molecules are characterized by an aldehyde group adjacent to an oxime moiety which can influence several properties such as redox potential, pKa, and BDE. Similarly to α-ketoximes, the vicinal aldehyde group can also influence the *E/Z* photoisomerization of the oxime group provide complex H-bond patterns in aqueous solution. Besides, the aldehyde group can be used as a handle to bind bioactive molecules through the formation of hydrazones or imines.[86,87] Over the years, several HIAs with different R substituents have been synthetized and characterized in order to asses structure-properties relationship.[88]

Acidity of HIAs is higher with respect to that of simple oximes thanks to stabilization of negative charge by aldehyde group. Indeed, their pKas ranging from 7.7 to 9.9 are comparable to that of hydroxamic acid (approximately from 7.9 for $C_6H_5C(O)N(OH)CH_3$[89] to 9.9 for $(CH_3)_3C(O)N(OH)CH_3$),[90] but they are higher than that α-arylcyanoximes (range 4.5–6.2) (Table 1.1).[91] HIAs, similarly to simple ketoximes and aldoximes, cannot be oxidised up to 2 V vs NHE. On the other hand, their anions possess oxidation potentials in the range of 0.38 to 0.64 V vs. NHE depending on steric hindrance of the adjacent R group. Deprotonated α-ketoximes bearing a carbonyl group conjugated to the $>C=NO^{-}$ moiety can be oxidised at similar potentials ($CH_3COCH=NO^{-}$, Ep=0.558 V/NHE; $PhCOCH=NO^{-}$, Ep=0.540 V/NHE).[89]

Table 1.1. pKa values of several 2-(hydroxyimino)aldehydes and the oxidation potentials (E^p) of the corresponding anions. Adapted with permission from Ref.[88]

RC(N=OH)CHO	pKa	E^p [V vs NHE]
$CH_3(CH_2)_7$-	8.8 ±0.2	0.55±0.01
$[CH_3(CH_2)_7][CH_3(CH_2)_9]CH$-	8.7 ±0.2	0.52±0.02
$(CH_3)_3C$ -	9.90 ±0.03	0.38±0.01
Cyclohexyl-	8.7 ±0.3	0.51±0.01
Ph-	7.69 ±0.02	0.63±0.01
$PhCH_2$-	8.05 ±0.07	0.61±0.01
Np-	7.94 ±0.06	0.60±0.01

A preliminary investigation of photoisomerization, carried out by using two HIAs with different R group, has demonstrated that both the initial *E/Z* population, photoisomerization and the rate of thermal re-equilibration to the initial population depend on the bulk of the substituent (Table 1.2). In fact, in contrast to the linear one, the *t*-Bu HIA exists mainly in the *Z* form and gives an almost complete inversion of configuration after 2 hours photoisomerization at 350 nm. Furthermore, the initial *E/Z* ratio is not recovered after 40 days thermal relaxation at 40°C. In contrast, only 10% of *E* isomer present before photostimulation in linear HIA inverts to *Z*. In addition, thermal isomerization is much faster than that of bulker HIA. Furthermore, the combination of *E/Z* isomers and the bulk of R group is expected to influence the ability to form dimers, trimers, tetramers or catamers[92] and H-bonding pattern.

Table 1.2. Preliminary investigation on photoisomerization of HIAs

RC(N=OH)CHO	*E/Z* (t_0)	*E/Z* λ=350 nm (2 h)	*E/Z* Δ, 40°C (t)
$CH_3(CH_2)_7$-	*E* only	10:1	*E* only (8 d)
$(CH_3)_3C$ -	1:10	5:1	1:2 (40 d)

In summary, 2-(hydroxyimino)aldehydes are endowed with intriguing properties which make them ideal candidates as responsive groups for smart polymers. Indeed, they can respond to light, pKa and redox stimuli proving a high versatility. (Figure 1.7).

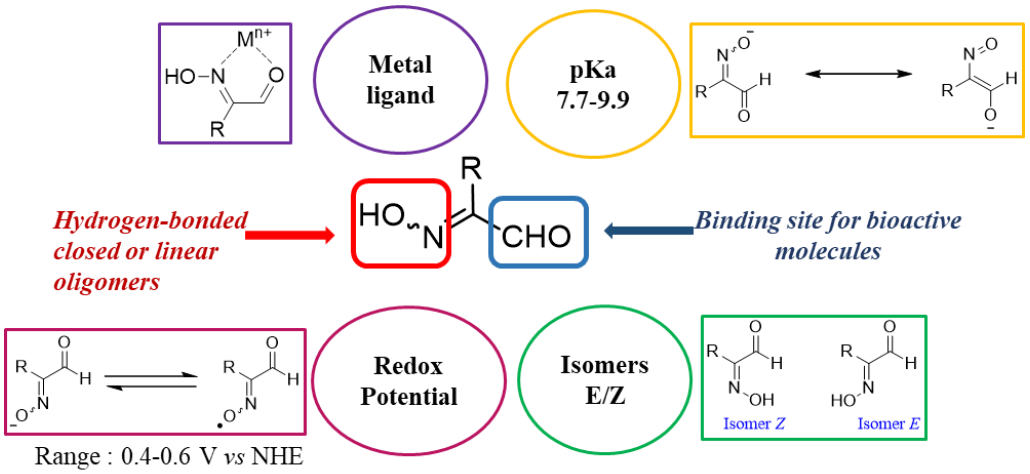

Figure 1.7. Properties of HIAs.

1.5 AIM OF THE PROJECT

The purpose of this PhD thesis is to prepare and study copolymers of OEGMA with methacrylates bearing the HIA group in the side chain. These copolymers combine the properties of HIA with temperature responsiveness of OEGMA, so that their behavior in response to different stimuli can be investigated. Moreover, a part of this thesis work was dedicated to the study of photochemical behavior of HIAs with different substituents in order to predict the photochemical response of HIA group in a polymer.

The first part of the thesis project was dedicated to the synthesis and characterization of a methacrylate monomer bearing the HIA group in the side chain. In particular, >CNO-*H* pKa and BDE, oxidation potential of oxime and oximate anion were assessed. Then, monomer encompassing HIA was copolymerised with OEGMA of different lengths through RAFT method.

In the second part of the work, the above-mentioned preliminary study on isomerization of HIAs was expanded to further small HIAs bearing different R groups adjacent to oxime. Moreover, the use of monochromatic source (LED) was compared to that of mercury lamps. The effect of light in a copolymer encompassing HIA in the side chain was also investigated.

Finally, the investigation on thermal behavior of copolymers aqueous solutions was carried out through turbidimetry and DLS measurement. Such investigation was also carried out on photostimulated polymer solutions, so as assess the interplay between light and temperature stimuli.

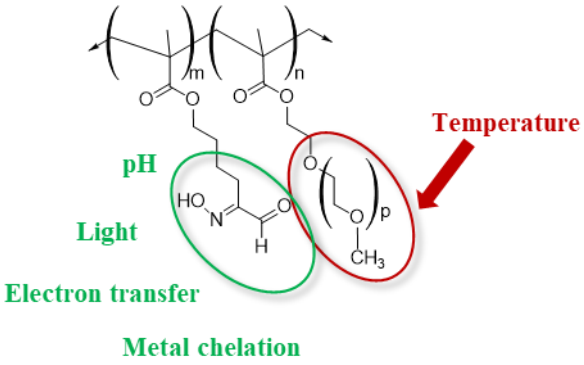

Figure 1.8. Polymers bearing HIA in the side chain

.

Chapter 2: Synthesis of copolymers bearing the HIA group

2.1 INTRODUCTION

The present chapter is dedicated to the preparation of copolymers of OEGMA with a methacrylate bearing HIA moiety. Two different strategies can be envisaged. A possible route may be the synthesis of a methacrylate encompassing an aldehyde group in the side chain, followed by copolymerization with OEGMA and a final post-polymerization reaction giving a polymer with HIA moieties. This procedure is actually employed to prepare polymers with a simple oxime group.[82,93] In fact, the condensation of primary amines with aldehyde and ketones is endowed with the requirements of an ideal polymer functionalization reaction: high yield, adaptable to large scale purification, simple, rapid and efficient under equimolecular conditions.[94] On the other hand, α-oximation reaction of aldehydes usually gives 60-90% yields on small molecules[85] that does not guarantee a complete functionalization of each repeat unit of polymers, especially with brush-type as OEGMA copolymers. Moreover, removal of reaction by-products, such as iron salts, may not be a user-friendly procedure. For these reasons, we prepared a fully-functionalized monomer **1** (HIABMA) by three-step synthesis from 1,6-hexandiol with the aim to use it directly in polymerization reactions (Scheme 2.1).[95]

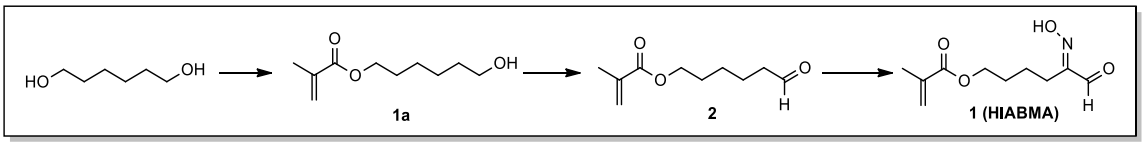

Scheme 2.1. Preparation of a monomer bearing HIA moiety.

The HIA functional group poses several challenges for radical polymerization. Initiating or propagating radicals may cleave the C(NO-H) bond[96] or add to the C=N bond. In fact, C=N bonds of some oxime ethers and conjugated oximes can act as radical acceptor, whereas glyoxyl oxime ethers have been shown to inhibit or retard radical polymerization of vinyl monomers.[97,98] In any case, these potential issues may not occur in a controlled radical polymerization. The choice of the most suitable

polymerization method is thus fundamental. NMP was discarded in the first place because it is scarcely successful with methacrylates,[50] as tertiary propagating radicals can disproportionate with nitroxyl radical, giving hydroxylamines and unsaturated chain terminals. As mentioned in the first chapter, HIA may form metal complexes,[99,100] subtracting them from the equilibria promoted by metal-based catalyst in ATRP methods. Therefore, for copolymerization of HIABMA with OEGMA we opted for RAFT method with AIBN as radical initiator, and CPDB (2-cyano-2-propyl benzodithioate), which has been already employed in polymerization with $OEGMA_{475}$,[101] as chain transfer agent. To the best of our knowledge, it was the first time that RAFT polymerization was carried out in presence of a free oxime moiety. For comparison, analogous monomers encompassing only aldehyde (OHMA) or simple oxime group (HIHMA) was also synthetised and copolymerised with OEGMA in order to highlight any peculiarities of HIA moiety, and to verify general applicability of RAFT to free-oxime-containing monomers (Figure 2.1).

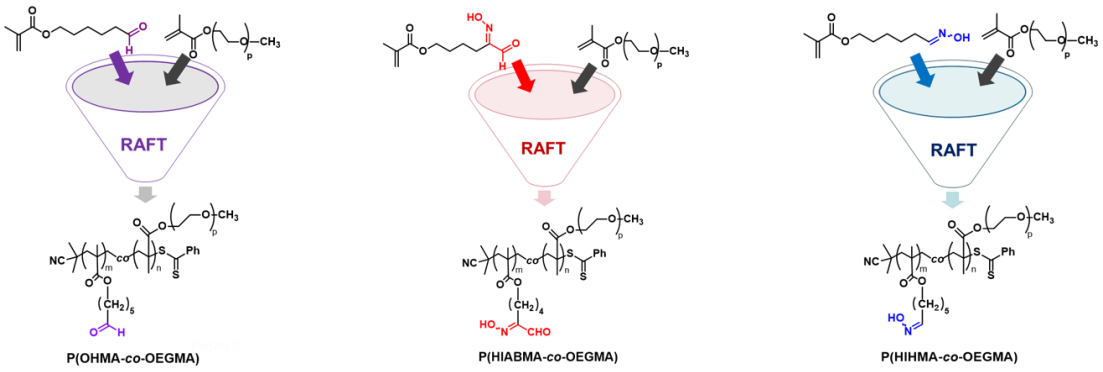

Figure 2.1. Target monomers and their copolymers with OEGMA.

Along with investigation on RAFT polymerizations, assessing the properties of HIABMA monomer is also fundamental with an outlook on multi-stimuli responsive polymers. Acidity, oxidation potential and UV absorption bands were therefore evaluated. A deeper analysis on photochemistry of HIABMA together with other HIAs can be found in Chapter 3. Moreover, computational studies, with a special attention on BDEs calculations, of HIABMA and another HIA bearing a *tert*-butyl group adjacent to oxime were conducted by Prof. M. D'Abramo research group to support experimental data and to evaluate the possibility of hydrogen abstraction during radical polymerization.[88]

Besides the successful preparation of the linear HIABMA monomer and of its copolymer with OEGMA, we have attempted the synthesis of a monomer with tertiary HIA. Indeed, we have shown that photostimulation of HIAs with bulkier substituents result in a more effective *E/Z* inversion. Unfortunately, it was not possible to obtain a monomer bearing a tertiary group in sufficient quantity and purity to allow polymerization. The several attempts are discussed in paragraph 2.2.3.

2.2 MONOMERS SYNTHESIS AND CHARACTERIZATION

2.2.1 Monomers synthesis

The monomer HIABMA **1** (4-[(hydroxyimino)aldehyde]butyl methacrylate) bearing a 2-(hydroxyimino)aldehyde (HIA) group, was obtained by multistep synthesis reported in Scheme 2.2. Monoacylation of 1,6-hexandiol was carried out using methacrylic anhydride and DMAP (4-dimethylaminopyridine) as catalyst.[102] The optimized ratio between diol and methacrylic anhydride is 2:1, even though reasonable loss of unreacted diol and a small amount of undesired bifunctional product **1b** are inevitable. Furthermore, monoprotection of symmetrical diol proved unnecessary, since product **1a** was obtained in satisfactory yield (59%).

Table 2.1. Reaction condition screening of monoacylation.

1,6 hexandiol / DMAP/ methacrylic anhydride	Yield 1a (%)	Ratio 1a/1b
0.5/0.2/1	- (only **1b**)	-
2/0.2/1	59	4.5/1
1/0.2/1	56	1.5/1

Product **1a** was oxidized to aldehyde **2** through Parikh-Doering oxidation[103] without prior purification on silica gel chromatography. The presence of by-product **1b** does not affect the reaction that proceed smoothly (98% of yield of isolated product) without over-oxidation of aldehyde **2** to carboxylic acid. Purification of product **2** by silica gel chromatography was necessary to perform subsequent reactions, i.e. α-oximation and RAFT polymerization (Scheme 2.2).

Monomer HIABMA **1** was thereby obtained by α-oximation[85] of aldehyde **2** as the main product of the reaction. A small amount of by-products were detected by GC-FID analysis at the end of reaction. Two of these compounds were identified by GC-MS analysis and ^{1}H-NMR, specifically aldehyde **2** self-condensation product and the nitrile resulting from **1** by-elimination of formic acid. Moreover, since the reaction was

carried out in presence of a stoichiometric amount of $FeCl_3$, removal of iron salts resulted in a partial loss of product **1**. After purification on silica gel chromatography monomer **1** was obtained in 60% yield.

Monomer **3** encompassing only free oxime group (HIHMA) was prepared in high yield by simple oximation reaction of purified aldehyde **2** with $NH_2OH{\cdot}HCl$ (Scheme 2.2).

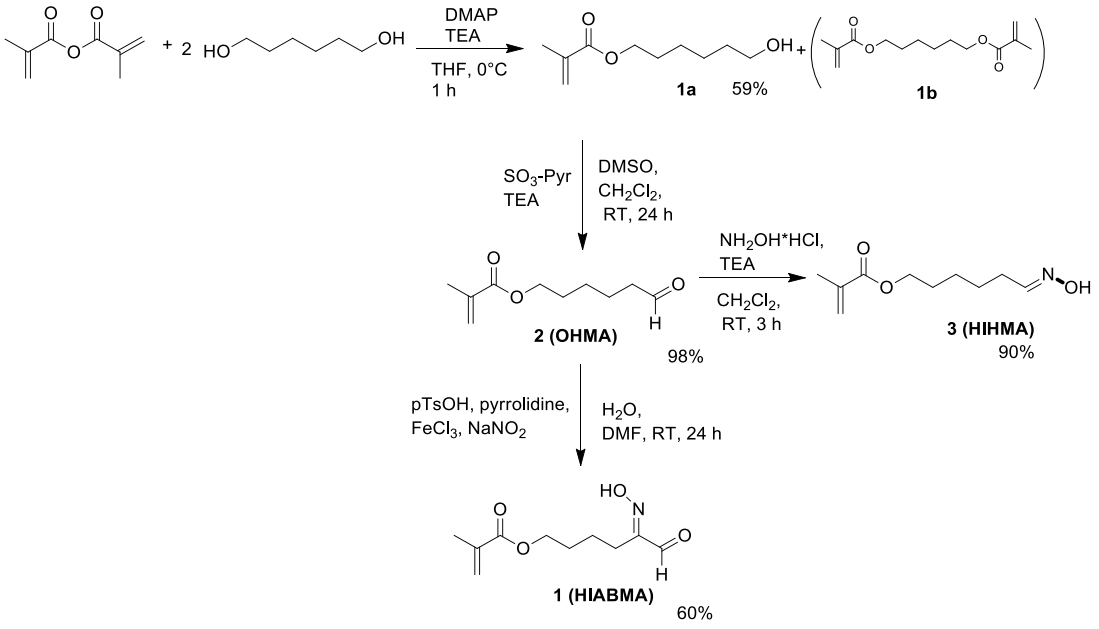

Scheme 2.2. Synthesis of methacrylates 4-[(hydroxyimino)aldehyde]butyl methacrylates (HIABMA), 6-(hydroxyimino)hexyl methacrylate (HIHMA) and 6-oxohexyl methacrylate (OHMA).

2.2.2 Characterization of HIABMA

Acidity, redox potential and UV-visible absorption bands of HIABMA were investigated and compared with those of other HIAs. Moreover, Bond Dissociation Energy of O-H bond of compound **1** and of a bulker HIA were calculated by DFT method in order to evaluate possible hydrogen atom abstraction by radical species during polymerization. Further investigations on the stability of *E*/*Z* isomers and photoisomerization of HIABMA are addressed in Chapter 3.

UV-visible spectroscopy

Absorption maxima and extinction molar coefficients of HIABMA were measured in a protic solvent (*i*-PrOH) and in three aprotic solvents of different polarity ($CHCl_3$, CH_3CN and DMSO) in order to evaluate solvatochromic effects. Moreover, the same investigation was carried out after deprotonation of **1** with an excess of

$(CH_3)_4NOH$. The results in Table 2.2 show a band at 230-260 nm ascribable to an allowed $\pi \rightarrow \pi^*$ transition that does not present significant solvatochromic effect. A weak band at 334 nm ascribable to the forbidden $n \rightarrow \pi^*$ transition becomes detectable as the concentration of **1** is increased to 1.2 mM. These values are in accordance with those of α-oxo-oximes[104] and of other HIAs.[88] When monomer **1** was deprotonated, a bathochromic shift combined with a hyperchromic effect of the allowed band was observed for all solutions. This is probably due to delocalization of negative charge on the carbonyl moiety.

Table 2.2. UV-vis data of HIABMA and its anion.

	***i*-PrOH** **λ/nm** **(ε/ $M^{-1}cm^{-1}$)**	**$CHCl_3$** **λ/nm** **(ε/ $M^{-1}cm^{-1}$)**	**CH_3CN** **λ/nm** **(ε/ $M^{-1}cm^{-1}$)**	**DMSO** **λ/nm** **(ε/ $M^{-1}cm^{-1}$)**
1	234 (16864)	235 (4458)	232 (18674)	260 (855) 334 (29)
1^-	290 (34556)	292 (38962)	292 (42944)	304 (6017)

[a] Concentrations: 1.2×10^{-3}M.

Determination of the pK_a value

The pKa of 2-(hydroxyimino)aldehyde **1** was determined by potentiometric titration. Owing to low solubility of HIABMA in water, it was dissolved in three mixtures of DMSO/H_2O (10:90, 20:80, 30:70 v/v) and titrated with KOH 0.1 M. The concentration of **1** in all DMSO/H_2O mixtures was 2 mM. The ionic strength was kept constant by addition of KCl (0.15 M). For each DMSO/water mixture, the cosolvent dissociation constant (p_sK_a) was obtained through the Henderson-Hasselbalch (Equation 2.1) equation by plotting the values of $\log([A^-]/[HA])$ versus pH before and after the equivalence point. The p_sK_a of a given mixture correspond to the intercept of the resulting linear regression. (Equation 2.1)

$$\mathrm{pH} = \mathrm{p}_s\mathrm{K}_a + \log([\mathrm{A}-]/[\mathrm{HA}]) \qquad \text{Equation 2.1}$$

The aqueous pKa value was, therefore, obtained by plotting the data collected for each DMSO/water mixture according to Yasuda-Shedlovsky equation[90] (Equation 2.2).

$$\mathrm{p}_s\mathrm{K}_a + \log[\mathrm{H_2O}] = \mathrm{a} + b/\mathcal{E} \qquad \text{Equation 2.2}$$

Here, $[H_2O]$ is the molar concentration of water and ε[105] is the dielectric constant of the given mixture, respectively. Intercept *a* and angular coefficient *b* are determined

by linear plotting of p_sK_a + log[H_2O] versus 1/ε. Finally, the aqueous pKa value was derived by Yasuda-Shedlovsky equation using *a* and *b* previously derived and dielectric constant of pure water (ε =78.36). The value 7.68 for the pKa of HIABMA is lower than that of simple linear HIAs (8.8) but it is comparable to aromatic HIAs. (Figure 2.2) This may be due to a remote inductive electron-withdrawing effect promoted by methacrylate that stabilize the oximate ion.

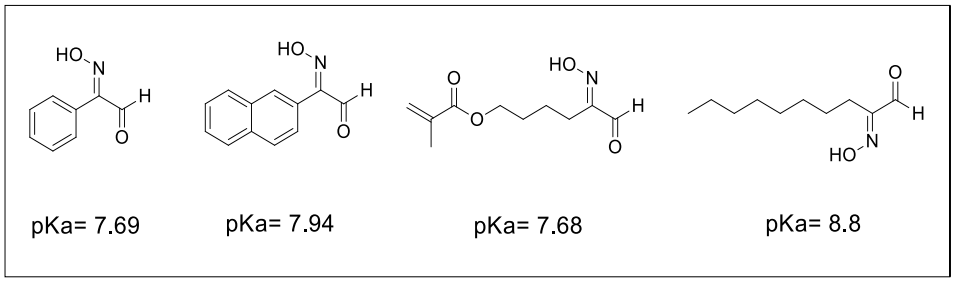

Figure 2.2. pKa values of HIAs.

Determination of oxidation potentials

The HIABMA oxidation potential was determined by cyclic voltammetry using DMF as solvent, 0.1 M Bu_4NBF_4 as supporting electrolyte, a glassy carbon working electrode, and Ag/AgCl/KCl (3 M) as reference electrode. First the potential was increased to 2 V *vs* NHE at a scan rate of 0.5 V/s. Compound **1** was not oxidazed up to this potential resulting in no flow of electrical current in the circuit. Then, a four-fold excess of Me_4NOH was introduced to deprotonate HIABMA. The resulting oximate ion showed an oxidation peak at 0.62 V vs NHE that results partially reversible as the potential is switched to 0.8 V *vs* NHE (Figure 2.3).

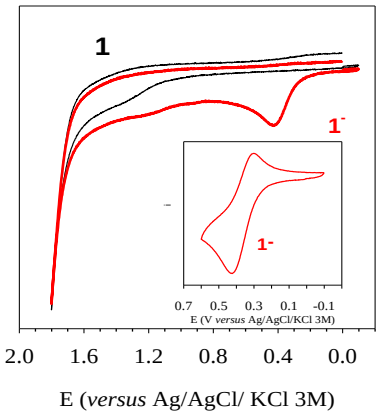

Figure 2.3. Cyclic voltammogram of compound **1** and its anion in DMF at 0.5 V/s. Reproduced with permission from Ref.[88]

Calculation of O-H bond dissociation enthalpy

HIAs can exist in different configurational (*E/Z*) and conformational isomers (*syn/anti*) showed in Figure 2.4. Since BDEs of NO-H bond of ketoximes depend on several factors, such as geometrical isomerism, steric effects, dipole-dipole interactions, and intramolecular hydrogen-bonding,[96] two different HIAs were taken into account in this investigation. One is the linear monomer **1** (HIABMA), while the other bearing a *t*-Bu group was chosen as a model for a potential monomer having considerable steric hindrance close to the oxime moiety (**4**).

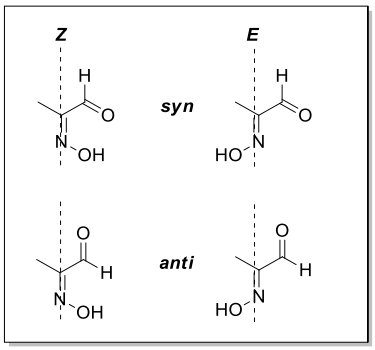

Figure 2.4. Configurational (*E/Z*) and conformational (syn/anti) isomers of 2-(hydroxyimino)aldehydes.

The calculated BDEs of **1** and **4** are shown in Table 2.3 together with BDE values of some symmetric ketoximes encompassing different alkyl substituent.[96,106] The presence of an aldehyde substituent leads to BDEs 3-10 kcal/mol lower than BDE of simple oximes having alkyl group as substituents. Linear HIA **1** exhibits higher BDEs of isomers *E* with respect to *Z*, while the hindered HIA **4** shows an opposite trend. Small differences are also found for *syn*/*anti* isomers resulting from the relative stability of each geometry. In fact, both **1** and **4** show BDEs of *Z-syn* isomers 1-2 kcal/mol larger than that of *Z-anti* likely owing to intramolecular hydrogen bond between the oxygen atom of CHO and hydrogen atom of oxime moiety. Calculations of O-H-O distances in the optimized geometries of *syn*-(*Z*)-**4** and *syn*-(*Z*)-**1** (2.57 and 2.60 Å, respectively) supports this hypothesis.

Table 2.3. Gas-phase NO-H BDEs of 2-(hydroxyimino)aldehydes **1** and **4** at 298 K.[a] Reproduced with permission from Ref.[88]

RC(=NOH)CHO	***Z-syn***	***Z-anti***	***E-syn***	***E-anti***
(**1**) CH_2=C(CH_3)CO_2(CH_2)$_4$-	75.5	74.4	75.7	77.5
(**4**) (CH_3)$_3$C-	74.8	72.7	72.9	72.5
t-Bu_2C(N=OH)		75.6[b]		
i-Pr_2C(N=OH)		80.7[b]		
Et_2C(N=OH)		81.8[b]		
Me_2C(N=OH)		82.6[b]		

[a] Calculated by DFT at the B3LYP/6-311+G(2d,2p). [b] Ref.[96]

Calculations in the gas phase of the relative energy of each isomer (Appendix A) indicate that *anti*-(*E*)-**1** is more stable of about 5-7 kcal/mol than other isomers of **1**, while the energies of (*Z*)-**4** isomers are lower than that of (*E*)-**4**. This opposite trend should be ascribed to a combination of effects of the *tert*-butyl bulk and dipole moment interactions. Values for ∠CCN angles along with a representation of dipole moments of all isomers are shown in Figure 2.5. Although *Z* isomer of **1** and **4** have similar values for ∠CCN angles, the steric hindrance of *tert*-butyl group brings CHO and C(NOH) groups closer in *E* isomers with respect to CH_2=C(CH_3)CO_2(CH_2)$_4$- group of **1**. As a consequence, the dipolar interactions become more destabilizing in (*E*)-**4** than in (*E*)-**1**. A deeper insight on the optimized structures of iminoxyl radicals of **1** and **4** in gas phase and in DMF (Appendix A) show that almost all bond lengths are similar to those of their precursors except for N-O bond that is 0.15-0.17 Å smaller. Unpaired radical electron is shared by N and O atom as demonstrated by spin density computed at B3LYP/6-311+G(2d, 2p) level. In fact, N and O of C(NOH) moiety have spin density values of 0.52-0.55 and 0.43-0.47 respectively, whereas all other carbon atoms and oxygen of aldehyde group have values close to zero. These results are in agreement with those of other oximes,[96,106] and demonstrated that the unpaired electron is σ-type lying in the plane of molecular framework. This is reflected on ∠CNO angles of iminoxyl radicals that are 13°-20° larger than in parent HIAs. The larger relief in the radical structures makes the dipole-dipole interactions less significant and, thus, could rationalize the smaller BDE of (*E*)-**4** with respect to (*E*)-**1**.

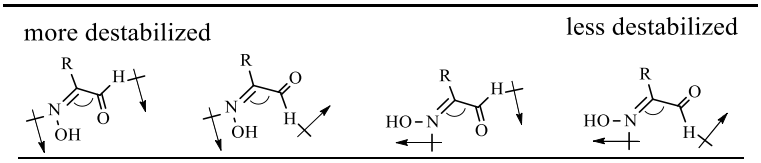

	∠CCN			
	Z-syn	***Z-anti***	***E-syn***	***E-anti***
1	123.3°	123.7°	115.4°	112.2°
4	122.9°	121.3°	110.7°	106.7°

Figure 2.5. Dipolar repulsions in the different isomers of HIAs **1** and **4**. ∠ CCN angles of the optimized geometries in the gas-phase calculated at the B3LYP/6-311+G(2d,2p) level of theory. Reproduced with permission from Ref.[88]

To summarize, BDEs of HIAs fall in the range of 72-78 kcal/mol, approximately 3-10 kcal/mol lower than that of simple oximes. Hydrogen abstraction from radical species participating in polymerization reaction may therefore be possible. For example, 2-cyano propyl radicals $Me_2\dot{C}CN$ used in the present work as initiator radicals of RAFT polymerization, may abstract the hydrogen atom from C(=NOH) group of **1** in an exothermic process of about 10 kcal/mol:

$$Me_2\dot{C}CN + RC(NOH)CHO \rightarrow Me_2CHCN + RC(NO^{\bullet})CHO$$

$$\Delta H_{reaction}\ (kcal/mol) = BDE_{reagents} - BDE_{products} = 78 - 85 = -7$$

Similarly, alkyl radicals derived from propagating chains could stop the growth of polymer chain by hydrogen abstraction from HIA, the BDE of non-conjugated C-H bonds being about 100 kcal/mol.[107] However, a simple comparison between gas-phase BDEs of all species present during the polymerization does not prove the interference of C(NOH) moiety in the reaction. Factors as solvent and radical philicity play also a fundamental role in hydrogen abstraction. Anyway, investigations on BDEs of HIAs with different structures is a preliminary indication to understand some aspects of the radical polymerization of HIA-functionalized monomers.

2.2.3 Attempts to synthesize an HIA-containing monomer bearing a tertiary group

As mentioned in the introduction, HIA with a tertiary group close to oxime moiety exhibits a large inversion of configuration upon irradiation, from 90% *Z* to 80% *E* (Table 1.2). Therefore, in order to obtain a monomer bearing HIA group able to give

an extensive *E/Z* inversion of configuration, two different monomeric structures were targeted.

The first synthetic route envisaged selective protection of the primary position of asymmetric diol **5a** by using sterically-hindered *tert*-butyldimethylsilyl chloride (TBDMS-Cl) as the silylating agent.[108] The subsequent esterification of tertiary alcohol (**6**) was then possible. Then, deprotection of primary alcohol would enable the oxidation to aldehyde **8** and the subsequent α-oximation to afford HIA with a tertiary group adjacent to oxime moiety (**9**) (Scheme 2.3). Steps I-III were performed one-pot without isolation of intermediates **5** and **6**. ^{1}H-NMR analysis showed the primary alcohol was indeed protected selectively, and, then, only tertiary alcohol reacted with methacrylic chloride. However, deprotection of primary alcohol with tetrabutylammonium fluoride resulted in 50% rearrangement of ester **7a** to ester **7b** through undesired transesterification.[109] This lowered the yield of **7a** to less than 50%. Then, several attempts were made to oxidize **7a** to **8**. Both Parikh-Doering modification of Swern reaction and oxidation with TEMPO and BAIB consumed all alcohol **7a** but without the formation of aldehyde **8**. Oxidation with pyridinium chlorochromate afforded aldehyde **8**, but the product turned out to be volatile, and, therefore, difficult to handle. This disadvantage, along with the desire to avoid Cr(VI) reagents, and transesterification of ester **7a** prompted us to change target a slightly different monomer (Scheme 2.4).

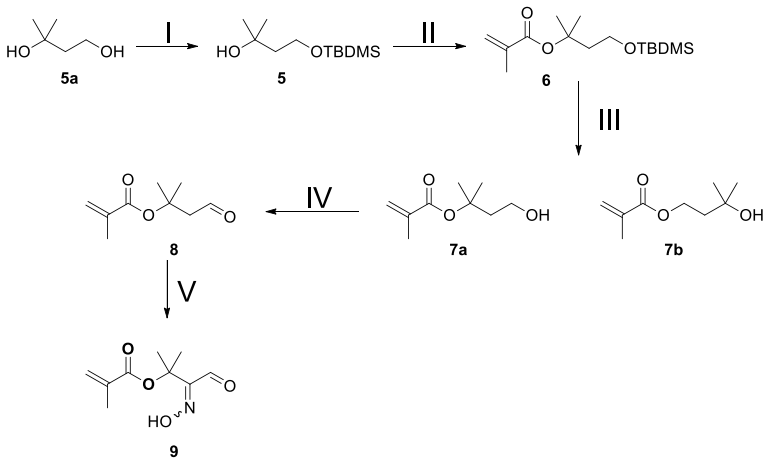

Scheme 2.3. First synthetic strategy to obtain a HIA-containing monomer with tertiary group adjacent to oxime. I) TBDMSCl, TEA, DMAP, Et_2O; II) Methacrylic chloride, DMAP, TEA, Et_2O. III) TBAF, THF, Et_2O (Yield of **7a** 35%, **7b** 30%); IV) (a) SO_3-Pyr, DMSO, TEA, DCM; (b) TEMPO, BAIB, DCM; (c) PCC, DCM; V) pyrrolidine, H_2O, TsOH, $FeCl_3$, $NaNO_2$, DMF.

In fact, our second attempt for a tertiary HIA monomer was aimed at avoiding protection/deprotection steps and at preventing the hypothetical interference of the methacrylate group on the oxidation step. We therefore decided to obtain the methacrylate of symmetrical 3,3-dimethylpentanediol as precursor, so as to move the methacrylic ester one position away from the tertiary group (**11a** *vs.* **7a**) (Scheme 2.3). In step I, 3,3-dimethylglutaric acid was reduced quantitatively to diol **10** using lithium aluminium hydride. Then ester **11a** was obtained through acylation of diol **10** with 0.5 equivalents of methacrylic anhydride, in the presence of DMAP as catalyst, resulting in an acceptable loss of diol and limited formation of diester **11b** (20%) (Step II). Oxidation of **11a** to **12** with Parikh-Doering reaction afforded good yield (62% of isolated product, Step III) with no over-oxidation to carboxylic acid, thus confirming that the failure of the oxidation step in Scheme 2.3 can be ascribed to the relative proximity of the methacrylates group. α-oximation of **12** proceeded more slowly with respect to aldehydes with a primary or secondary group in β-position (Step IV). However, only 10% of aldehyde was left by continuing the reaction for 72 hours and **13** was the main product of reaction detected by GC-MS. After silica gel chromatography with ethyl acetate and hexane, only 26% **13** recovered. Furthermore, some impurities could be detected both by GC-MS and ^{1}H-NMR. This unsatisfactory outcome may be due to non-optimized purification procedure and/or instability of the compound itself. In summary this synthetic strategy had proved to be better than the previous one. Step I-III proceeded with good to quantitative yields, while optimization of step IV is necessary to obtain HIA **13** in higher yield to use it in polymerization reaction.

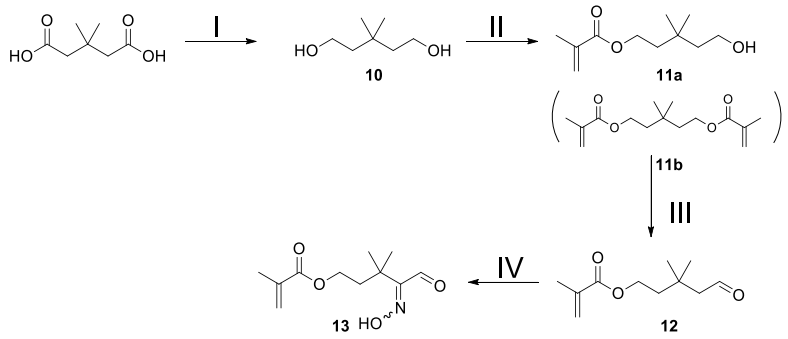

Scheme 2.4. Second synthetic strategy to obtain a HIA-containing monomer with tertiary group adjacent to oxime. I) $LiAlH_4$, THF, Et_2O (Yield 98%); II) methacrylic anhydride, DMAP, TEA, Et_2O (Yield of **11a** 47%, **11b** 20%). III) SO_3-Pyr, DMSO, TEA, DCM (Yield 62%); IV) pyrrolidine, H_2O, TsOH, $FeCl_3$, $NaNO_2$, DMF.

2.3 POLYMERIZATION REACTIONS

2.3.1 Random copolymerization of OEGMA and target monomers

The target monomers HIABMA, HIHMA and OHMA were copolymerized with $OEGMA_{475\text{-}500}$ and $OEGMA_{300}$ using CPDB as chain transfer agent and AIBN as initiator, so that only one type of initiating radical was present during the polymerization. (Scheme 2.5). Monomers feed ratio was varied from 1:9 to 3:7 (M/OEGMA), while the total concentration of monomers to chain transfer agent and initiator was kept at [M]:[CPDB]:[AIBN] 75:1:0.25. All polymerizations were carried out in dimethylformamide at 70-75 °C. No significant differences in the outcomes of polymerizations were found in this temperature range.

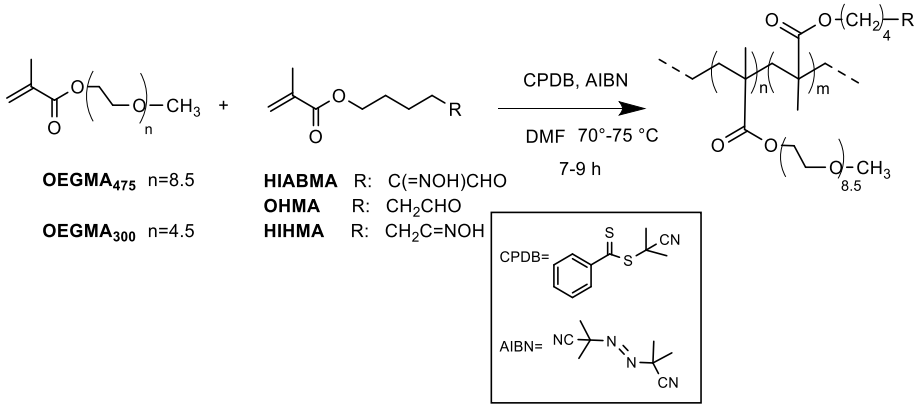

Scheme 2.5. RAFT polymerization of OEGMA and HIABMA, OHMA or HIHMA.

Table 2.4 shows the characterization data of copolymerization reactions of OEGMA with HIABMA, HIHMA and OHMA. Homopolymerizations of $OEGMA_{475}$ and $OEGMA_{300}$ (entry 1, 7 and 8) were used as references. Moreover, M_n and Degree of Polymerization (DP) data derived from GPC analysis may be underestimated by a factor of approximately two since comb-shaped polymers have smaller hydrodynamic radii with respect to linear calibration standards as demonstrated by Pietsch *et al.*[110] However, this underestimation may depend on the length of side chain, composition and molecular weight of copolymers. For this reason, interpretation of M_n and DP data from GPC analysis should be handled with great care, keeping in mind that any correction factors are just an approximation.

For homopolymerizations and copolymerizations of $OEGMA_{475,}$ monomers conversion values were determined directly from GPC traces, as the signal of monomers is well resolved from that of the polymer at each stages of polymerization

(in Figure 2.6 are reported GPC traces of polymerization of $OEGMA_{475}$ and HIABMA/$OEGMA_{475}$ 3:7 as examples). This approach was already used by Pietsch *et al.* to follow the monomer consumption over time of $OEGMA_{1100}$ polymerization.[110] The reliability of this determination was confirmed through two further approaches. First, the area of monomers peaks was plotted towards monomers weight fraction of injected GPC samples, resulting in a linear response of RI detector. Then, for HIABMA/$OEGMA_{475}$ 3:7 copolymerization, GPC conversion was compared with conversion obtained by ^{1}H-NMR, as is shown in Figure 2.7. Furthermore, the conversions obtained by GPC analysis were found in excellent agreement with ^{1}H-NMR data at the final time-point of all copolymerizations. (Table 2.5). Differently, for homo- and copolymerization of $OEGMA_{300}$ calculation of monomer conversions was performed only by ^{1}H-NMR analysis of crude mixture, since GPC results were of limited reliability.

Table 2.4. Characterization data of homo- and copolymerization of OEGMA with HIABMA, OHMA and HIHMA. The reactions were carried out at 70°C[(e)] or 75°C[(f)].

Entry	Monomers (mol/mol)	C_{tot}[(a)] (M)	Reaction time[(b)] (h)	Monomer conv.[(c)] (%)	M_n (GPC) (Da)	Đ	DP (GPC)	DP theor[(d)]
1	$OEGMA_{475}$ [(e)]	0.8	7	77	13400	1.12	28	58
2	HIABMA/$OEGMA_{475}$ 1:9 [(e)]	0.8	8	81	13000	1.13	29	61
3	HIABMA/$OEGMA_{475}$ 3:7 [(e)]	0.8	9	58	9800	1.10	25	44
4	HIABMA/$OEGMA_{475}$ 3:7 [(f)]	0.8	8 (6)	55	10400	1.09	26	42
5	HIHMA/$OEGMA_{475}$ 3:7 [(f)]	0.8	8 (6)	85	11200	1.10	28	64
6	OHMA/$OEGMA_{475}$ 3:7 [(f)]	0.8	8 (6)	73	11000	1.11	33	55
7	$OEGMA_{300}$ [(f)]	0.8	7.5	63	8200	1.08	27	47
8	$OEGMA_{300}$ [(f)]	1.1	7.5 (6)	94	10700	1.15	36	71
9	HIABMA/$OEGMA_{300}$ 3:7 [(f)]	1.1	7.5 (6)	94	11100	1.14	43	71
10	HIHMA/$OEGMA_{300}$ 3:7 [(f)]	1.1	8	84	9700	1.13	36	63

[(a)] Total concentration of monomers (mol/L)

[(b)] Time of polymerization quenching (hours); in parenthesis, time at which no polymerization progress is observed by GPC.

[(c)] Entries 1-6: Monomer conversions are calculated from GPC traces. Entries 7-10: Monomer conversions are calculated by ^{1}H-NMR analysis of crude mixture using terminal OCH_3 of $OEGMA_{300}$ as internal standard.

[(d)] DP (theor.) are calculated according equation $DP=\frac{M_0-M_t}{[CTA]}$ (eq. 2.3)

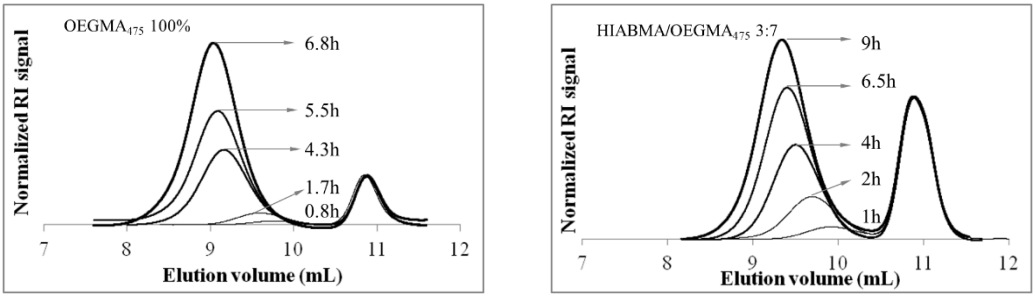

Figure 2.6. Time evolution of the GPC traces of the RAFT polymerization crudes of $OEGMA_{475}$ and of HIABMA/$OEGMA_{475}$ 3:7. RI signals are normalized to the height of the monomers peak. Reproduced from Ref. [95] with permission from The Royal Society of Chemistry.

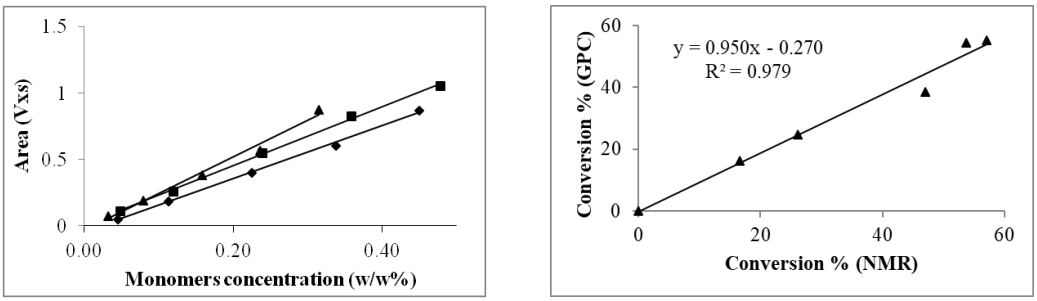

Figure 2.7. Left: plot of the GPC peak area of co-eluted monomers against their weight fraction (w/w%) in the injected sample. OHMA/$OEGMA_{475}$ 3:7 (◆); HIHMA/$OEGMA_{475}$ 3:7 (■); HIABMA/$OEGMA_{475}$ 3:7(▲). Right: Correlation between total monomers conversion values (HIABMA/$OEGMA_{475}$ 3:7) obtained through analysis of crude samples drawn at fixed time-points by ^{1}H-NMR and by GPC. Reproduced from Ref. [95] with permission from The Royal Society of Chemistry.

All the polymers reported in Table 2.4 show Đ values below 1.2, as expected in controlled radical polymerizations. $OEGMA_{475}$ and $OEGMA_{300}$ homopolymer and all copolymers of OHMA, HIHMA and HIABMA reach conversions higher than 55%. Copolymers of HIABMA show differences depending on monomers ratio and length of OEGMA. While HIABMA/$OEGMA_{475}$ 1:9 (entry 2) copolymer has very similar characteristics as $POEGMA_{475}$, an increase in the monomers ratio to 3:7 (entry 3 and 4) results in a decrease of monomer conversion (58%), with a slightly lower DP of 25. In contrast, HIHMA/$OEGMA_{475}$ 3:7 (entry 5) and OHMA/$OEGMA_{475}$ 3:7 (entry 6) reach higher conversions (85% and 73%, respectively) comparable to $POEGMA_{475}$. An opposite situation was found in $OEGMA_{300}$ copolymerizations. In fact, HIABMA/$OEGMA_{300}$ 3:7 (entry 9) results in the same monomer consumption as $POEGMA_{300}$ (entry 8), while HIHMA/$OEGMA_{300}$ 3:7 (entry 10) shows a slightly lower monomer conversion. In Figure 2.8 are reported the kinetics of homopolymerization of $OEGMA_{475}$ and $OEGMA_{300}$. All homopolymerizations show a linear first-order kinetics that is indicative of a constant concentration of radicals

through time. However, reaction of $OEGMA_{300}$ carried out at 0.8 M exhibits an induction period at the beginning of the polymerization and proceeds with an apparent kinetic rate constant that is approximately half that of the same polymerization carried out at 1.1 M. $OEGMA_{475}$ homopolymerization does not exhibit the same induction period at 0.8 M and proceeds with a comparable rate as $OEGMA_{300}$ (C=0.8 M). As a result, concentration of 0.8 M is sufficient to reach 77% monomer conversion after 7 hours.

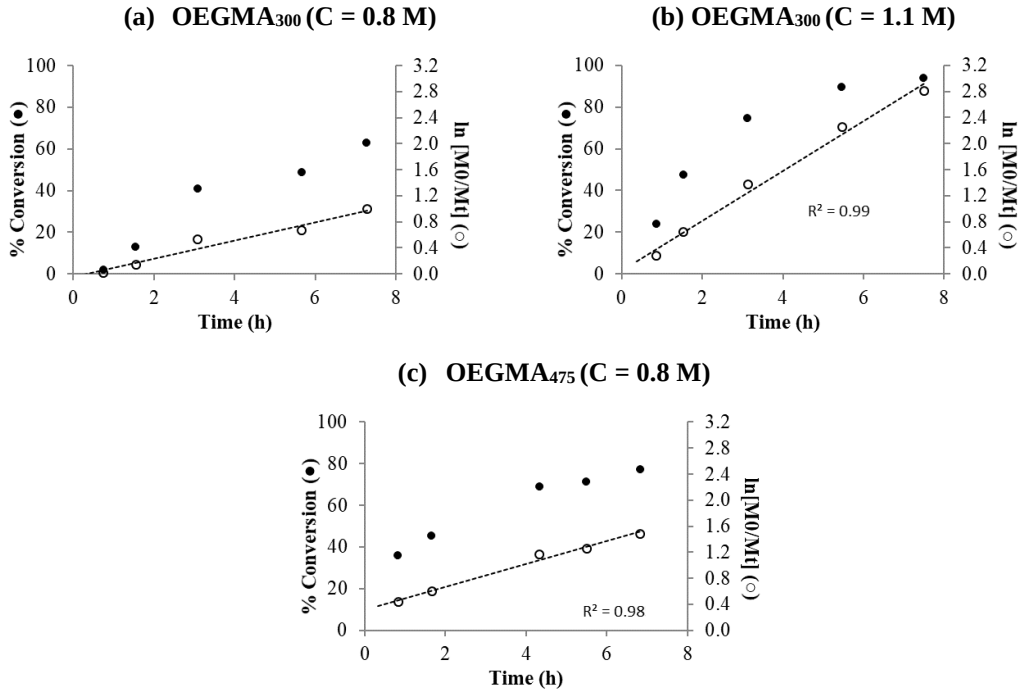

Figure 2.8. Monomers conversion (filled symbols) and first-order kinetics (empty symbols) for $OEGMA_{300}$ (a,b), and $OEGMA_{475}$ homopolymerization (c). The dotted lines in (a), (b) and (c) are the linear fit of the first-order kinetic plot. Adapted from Ref. [95] with permission from The Royal Society of Chemistry.

The kinetics of all OEGMA copolymerizations (ratio M/OEGMA 3:7) are shown in Figure 2.9. $OEGMA_{475}$ homopolymerization (Figure 2.8 (c)) and $OEGMA_{475}$ copolymerization with 30% HIABMA (Figure 2.9 (a)) both show a linear first order kinetics. However, HIABMA/$OEGMA_{475}$ 3:7 copolymerization has a lower initial conversion with respect to 100% $OEGMA_{475}$ (10% *vs* 40% at 1 h) and proceeds up to 58% conversion in 9 h, while $OEGMA_{475}$ homopolymerization show more than 60% conversion already after 4 h. Copolymerization of $OEGMA_{475}$ with HIHMA showed a similar initial conversion (17%) to that with HIABMA (19%), but continued faster reaching 80-85% conversion after 4 h. When $OEGMA_{475}$ was copolymerized with OHMA, conversion after 1h is slightly higher (30%) than with HIABMA or HIHMA,

and, in this case as well, high conversion (70%) were found after only 4h reaction. Moreover, both copolymerization of $OEGMA_{475}$ with OHMA and HIHMA stopped after 4-6 hours of reaction, showing loss of living character towards the end of reaction. HIABMA/$OEGMA_{300}$ 3:7 copolymerization is even faster than HIHMA/$OEGMA_{300}$ 3:7 copolymerization (Figure 2.9 (d) and (e)), while it shows a similar reactivity than $OEGMA_{300}$ homopolymerization (Figure 2.8 (b)). While both HIHMA/$OEGMA_{300}$ 3:7 and $OEGMA_{300}$ homopolymerization have a similar initial conversion (~20%), HIABMA/$OEGMA_{300}$ copolymerization results in more than 40% monomer consumption at the beginning of the reaction. This behavior contrasts with that of copolymerization with $OEGMA_{475}$. It is worth noting that these differences in kinetics behavior suggest an influence of the side chain of the target methacrylates in monomer reactivity. However, the incorporation of monomers remains constant and close to feed ratio of 3:7 over time in all copolymerizations. (Table 2.5 and Table 2.6)

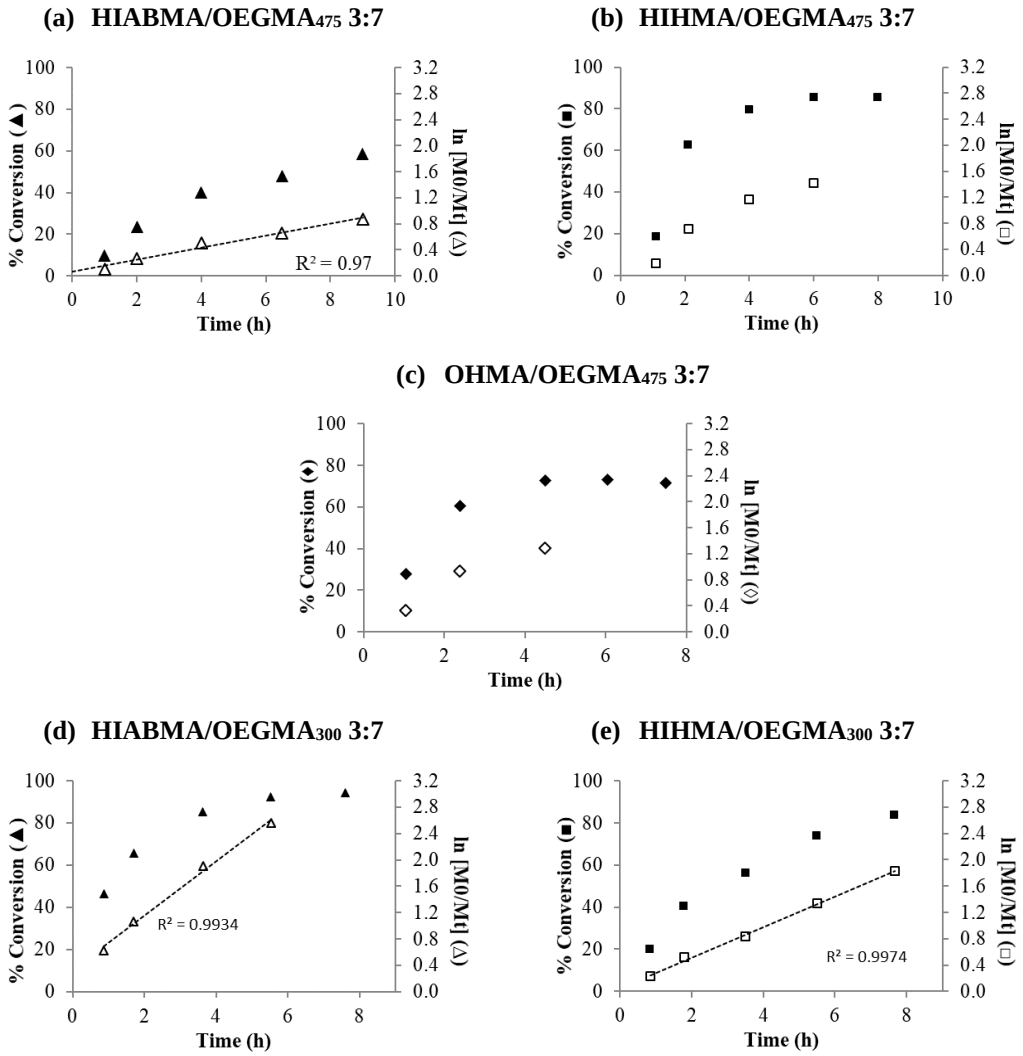

Figure 2.9. Monomers conversion (filled symbols) and first-order kinetics (empty symbols) for $OEGMA_{475}$ copolymerization with HIABMA (a), HIHMA (b) or HIHMA (c) and $OEGMA_{300}$ copolymerization with HIABMA (d) and HIHMA (e) at 70% (mol/mol) OEGMA in the reaction feed. The dotted lines are the linear fit of the first-order kinetic plot. Adapted from Ref. [95] with permission from The Royal Society of Chemistry.

Table 2.5. Monomer conversions and incorporation of the monomers as a function of conversion of copolymerization of OHMA, HIHMA, or HIABMA with $OEGMA_{475}$ (3:7 nominal monomer molar ratio). Reproduced from Ref.[95] with permission from The Royal Society of Chemistry.

	OHMA/$OEGMA_{475}$ 3:7 (mol/mol)		**HIHMA/$OEGMA_{475}$ 3:7 (mol/mol)**		**HIABMA/$OEGMA_{475}$ 3:7 (mol/mol)**	
t (h)	**Conv.[a] %**	**Ratio of repeat units[b]**	**Conv.[a] %**	**Ratio of repeat units[b]**	**Conv.[a] %**	**Ratio of repeat units[b]**
1	28	2.6:7	19	3.5:7	17	3.2:7
2	61	2.3:7	63	2.9:7	26	3.2:7
4	73	2.7:7	80	3.0:7	47	2.9:7
6	73	2.6:7	85	2.6:7	54	3.0:7
8	72	2.7:7	86	3.0:7	58	3.0:7
	(73)[d]	(3.1:7)[c]	(86)[d]	(3.4:7)[c]	(57)[d]	(3.1:7)[c]

[a] Determined by GPC analysis.
[b] Determined by ^{1}H-NMR analysis of the polymerization mixtures (Experimental section 6.3.4)
[c] Determined by ^{1}H-NMR analysis of isolated polymers.
[d] Determined by ^{1}H-NMR analysis of the polymerization mixtures.

Table 2.6. Monomer conversions and incorporation of the monomers as a function of conversion of copolymerization of OHMA, HIHMA, or HIABMA with $OEGMA_{300}$ (3:7 nominal monomer molar ratio).

	HIHMA/$OEGMA_{300}$ 3:7 (mol/mol)		**HABMA/$OEGMA_{300}$ 3:7 (mol/mol)**	
t (h)	**Conv.[(a)] %**	**Ratio of repeat units[(b)]**	**Conv.[(a)] %**	**Ratio of repeat units[(b)]**
1	20	2.9:7	46	2.9:7
2	40	3.1:7	65	2.9:7
4	56	3.2:7	85	3.0:7
6	74	3.0:7	92	3.0:7
8	84	2.9:7	94	3.0:7
		(2.9:7)[(c)]		(2.9:7)[(c)]

[(a)] Determined by ^{1}H-NMR analysis of the polymerization mixtures.
[(b)] Determined by ^{1}H-NMR analysis of the polymerization mixtures (Experimental section 6.3.4).
[(c)] Determined by ^{1}H-NMR analysis of isolated polymers.

In RAFT polymerization, the degree of polymerization (DP) can be estimated from equation 2.3:[111]

$$\mathrm{DP(t)} = \frac{[M]_0 - [M]_t}{[CTA]_0 + df([I]_0 - [I]_t)} \qquad \text{Equation 2.3}$$

where $[M]_{0,t}$ is monomer concentration, d is the fraction of chains derived from termination events, f is the initiator efficiency, and $[I]_{0,t}$ is the initiator concentration. In an ideal RAFT polymerization, the reaction conditions are chosen in order to neglect the contribution of the fraction of initiator-derived chains (that usually is greater or equal to number of chains derived by radical-radical termination events). The equation 2.3 can be therefore simplified as follows:[111]

$$\mathrm{DP(t)} = \frac{[M]_0 - [M]_t}{[CTA]_0} \qquad \text{Equation 2.4}$$

As in other living polymerization, equation 2.4 shows a linear dependence of degree of polymerization with monomer consumption, assuming the complete usage of CTA already at the early reaction steps.

DP *vs*. conversion dependence is linear and Đs are low throughout the polymerization process (Figure 2.10) showing that chain growth proceeds almost exclusively through monomer incorporation. Dotted lines represent ideal correlation between DP and conversion, although the underestimation of brush type polymers by GPC was roughly taken into account with a correction factor of two:[110]

$$\mathrm{DP(t)} = \frac{[M]_0 - [M]_t}{2[CTA]_0} \qquad \text{Equation 2.5}$$

Homopolymerization of $OEGMA_{475}$ showed a good fit between equation 2.5 and experimental DP data (Figure 2.10 (a)). On the contrary, $OEGMA_{300}$ homopolymerization (Figure 2.10 (b)) exhibits a positive deviation of DP values at low conversions that levels off towards the expected values at high conversation. It is worth noting how the difference in the rate of reaction was not reflected on DP *versus* conversion plot that shows similar trend at both monomer concentrations (0.8 and 1.1 M).

The same positive intercept at the beginning of reaction was found for all 3:7 copolymerization reactions. This may be ascribed to the so-called *hybrid behavior*, in which an incomplete usage of CTA occurs at the beginning of reaction. This behavior has been also observed by Pietsch *et al.* for RAFT homo- and copolymerization of DEGMA and $OEGMA_{1100}$ in ethanol,[110] and it is accompanied by higher Đ at the beginning of reaction. In our case, we did not detect any decrease of Đ with monomer consumption in any polymerization reactions. As the reaction proceeded beyond the hybrid phase, DP of all $OEGMA_{475}$ copolymers grows linearly with conversion towards the expected values, while $OEGMA_{300}$ DPs grow parallel to ideal values with monomer consumption. In conclusion, for $OEGMA_{475}$ copolymers HIA group does not exhibit any peculiarities in terms of chain growth *vs*. monomer incorporation with respect to OHMA and HIHMA. On the contrary, HIABMA/$OEGMA_{300}$ 3:7 show higher DPs than HIHMA/$OEGMA_{300}$ 3:7 over monomer consumption.

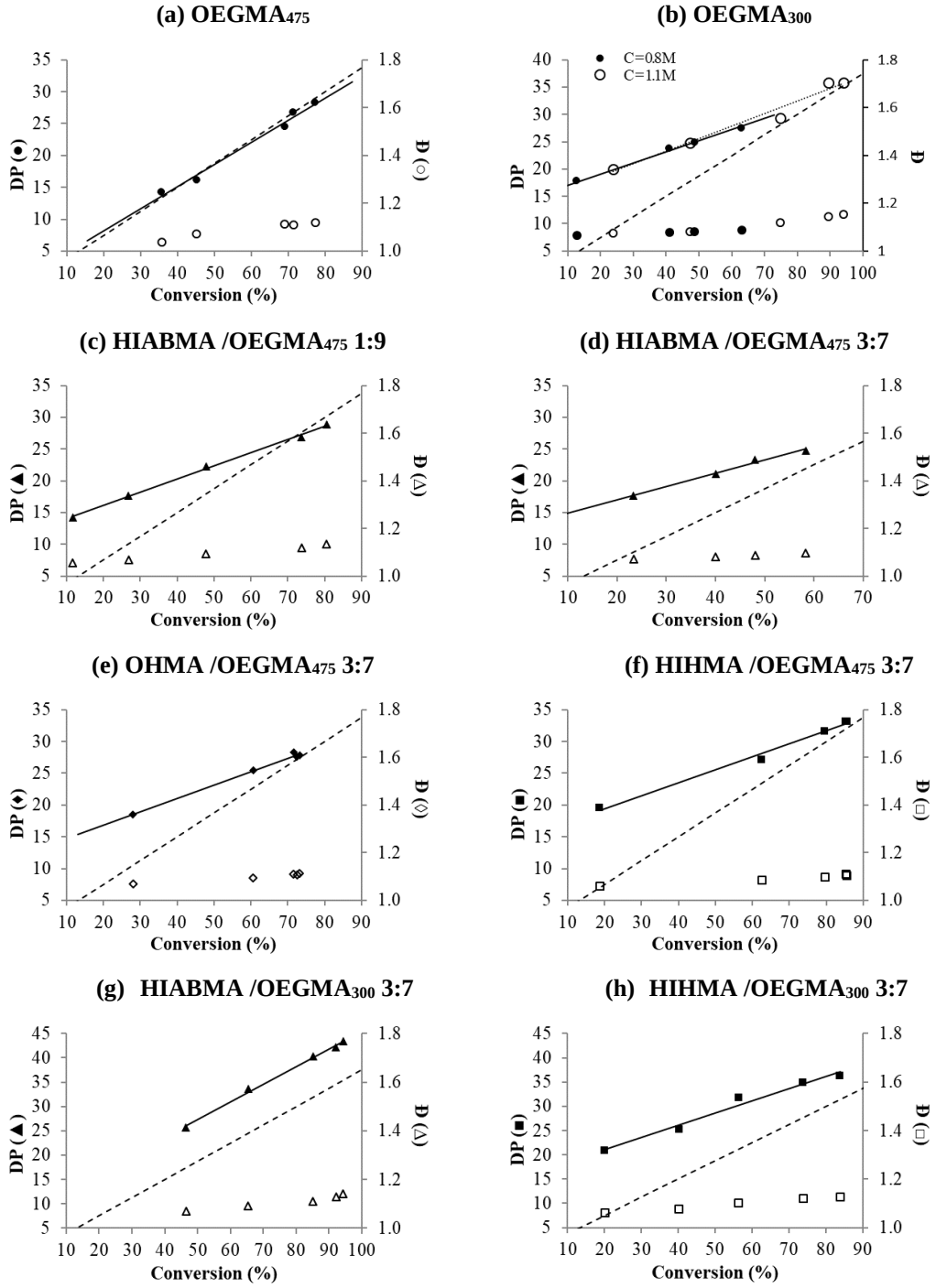

Figure 2.10. DP(GPC) and Đ plots against overall monomers conversion for $OEGMA_{475}$ and $OEGMA_{300}$ homopolymerization (a,b) and for HIABMA/$OEGMA_{475}$ 1:9 (c), HIABMA/$OEGMA_{475}$ 3:7 (d), OHMA/$OEGMA_{475}$ 3:7 (e), HIHMA/$OEGMA_{475}$ 3:7 (f), HIABMA/$OEGMA_{300}$ 3:7 (g), HIHMA/$OEGMA_{300}$ 3:7 (h) copolymerizations. The dotted line is a plot of equation 2.5. Adapted from Ref. [95] with permission from The Royal Society of Chemistry.

NMR spectra of purified copolymers of $OEGMA_{475}$ in Figure 2.11 show that HIA group in HIABMA as well as aldehyde and oxime moiety in OHMA and HIHMA, respectively, are incorporated intact in the structure of copolymers, as demonstrated by the presence of all diagnostic signals. Specifically, in the case of HIABMA/

$OEGMA_{475}$ copolymers the area of C=NO*H* proton is equal to that of C*H*O, thus proving the integrity of HIA group in the copolymers. FTIR spectroscopy also confirms the presence of functional groups in all polymers (Chapter 6, Experimental section). Another important indication of the integrity of aldehyde, aldoxime and HIA group during polymerization is provided by the analysis of reaction mixtures at the initial (t_0) and final (t_f) timepoints of the polymerization reactions by ^{1}H-NMR (Table 2.7). In fact, the ratio between total diagnostic signals and the terminal OCH_3 of OEGMA, used as internal standard, remained constant and close to the theoretical values, within NMR uncertainty (5%).

Table 2.7. ^{1}H-NMR ($CDCl_3$) of C*H*O (OHMA and HIABMA) or *HC*(=NOH) (HIHMA) signals of the polymerization mixtures at initial (T_0) and final (T_f) time-point. Reproduced from Ref. [95] with permission from The Royal Society of Chemistry.

Monomers ratio (mol/mol)	**Intensity[(a)] (δ/ppm)**		
	Theor.	**T_0**	**T_f**
OHMA/$OEGMA_{475}$ 3:7	0.43	0.36 (9.76)	0.38 (9.78)
HIHMA/$OEGMA_{475}$ 3:7	0.43	0.39[(b)] (7.41; 6.79)	0.40[(b)] (7.41; 6.78)
HIABMA/$OEGMA_{475}$ 3:7	0.43	0.35 (9.44)	0.36 (9.45-9.44)
HIHMA/$OEGMA_{300}$ 3:7	0.43	0.41[(b)] (7.41; 6.79)	0.40[(b)] (7.41; 6.78)
HIABMA/$OEGMA_{300}$ 3:7	0.43	0.43 (9.44)	0.41 (9.44)

[(a)] Intensity of the total C*H*O or *H*C(=NOH) signals of both monomer and polymer, relative to the terminal -OCH_3 group of $OEGMA_{475}$.
[(b)] Two separate signals for the *E* and *Z* isomers.

P(OHMA-*co*-OEGMA$_{475}$) 3:7

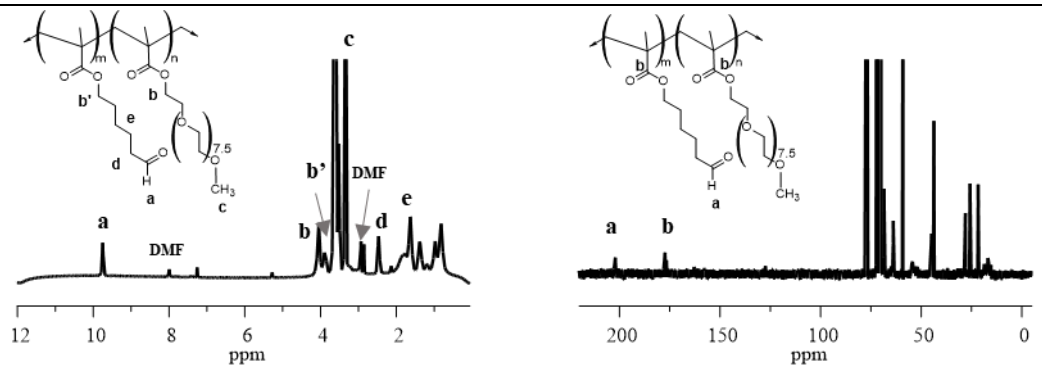

^{1}H-NMR ($CDCl_3$) δ (ppm): 9.79 (s, **a**); 4.07 (br, **b**); 3.92 (br, **b'**); 3.38 (s, **c**); 2.50 (br, **d**); 1.84 (br, **e**).

^{13}C-NMR ($CDCl_3$) δ (ppm): 202.24 (**a**), 177.45-176.93 (**b**), 71.87, 70.07, 68.78, 64.99, 64.30, 59.16, 45.06, 43.37, 25.84, 17.45, 16.92, 14.64.

P(HIHMA-*co*-OEGMA$_{475}$) 3:7

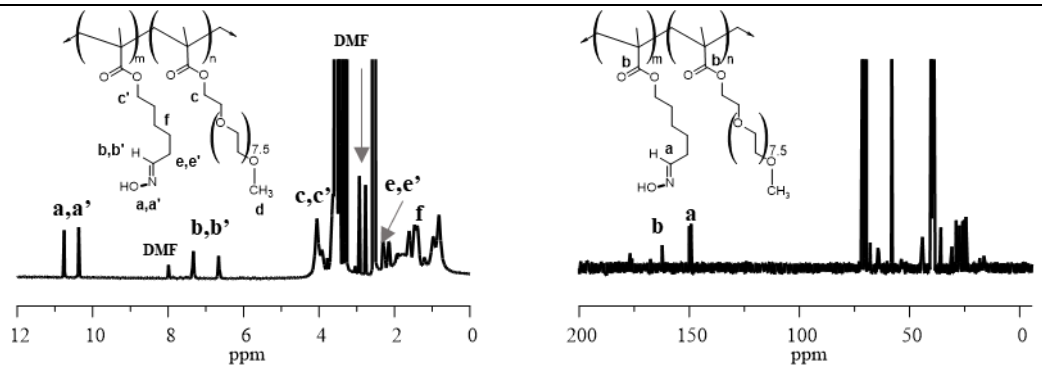

^{1}H-NMR (DMSO-d_6) δ (ppm): 10.72, 10.33 (s, 1H, **a** and **a'**); 7.29, 6.62 (s, 1H, **b** and **b'**); 4.02 (br, **c**); 3.88 (br, **c'**); 3.24 (s, **d**) 2.25, 2.12 (br, 2H, **e** and **e'**); 1.57 (br, **f**)

^{13}C-NMR ($CDCl_3$) δ (ppm): 176.83 (**b'**), 162.34 (**b**), 149.98-149.22 (**a**, *E*, *Z*), 71.31, 69.82, 69.62, 67.86, 64.40, 58.07, 58.05, 40.35, 40.07, 39.80, 39.52, 39.24, 38.96, 38.68, 28.87, 25.91, 25.26, 24.44.

P(HIABMA-*co*-OEGMA$_{475}$)

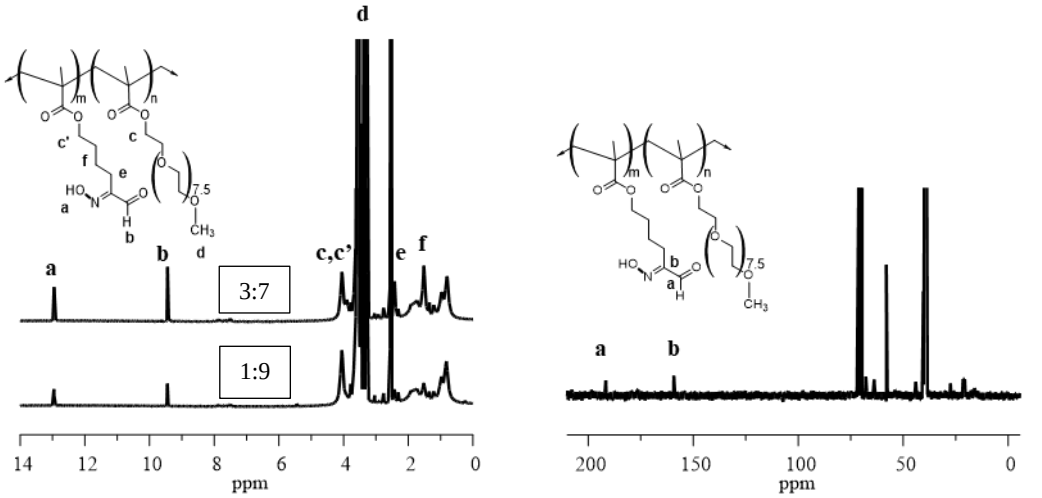

^{1}H-NMR (DMSO-d_6) d (ppm): 12.92 (s, **a**, *E* isomer); 9.40 (s, **b**, *E* isomer); 4.01 (br, **c**), 3.85 (br, **c'**); 3.24 (s, **d**); 2.38 (br, **e**); 1.48 (br, **f**).

^{13}C-NMR (DMSO-d_6) HIABMA/OEGMA$_{475}$ 3:7 δ (ppm): 191.82 (**a**), 159.68 (**b**), 71.64, 70.38, 67.69, 63.71, 57.95, 44.39, 27.61, 21.48, 20.96.

Figure 2.11. Characterization of the synthesized polymers through ^{1}H-, ^{13}C- NMR spectroscopy.

Notwithstanding the high conversion of OEGMA copolymerizations with all synthetized monomers, it was necessary to rule out possible undesired reactions promoted by the functional groups of monomers, especially the novel HIA moiety. In fact, in the previous paragraph NO-H bond BDEs of model HIA suggest that several radical species involved in RAFT polymerization may abstract H• from NO-H group to give iminoxyl radical. The resulting iminoxyl radical may couple with a growing propagating chain to yield a branch point. GPC traces of HIABMA/$OEGMA_{475}$ 3:7 polymerization (Figure 2.6) exhibit narrow monomodal weight distributions throughout the reaction without any detectable shoulders. So, no evidence is found for branch points.[112] However, reversible undesired formation of radical centers cannot be ruled out.

In summary, the feasibility of RAFT polymerization in the presence of free oxime and the highly functionalized HIA groups was demonstrated for OEGMA copolymerizations with up to 30% (mol/mol) of target monomers (respectively HIHMA and HIABMA). All reactions show low Đs throughout reaction time, a linear dependence of DP with monomer consumption and linear first order kinetics (except HIHMA/$OEGMA_{475}$ 3:7). Furthermore, all copolymerizations reached good to excellent monomer conversions. In addition, HIABMA and HIHMA monomers do not exhibit any peculiarities with respect to analogous monomer bearing only the aldehyde group (OHMA).

Reproducibility of HIABMA/OEGMA copolymerizations

$OEGMA_{475}$ copolymerizations with 50% of monomers bearing oxime group (HIHMA and HIABMA) were carried out several times to check for reproducibility. In the best scenario both copolymerizations (Table 2.8) show Đs lower than 1.2 and excellent monomer conversions within 7 hours (Table 2.8, entry 1 and 4). After purification no unexpected ^{1}H-NMR signals were found (HIABMA copolymer: Figure 2.12). When we ran duplicates, HIABMA/$OEGMA_{475}$ 1:1 reactions exhibited different monomer conversions depending on purification and storage conditions (Table 2.8 entry 2 and 3). Specifically, monomer conversion dropped to low values when HIABMA was stored at 4°C for an extended period of time. Most likely, monomer bearing HIA moiety is prone to degradation over time, yielding compounds able to inhibit polymerization. Unfortunately, even when the monomer affording the worst outcome in polymerization (Table 2.8, entry 3) was analysed, those hypothetical compounds

could not be detected by either GC-MS, GC-FID and ^{1}H-NMR. Furthermore, ^{1}H-NMR analysis of purified P(HIABMA-*co*-OEGMA$_{475}$) 1:1 obtained with the ill-performing monomer batch (Table 2.8 entry 3) demonstrated the presence of NO*H* and C*H*O signals of equal intensity (Figure 2.12). However, some additional unexpected signals of low intensity are present in the 5.5-7 ppm range in the ^{1}H-NMR spectrum of P(HIABMA-*co*-OEGMA$_{475}$) 1:1 obtained with the ill-performing monomer.

On the other hand, HIHMA/OEGMA$_{475}$ copolymerizations exhibited good reproducibility (Table 2.8, entry 5 and 6), thus showing that the HIA moiety is more prone than the corresponding simple oxime to yielding very small amounts of degradation products that are detrimental to the polymerization process.

Table 2.8. Characterization data of copolymerization (1/1) of OEGMA$_{475}$ with HIABMA and HIHMA and their reproducibility according to storage and purification of monomers ([M]/[CTA]/[I]$_0$ 75/1/0.25, T = 75°C).

Entry	Monomers (mol/mol)	C_{tot} (M)	Reaction time[(a)] (h)	Monomer conv.[(b)] (%)	M_n (GPC)	Đ	DP (GPC)	DP th[(c)]
1	HIABMA/OEGMA$_{475}$ 1:1[(d)]	1.1	7	94	12800	1.11	35	70
2	HIABMA/OEGMA$_{475}$ 1:1 [(e)]	1.1	7 (5)	54	10200	1.10	28	41
3	HIABMA/OEGMA$_{475}$ 1:1 [(f)]	1.1	6 (2)	15	6300	1.10	25	11
4	HIHMA/OEGMA$_{475}$ 1:1	1.1	6	80	11000	1.09	31	60
5	HIHMA/OEGMA$_{475}$ 1:1	1.1	8 (6)	69	10000	1.10	30	53
6	HIHMA/OEGMA$_{475}$ 1:1	1.1	6.5	76	10500	1.09	30	57

[(a)] Time of polymerization quenching; in parenthesis, time at which no polymerization progress is observed by GPC.

[(b)] Monomer conversions are calculated by ^{1}H-NMR analysis of crude mixture using terminal OCH$_3$ of OEGMA$_{475}$ as internal standard.

[(c)] DP (teo) are calculated according equation $DP=\frac{M_0-M_t}{[CTA]}$

[(d)] HIABMA purified by silica gel chromatography twice and used after a month conservation at -18°C

[(e)] HIABMA purified by silica gel chromatography twice and used after a month conservation at 4°C

[(f)] HIABMA purified by silica gel chromatography once and used after a month conservation at 4°C.

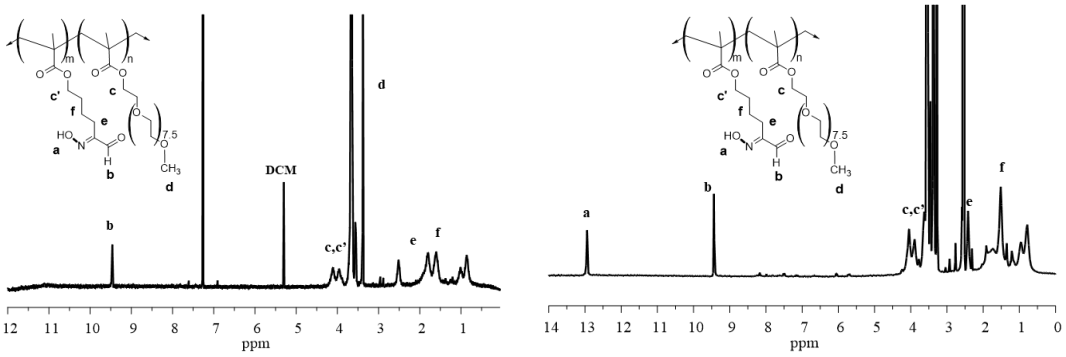

Figure 2.12. Characterization of purified P(HIABMA-*co*-OEGMA$_{475}$) 1:1 with 94% monomer conversion (left) and 15% monomer conversion (right) through ^{1}H-NMR spectroscopy.

A role of monomer purification procedure on polymerization outcome was also highlighted by running HIABMA/OEGMA$_{300}$ copolymerizations with HIABMA monomer purified by silica gel chromatography twice or only once (Table 2.9 and Figure 2.13 and 2.14). When HIABMA was purified only once by silica gel chromatography, HIABMA/OEGMA$_{300}$ 3:7 copolymerization was retarded showing both an induction period up to 1 h and a significantly smaller apparent kinetic constant (Figure 2.13 (b)) compared to monomer purified twice by silica gel chromatography. The scenario got worse when HIABMA was increased to 50% (Figure 2.13 (c)). The reaction stopped at 27% conversion, with an even more pronounced induction period at the beginning of reaction. It is worth noting that this marked effect of monomer purification procedure on polymerization outcomes does not correspond to detectable changes in GC-FID, GC-MS and ^{1}H-NMR analysis. Notwithstanding the differences in the rate of reaction, all copolymerizations exhibit Đ<1.2 and a linear relationship between DP and monomer consumption. Therefore, also where impurities are present during polymerization, chain growth with monomers containing the novel 2-(hydroxyimino)aldehyde group proceeds almost exclusively through monomer incorporation, rather than through chain coupling, and chain termination through disproportionation is kept to a minimum (Figure 2.14).

Table 2.9. Effect of HIABMA purification on outcomes of HIABMA/OEGMA$_{300}$ copolymerizations.

Entry	Monomers (mol/mol)	Tot Monomer concentration (M)	Reaction time[(a)]	Monomer conversion[(b)]	M_n (GPC)	Đ	DP (GPC)
1	HIABMA/OEGMA$_{300}$ 3:7 [(b)]	1.1	7.5 (6)	94	11100	1.14	43
2	HIABMA/OEGMA$_{300}$ 3:7[(c)]	1.1	8 (5)	46	7500	1.09	27
3	HIABMA/OEGMA$_{300}$ 1:1[(c)]	1.1	7 (2)	27	6600	1.07	24

(a) Time of polymerization quenching; in parenthesis, time at which no polymerization progress is observed by GPC.

(b) HIABMA purified by silica gel chromatography twice and used after a month conservation at -18°C. This reaction was reported from Table 2.4 entry 9.

(c) HIABMA purified by silica gel chromatography once and used after a month conservation at -18°C.

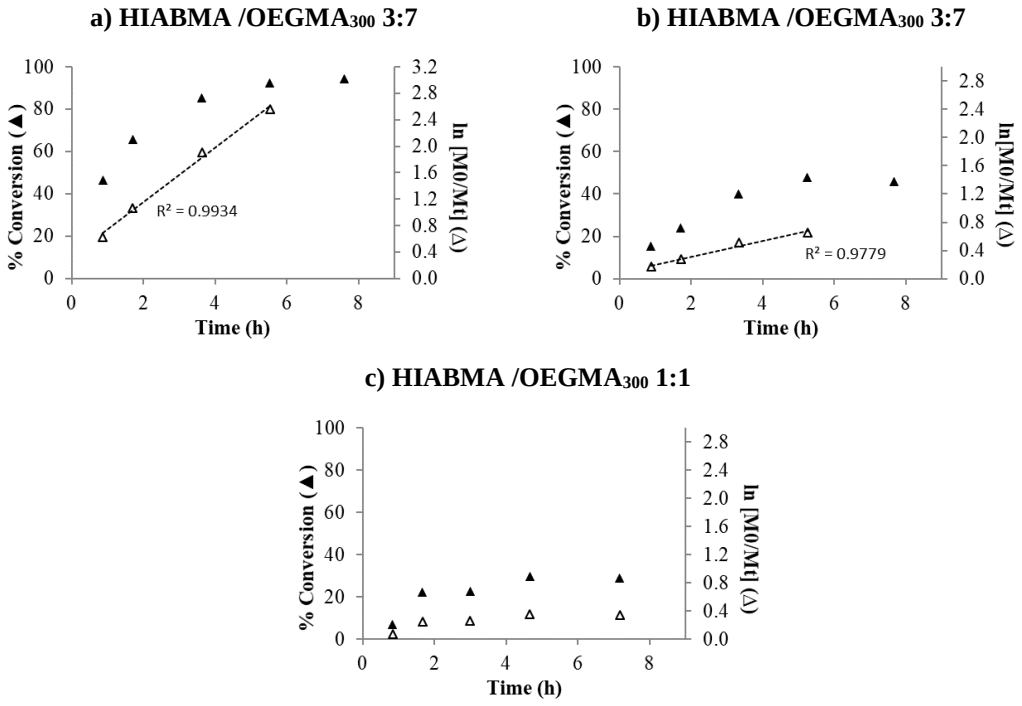

Figure 2.13. Monomers conversion (filled symbols) and first-order kinetics (empty symbols) for HIABMA/OEGMA$_{300}$ 3:7 copolymerization (a,b) and HIABMA/OEGMA$_{300}$ 1:1 copolymerization (c). The dotted lines are the linear fit of the first-order kinetic plot. HIABMA was purified by silica gel chromatography twice (a) or once (b and c).

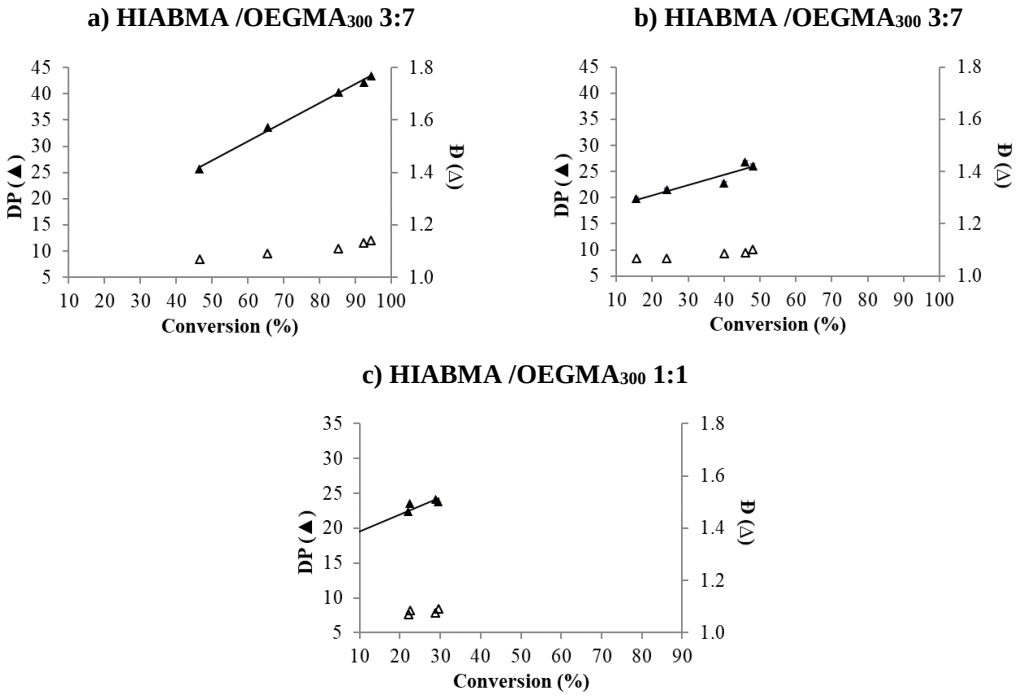

Figure 2.14. DP(GPC) (filled symbols) and Đ plots (empty symbols) against overall monomers conversion for HIABMA/OEGMA$_{300}$ 3:7 copolymerization (a,b) and HIABMA/OEGMA$_{300}$ 3:7 copolymerization (c) HIABMA was purified by silica gel chromatography twice (a) or once (b and c).

Generally, retardation/inhibition in RAFT polymerizations may be due to several causes. First, the slow fragmentation of RAFT agent in the pre-equilibrium (Chapter 1, Scheme 1.8) leads to inefficient re-initiation process with consequent variable inhibition time. Reversible and irreversible terminations of intermediate RAFT radical also decrease the rate of reaction with loss of molecular weight control. In fact, propagating polymer chain can add irreversible to intermediate radical to form a 3-arm star chain, while reversible self termination of two intermediate RAFT radicals leads to 4-arm star chain.[111] Besides these intrinsic problems of specific CTA/monomer system, other side reactions may occur during RAFT polymerizations. RAFT agents are dithioester compounds that are able to react with different functional groups such as primary and secondary amines, thiols and reducing agents.[113] Furthermore, they are susceptible to hydrolysis as other esters[113] and can decompose under the effect of temperature.[114] Some of the resulting products of these undesired reactions such as thiols and thiobenzoic acid are known to act as radical scavenger and/or retarders.

The retardation/inhibition observed in RAFT polymerizations of monomer bearing HIA group cannot be ascribed to the slow fragmentation model or to cross-termination of intermediate RAFT radical with propagating chain, but rather to some undesired side reaction promoted by impurities present in HIABMA. Plummer *et al.*

found a correlation on purification procedure and shelf life of cumyl dithiobenzoate with rate of polymerization,[115] while Favier *et al.* demonstrated that by-products derived from synthesis of Madix RAFT agent can act as inhibitors.[116] In our case, impurities derived directly from synthesis or storage of HIABMA have not been identified yet due to their low concentration. Their presence in polymerization reaction may cause degradation of CTA end groups or termination reaction of both propagating chain or intermediate RAFT radical. Further investigations are required to identify impurities and establish the shelf life of HIABMA stored at -18 °C. Moreover, an improved optimization of HIABMA purification is also necessary. An HPLC analysis protocol should also be developed as an alternative to GC for monomer quality control.

2.3.2 Preliminary investigation on block copolymers of HIABMA and $OEGMA_{500}$

Statistical RAFT copolymerization has been an useful tool for preparation of materials with novel properties thanks to its applicability to a wide range of monomers.[58] However, the opportunity to afford complex architectures has allowed the formation of macromolecules with tunable solution behavior and with self-assembling abilities to form high-order structures.[117] As shown in the previous paragraphs, HIABMA can be used to prepare random copolymers through a RAFT protocol. However, this study would not be satisfactorily complete without checking the possibility for building HIABMA blocks. Block copolymers of HIABMA and $OEGMA_{500}$ were prepared directly through the well-known chain extension method, in which the first block obtained via classical RAFT method is used as a macro chain transfer agent in the subsequent polymerization. This is possible only if the dithiobenzoate groups are preserved at chain-ends of polymers after the first reaction.

A $OEGMA_{500}$ based macroCTA having M_n of 11.00 KDa was synthetized using CPDB as chain transfer agent and AIBN as initiator. After isolation of the macroCTA from the polymerization mixture, chain extension with further $OEGMA_{500}$ was carried out to verify that the chain ends were preserved. $POEGMA_{500}$-*b*-PHIABMA was then prepared in the same way, only feeding HIABMA for chain extension. Both block copolymerizations were carried out in DMF at 72 °C using [M]/[macroCTA]/[I] ratio of 100/1/0.5. The outcomes of preparation of macroCTA (entry 1) and their subsequent chain extensions are reported in Table 2.10. The homopolymerization to form macroCTA was deliberately stopped at 50% monomer conversion in order to preserve

chain end functionality and minimize termination reactions. HIABMA block copolymerization reaches 60% monomer conversion after 4 hours with Đ of 1.14 exhibiting a monomodal distribution on GPC analysis throughout the reaction time (Figure 2.15). Here, the absence of additional shoulders indicates that chain extension was complete and that dead chains resulting from unavoidable termination processes in the synthesis of macroCTA were below detection.

Table 2.10. Characterization data of block copolymerization of $OEGMA_{500}$ with HIABMA. Reaction condition: T=75°C, $[M]/[CTA]/[I]_0$=75/1/0.25, C=0.5 M (Entry 1 and 3); T=75°C, $[M]/[macroCTA]/[I]_0$=100/1/0. 5, C=0.6 M (Entry 2 and 4).

Entry	Monomers (mol/mol)	Tot Monomer concentration (M)	Reaction time[(a)] (h)	Monomer conv.[(b)]	M_n (GPC)	Đ	DP (GPC)
1	$POEGMA_{500}$	0.5	3	55	10800	1.08	22
2	$POEGMA_{500}$-*b*-PHIABMA	0.6	6 (4.3)	61	18000	1.14	49
3	$POEGMA_{500}$-*b*-$POEGMA_{500}$	0.6	5 (3.8)	90	21400	1.27	43

(a) Time of polymerization quenching; in parenthesis, time at which no polymerization progress is observed by GPC.

(b) Entry 1 and 3: Monomer conversion calculated by GPC analysis. Entry 2: Monomer conversion calculated by ^{1}H-NMR analysis.

HIABMA block copolymerization showed a lower initial monomer conversion with respect to chain extension with $OEGMA_{500}$ (40% *vs.* 59% after 1 hour) (Figure 2.16 (a) and (b)). Then, reaction with HIABMA proceeds until 61% monomer consumption after 4 hours, while $OEGMA_{500}$ has almost quantitative conversion in the same time frame. Moreover, M_n *vs.* conversion dependence is linear for both chain extension with $OEGMA_{500}$ and HIABMA (Figure 2.16 (c) and (d)).

The ^{1}H-NMR spectrum in Figure 2.15 of the purified polymer shows that HIA functional group is incorporated in the final block copolymer and that the HIABMA/OEGMA ratio is 1:1.

In conclusion, it was possible to obtain a block copolymer starting from a $POEGMA_{500}$ as macro RAFT agent and freshly-synthesized, double-purified HIABMA. The resulting $POEGMA_{500}$-*b*-PHIABMA exhibits low Đ and a HIABMA/$OEGMA_{500}$ ratio of 1:1. The below-quantitative conversion of HIABMA in the chain extension step should be taken into account in planning the synthesis of block copolymers of defined composition.

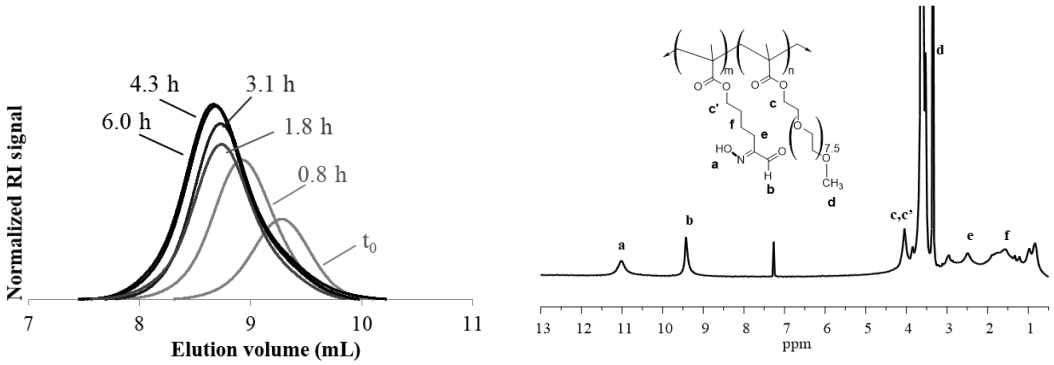

Figure 2.15. Time evolution of the GPC traces of the RAFT block copolymerization crudes of POEGMA$_{500}$-*b*-PHIABMA (RI signals are normalized at the same concentration) (left) and ^{1}H-NMR spectrum of purified copolymer (right).

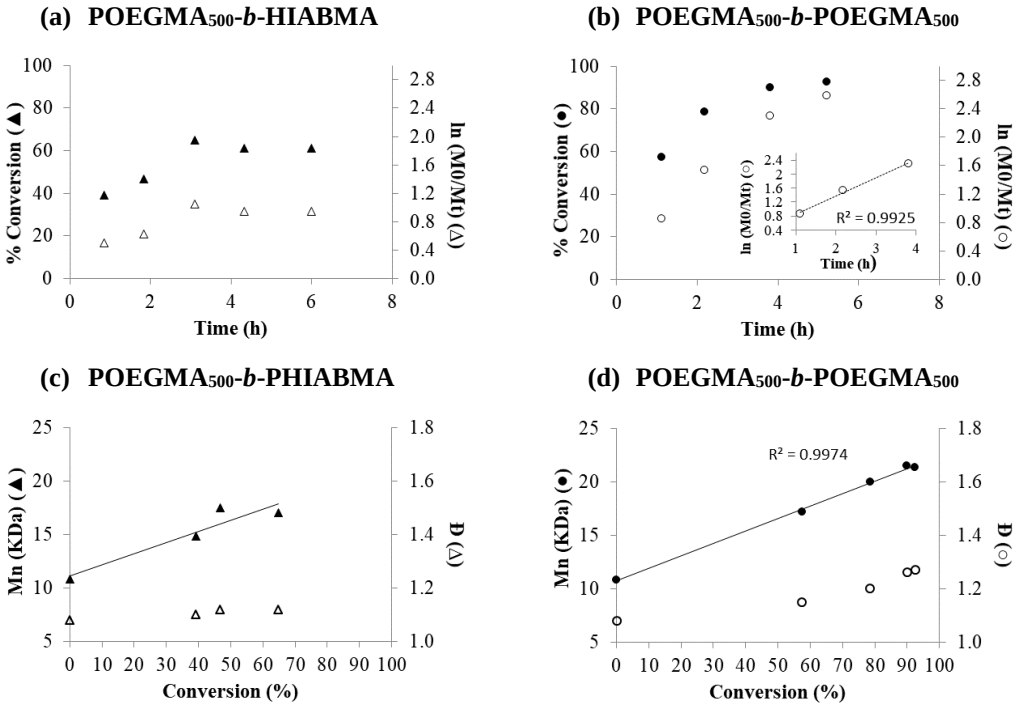

Figure 2.16. Above: monomers conversion (filled symbols) and first-order kinetics (empty symbols) for POEGMA$_{500}$-*b*-PHIABMA (a) and for its reference POEGMA$_{500}$-*b*-POEGMA$_{500}$ (b). The dotted lines in (b) are the linear fit of the first-order kinetic plot. Below: M_n (GPC) (filled symbols) and Đ plots (empty symbols) against overall monomers conversion for POEGMA$_{500}$-*b*-PHIABMA (c) and for its reference POEGMA$_{500}$-*b*-POEGMA$_{500}$ (d).

Chapter 3: Photochemical behavior of HIAs

3.1 INTRODUCTION

Similarly to oximes, all non-conjugated HIAs show an allowed band at 230-240 nm (ε *ca*. 10000 $M^{-1}cm^{-1}$) ascribable to the π→π* transition, that, in presence of an aromatic ring as substituent on the C(=NOH)CHO group, is shifted to *ca.* 270 nm. When the samples are concentrated up to 1.2 mM;[88] a weak band appears (ε <100 $M^{-1}cm^{-1}$) at 320-334 and, similarly to α-oxo-oximes,[104] it is ascribable to the forbidden *n*→π* transition.[118]

Oximes exhibit a complex photochemistry[104] involving isomerizations, rearrangements, dehydration to nitriles or loss of the hydroxylamine function to form the parent carbonyl. Moreover, due to the presence of the C=N double bond, different configurational and geometrical isomers can be envisaged for HIAs (Figure 3.1).

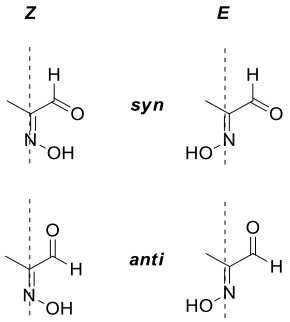

Figure 3.1. Configurational (*E/Z*) and conformational (*syn/anti*) isomers of 2-(hydroximino)aldehydes.

Since it was first observed in 1890, *E/Z* photo- and thermal isomerism has been the object of constant investigation, from the first NMR studies in the late 1950s to recent computational studies on isomers interconversion.[119] Concerning the mechanism for *E/Z* isomerization, the transition state may be either linear, with the nitrogen atom turning its hybridization from sp^2 to sp, or a state where the imine double bond character is weakened, thus lowering the barrier for rotation about the C=N(OH) bond. Blanco *et al.*[120] attribute the former to ground state interconversion and the latter to photoinduced isomerization. From literature inspection,[104] it is quite clear that the propensity for photoisomerization, the relative stability of the configurational isomers and the complexity of the resulting mixtures are peculiar to the specific substituent

adjacent to the oxime group. α-Oxo-oxime ethers were extensively investigated by Cerfontain and co-workers,[121] who showed that, in addition to *E/Z* interconversion, photolysis and/or a Norrish-Yang reaction can take place upon photoexcitation (Scheme 3.1). The photoreactivity of α-oxo-oxime esters has been known for over a century and is still being investigated for the photoinitiation of acrylic monomers polymerizations.[71]

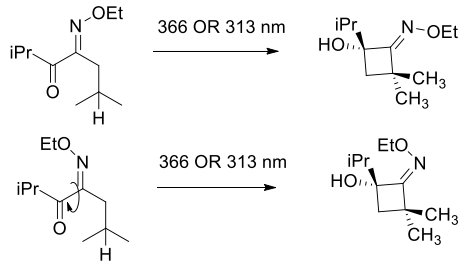

Scheme 3.1. Norrish-Yang cyclization of α-oxo-oxime ethers.[122]

In the present Chapter, we carried out an NMR-based investigation on photo- and thermal isomerism of several HIAs differing by the bulk of the aliphatic R group or by the type of substituent (phenyl or polymerizable group). Specifically, the work was organized in two phases.

The first part of the work, carried out at Sapienza University of Rome, was dedicated to the investigation of photoisomerization and thermal relaxation of target HIAs (Figure 3.2) by using a high pressure mercury lamp with an emission maximum at 350 nm. The emission spectrum of this lamp spans from 300 nm to 400 nm.

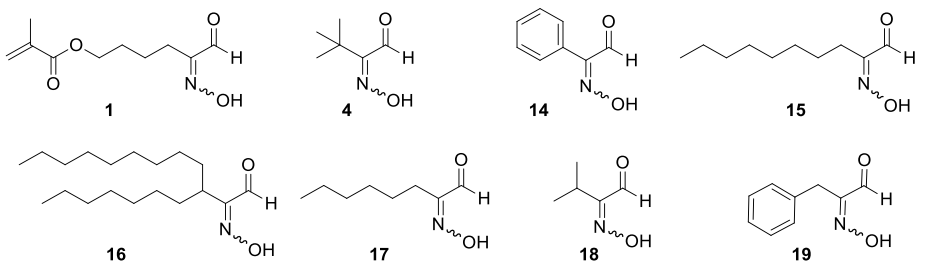

Figure 3.2. Selected HIAs for photochemical investigation.

The second part of the investigation was carried out in the laboratory of Prof. Gschwind at Institute of Organic Chemistry in Regensburg University (Germany). Irradiation was performed in different solvents by using two LED-based

monochromatic sources at 278 nm and 365 nm, with the aim to study the influence of wavelength and solvent polarity on observed photochemical behavior.

Finally, the last part of this chapter is dedicated to photoisomerization of HIA moieties of OEGMA copolymers previously prepared (see Chapter 2).

3.2 HIA-BEARING MOLECULES

3.2.1 Photoisomerization using mercury lamps

HIAs shown in Figure 3.3 were used for the first part of the investigation carried out at Sapienza University of Rome. HIA **4**, **15** and **16** were already available in the laboratory, whereas **14** was prepared directly from phenyl acetaldehyde through α-oximation reaction.[88] Compound **1** is the HIA-containing monomer used in the synthesis of copolymers with OEGMA (Chapter 2). Moreover, computational calculations were performed in Prof. M. D'Abramo group to support ^{1}H-NMR data (Appendix A).

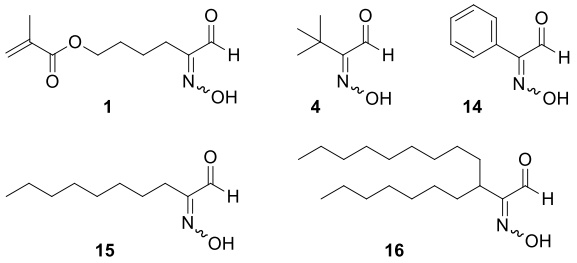

Figure 3.3. HIAs employed in the investigation of photochemical behavior using a high pressure mercury lamp with maximum a 350 nm.

To follow the N-OH and CHO signals of the irradiated samples by ^{1}H-NMR analysis, we chose DMSO-d_6 (UV cut-off: 265 nm) for our experiments. We observed different behavior for relatively short time (for up to 2h) of excitation compared to prolonged illumination (up to 22 hours). In fact, in order to observe mainly *E/Z* isomerization the samples were irradiated for 2 hours. The samples were then allowed to thermally equilibrate at 40°C in the dark and were monitored by NMR over time. In contrast, an extended photoexcitation (22 h) was necessary to promote the significant, if not quantitative, formation of a single new product. Based on the experimental evidence presented hereafter and on the behavior of α-oxo-oximes documented by Buys *et al*[123] we identified this product as a cyclobutanol oxime (CBO) derivative (Scheme 3.2) from the Norrish-Yang cyclization.[118]

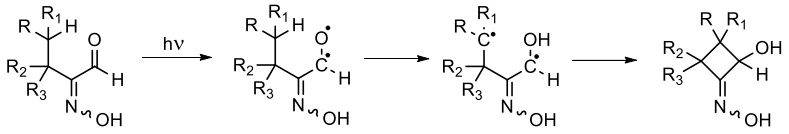

15: R=H, R_1=$CH_3(CH_2)_5$-, R_2=R_3=H
16: R=H, R_1=$CH_3(CH_2)_8$-, R_2=$CH_3(CH_2)_7$-, R_3=H
R=H, R_1=$CH_3(CH_2)_6$-, R_2=$CH_3(CH_2)_9$-, R_3=H
4: R=R_1=H, R_2=R_3=(CH_3)-

Scheme 3.2. Norrish-Yang cyclization of some HIAs.[88]

E/Z photo- and thermal isomerism

^{1}H-NMR signals of C=NO*H* and C*H*O are diagnostic for *E/Z* isomerism of HIAs. In Figure 3.4, the expansions of spectra encompassing all aldehyde and oxime signals are shown with their intensities. ^{1}H-NMR spectra of as-synthesized **1** and **15**, i.e. of the two compounds that bear a primary carbon next to the oxime group, only exhibit, respectively, one C*H*O peak (1H) at 9.39 and 9.40 ppm and one NO*H* peak (1H) at 12.89 and 12.92 ppm. After 2h light exposure of **1** or **15** in the photoreactor, two small additional peaks appear: 10.28 ppm (C*H*O) and about 12.00 ppm (NO*H*). The chemical shifts of the *aldehyde hydrogens* computed by DFT methods for the different isomers (Figure 3.4) of selected HIAs are reported in Table 3.1. The effect of DMSO was modeled using a continuum approach, i.e. by means of the Polarizable Continuum Model (PCM).[124] The computed chemical shift values for the *(Z)-syn* isomers are at most 0.4 ppm upfield of (*E*) isomers. Hence, it is not possible to assign any CHO aldehyde signals falling in the 9.1-9.7 ppm region of the spectrum to either configuration based on chemical shift calculations alone. However, the downfield NOH signal of unhindered α-oxo-oximes was assigned by Baas and Cerfontain [125] to the *(E)-anti* isomer, the most stable due to dipolar interactions. On these grounds, we assume that signals around 12.9 ppm of unhindered HIAs **1** and **15** should be assigned to NOH in the *E* form. Hence, the signals around 9.4 ppm are attributed to the CHO of the *E* isomers. The calculated CHO chemical shifts for the *(E)-syn/anti* isomers (Table 3.1) are in good agreement with the experimental signals (Figure 3.4). However, since rapid interconversion (on the NMR timescale) of *E* conformers cannot be ruled out with such little hindrance to rotation of the CHO group, we are not assigning the (*E*)-**1** and (*E*)-**15** signals to either conformation. The calculated CHO shift for the *(Z)-anti* isomer (10.4 ppm) lies very close to one of the two signals (b': 10.28 ppm) appearing after 2h irradiation. Since the intensity of the (*Z*)-NOH (12.00 ppm) signal matches that of *(Z)-anti* CHO, we surmise that only the *(Z)-anti* isomer is formed upon

photostimulation. The pristine secondary compound **16** is also in the *E* form only (C*H*O peak at 9.34 ppm and NO*H* peak at 12.83 ppm). Upon photoexcitation, two small signals appear at 12.04 and 10.32 ppm, which we assign to the *Z* form in analogy with the primary compounds. The assignment of a further significantly intense signal at 10.15 ppm will be discussed later. As for tertiary **4**, similar arguments as for **1, 15** and **16** hold for the assignment of NMR signals to the *E* and *Z* isomers. However, in contrast with these compounds, the *Z* isomer (NOH and CHO signals of equal intensity at 11.78 and 10.24 ppm, respectively) is predominant over *E* (12.89 and 9.28 ppm of same intensity) prior to irradiation. In fact, (*E*)-**4** may be destabilized by overcrowding of the *t*-Bu group and N-OH group on the same side of the C=N bond. Photostimulation induces a complete switch in the configuration ratio and the appearance of a further signal at 10.14 ppm, which will be discussed later. In the case of compound **14**, the most relevant changes upon irradiation are detected in the aromatic region, whereas evidence for *E/Z* isomerization is too weak for any interpretation. Quantitative results for *E/Z* photoisomerization and subsequent thermal relaxation are summarized in Table 3.2. When HIAs bearing a primary R group (compounds **1** and **15**) are irradiated for two hours, limited inversion of configuration is observed (*E/Z*= 10/1). Thermal relaxation to *E*-isomer is quantitative in **15** within 8 days, while with HIA **1** the *E/Z* ratio is essentially unchanged after about three weeks. The remote methacrylate group, therefore, appears to slow down the thermal isomerization process. Also in the case of secondary **16** the *E* isomer is still predominant after 2h irradiation (*E/Z*~ 5/1) and thermal reversal to the *E* form is not completed after one week (*E/Z*~ 7/1). The most remarkable effect of 2h photostimulation is that observed with compound **4**. In fact, *E/Z* ratio switched from 1/10 to 5/1 and thermal relaxation was still incomplete after 40 days (*E/Z*= 1/2).

Table 3.1. ^{1}H-NMR computed chemical shifts[a] for the CHO of the different configurational and conformational isomers of HIAs. Reproduced with permission from Ref.[88]

RC(NOH)CHO	(*Z*)-*anti* (δ)	(*Z*)-*syn* (δ)	(*E*)-*anti* (δ)	(*E*)-*syn* (δ)
(1) $CH_2=C(CH_3)CO_2(CH_2)_4$-	10.4	9.2	9.2	9.6
(4) $(CH_3)_3C$-	10.4	9.3	9.2	9.7
(15) $CH_3(CH_2)_7$-	10.4	9.1	9.1	9.3

[a]Geometry optimization in vacuum at the B3LYP/6-31+G(d, p) level; Chemical shift calculations with WPO4/aug-cc-pVdZ; effect of the solvent modeled by means of the PCM. δ: ppm.

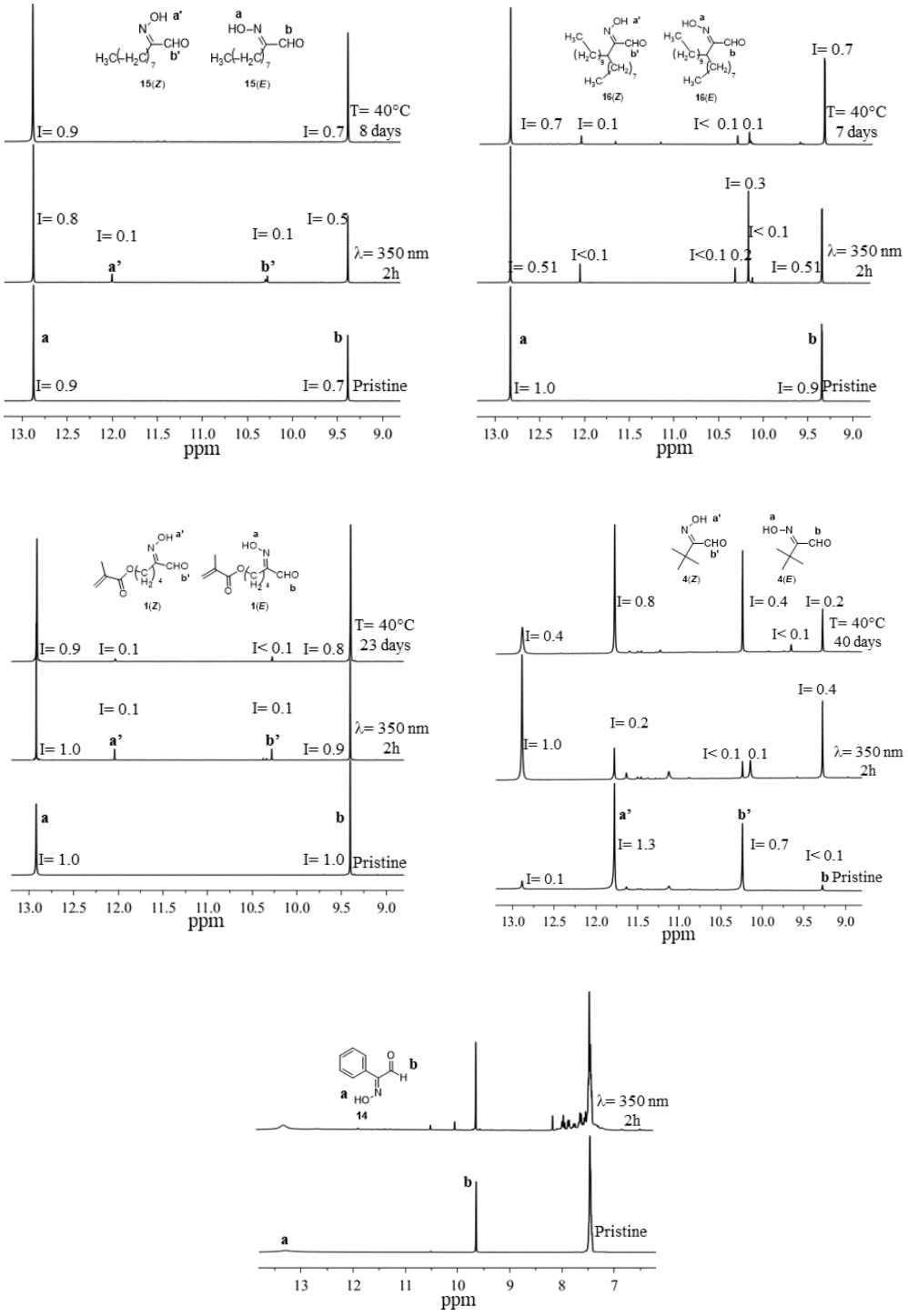

Figure 3.4 Expansion of the ^{1}H-NMR spectra (DMSO-d$_6$, δ: ppm) for the study of *E/Z* isomerism of compounds **1**, **4**, **14**, **15** and **16** after 2h photostimulation (λ= 350 nm) followed by annealing at 40°C. Intensities are normalized to terminal –C*H*$_3$ (**4**, **15**, **16**) or -OC*H*$_2$- (**1**). Broken lines are a pictorial of the calculated chemical shifts (Table 3.1) for different geometrical and conformational isomers of HIAs. Full spectra in the Experimental section. Adapted with permission from Ref.[88]

Table 3.2. *E/Z* photoisomerization[a] and thermal re-equilibration[b] of selected HIAs. Reproduced with permission from Ref.[88]

RC(NOH)CHO	Time	*E/Z*
(1) $CH_2=C(CH_3)CO_2(CH_2)_4$-	t=0	*E* only
	2h, 350 nm[a]	10/1
	23 days, 40°C [b]	10/1
(4) $(CH_3)_3C$-	t=0	1/10
	2h, 350 nm[a]	5/1
	40 days, 40°C [b]	1/2
(15) $CH_3(CH_2)_7$-	t=0	*E* only
	2h, 350 nm[a]	10/1
	8 days, 40°C[b]	*E* only
(16) $[CH_3(CH_2)_9][CH_3(CH_2)_7]CH$-	t=0	*E* only
	2h, 350 nm[a]	~5/1
	7 days, 40°C [b]	~7/1

[a] Irradiation (λ= 350 nm) in DMSO-d_6 followed by ^{1}H-NMR analysis.
[b] After irradiation, the samples were stored in the dark at 40°C and analyzed by ^{1}H-NMR at suitable time intervals.

Photoisomerization to cyclobutanol oxime (CBO)

As anticipated in the previous paragraph, compounds **4** and **16** exhibit additional ^{1}H-NMR peaks (10.15 and 10.14 ppm, respectively) besides those ascribed to *E/Z* isomerization, already within 2h of photostimulation. Indeed, halving of the *E*-isomer CHO and NOH peak intensities to the benefit of one single signal at 10.15 ppm is the most prominent effect of the 2h irradiation of compound **16** (Figure 3.4). In order to better observe any photoreactions that may occur over longer timescales than *E/Z* interconversion, photostimulation of compounds **4**, **15** and **16** was continued overnight (22h). Some features can be observed in the ^{1}H-NMR spectra of the resulting solutions (see Experimental section, paragraph 6.4.4 and Figure 3.5):

i) *(Z)-anti* signals are negligible; *(E)*-isomers signals are still present;

ii) The main photoproduct formed exhibits a singlet at 10.1-10.2 ppm (^{1}H) and a set of signals in the 5.5 (^{1}H) and 4-5 ppm (^{1}H) regions of the spectra. D_2O exchange shows that protons at 5.5 ppm exchange rapidly and couple with the 4-5 ppm protons (Experimental section, paragraph 6.4.4);

iii) A signal at 8.13 ppm peak is observed independently of the HIA substituent. This signal can be attributed to formic acid, i.e. the by-product formed by decomposition of HIAs to nitriles.[104]

In order to identify the product originating the new set (see feature ii above) of ^{1}H-NMR signals, we focused on compound **16**, which shows the least amount of residual HIA and of minor decomposition products. Full ^{1}H- and ^{13}C- NMR spectra of **16** after 22h irradiation, shown in Figure 3.5, are compatible with the formation of a cyclobutanol oxime (CBO) from Norrish-Yang cyclization,[118] as depicted in Scheme 3.2.

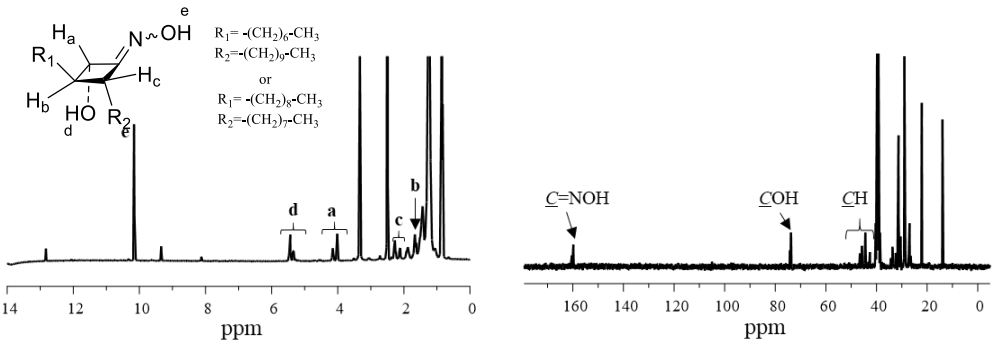

Figure 3.5. ^{1}H-NMR and ^{13}C-NMR (DMSO-d_6) spectra of **16** after 22h photostimulation (λ= 350 nm) followed by 4h at room temperature. δ (ppm): 12.8 (HIA, C=NO*H*, 0.1); 10.2 (H_e, 1.2); 9.34 (HIA, C*H*O, 0.1); 5.45 and 5.35 (H_d, 0.6 and 0.3); 4.15 and 4.02 (H_a, 0.3 and 0.7); 2.27 and 2.12 (H_c, 0.7 and 0.3); 1.65 (H_b, 1.0). Reproduced with permission from Ref.[88]

Unequivocal evidence is provided by D_2O exchange and 2D NMR experiments (Experimental section, paragraph 6.4.4). Specifically, the ^{1}H-NMR spectrum is simplified upon the addition of D_2O due to the disappearance of two exchangeable protons (10.15 ppm and 5.45 ppm). These signals can be attributed, respectively, to the C=NOH and CH-OH protons of the CBO structure. Further NMR experiments (COSY, DEPT 135, NOESY, HSQC; Experimental section) contribute to the assignment of the CH ring signals (reported in Figure 3.5), whereas the HMBC experiment clearly confirms the cyclic structure. In fact, the oxime carbon (159.8 ppm) shows long-range correlation with C-H_a and C-H_c, while C-H_b has $^{2}J_{CH}$ with the alcoholic carbon (74.3 ppm). It is worth noting that the formation of the cyclobutanol ring (Scheme 3.2) requires the HIA to be in the *anti* conformation, regardless of geometrical isomerism.[122] Upon thermal annealing, occurring even as the NMR spectra are acquired at room temperature, *E/Z* equilibration of the oxime group in the CBO structure takes place, as shown by the more complex NMR spectrum (Figure 3.5) with different CH-OH signals and splitting of its oxime signal (Experimental section). When compound **15** is irradiated for 22 h (Experimental section), the HIA oxime and aldehyde (*E* isomer, 12.89 and 9.39 ppm) signals are only partially reduced and signals

at 10.3 ppm, 5.64 and 5.46 ppm, 4.21 and 4.72 ppm are present, which are consistent with the formation of both *E* and *Z* isomers of CBO. 22h irradiation of compound **4** also yields the CBO structure (experimental section; 10.15, 5.50, 4.61 ppm) along with residual HIA. However, a number of unidentified minor signals are also detected. Table 3.3 shows the quantitative outcome of *E/Z* and Norrish-Yang photoisomerization of **4**, **15** and **16**.

Table 3.3. *E*/*Z* vs. Norrish-Yang photoisomerization of selected HIAs.[a] Reproduced with permission from Ref.[88]

RC(NOH)CHO	**Time**	**HIA *E/Z***	**CBO/HIA[b] (CBO%)**
(4) $(CH_3)_3C$-	t=0	1/10	nd[b]
	2h, 350 nm	5/1	0.1/1 (9%)
	22h, 350 nm	6/1	12/1 (77%)
(15) $CH_3(CH_2)_7$-	t=0	*E* only	nd[c]
	2h, 350 nm	10/1	<1%
	22h, 350 nm	*E* only	0.7/1 (40%)
(16) $[CH_3(CH_2)_9][CH_3(CH_2)_7]CH$-	t=0	*E* only	nd[b]
	2h, 350 nm	~5/1	0.5/1 (30%)
	22h, 350 nm	*E* only	20/1 (95%)

[a] Irradiation (λ= 350 nm) in DMSO-d_6 followed by ^{1}H-NMR analysis.

[b] Intensity of NO*H* signal of CBO/total C*H*O signal (both *E* and *Z*); CBO% = 100xCBO/(CBO+HIA).

[c] No CBO detected by NMR.

The *Z* isomers of **15** and **16** are only observed upon short time irradiation (*E/Z* 10/1 and 5/1, respectively) and are no longer detected after 22h exposure to light. After 22h, **4**- and **16**-CBO formation is almost quantitative (77 and 95%, respectively) and less remarkable in **15** (40%). It should be noted that in these experimental conditions configuration inversion of HIA **16** appears to be associated with sizable amounts of CBO at all irradiation times. In the case of **4**, instead, it is possible to obtain inversion of configuration after 2h photostimulation with less than 10% CBO formation.

3.2.2 Photoisomerization using LEDs

In this part, *E/Z* photoisomerization and Norrish-Yang cyclization of several HIAs bearing different R group (Figure 3.6) was investigated by using two LEDs at 278 nm and 365 nm in DMSO-d_6, DMF-d_7 or CD_3CN (UV cut-off 265, 268 and 190 nm respectively). Moreover, evaluation of Arrhenius activation energy of the thermal

back isomerization by ^{1}H-NMR analysis was carried out when HIA reached a substantial *E/Z* photo-inversion. In this paragraph, we adopted the same considerations of the previous section for ^{1}H-NMR data analysis and CBO formation.

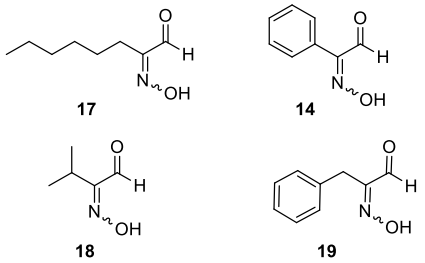

Figure 3.6. HIAs employed in the study of photochemical behavior using monochromatic LEDs at 278 nm and 365 nm.

The HIAs shown in Figure 3.6 were prepared according to α-oximation reaction reported by our group.[88] Yield of reactions and NMR characterizations can be found in the Experimental section (Chapter 6).

Photoisomerization at λ= 278 nm

The outcomes of photoisomerization with LED at 278 nm of selected HIAs are reported in Table 3.4. HIA **17** and **18** bearing, respectively, primary and secondary alkyl group adjacent to the oxime moiety are present only in the *E* form before irradiation (entry 1-4). After a variable period of irradiation time (up to 24 hours), only a limited inversion of configuration is observed for both **17** and **18** (respectively, *Z/E* 0.05 and 0.10-0.14) just as high pressure mercury lamps (λ=350 nm) (Table 3.3) for primary (**15**) and secondary (**16**). Photoisomerizations carried out in DMSO-d_6, DMF-d_7 or CD_3CN show no significant differences. The only substantial difference with the first set of experiments carried out in the high pressure mercury lamp (λ=350 nm) is nearly complete absence of CBO. In fact, even when compound **18** was irradiated for 24 hours in DMSO-d_6, ^{1}H-NMR analysis shows only traces of the product derived from Norrish-Yang cyclization (<5%) (full ^{1}H-NMR spectra are reported in the Experimental section, paragraph 6.4.5). Differently from irradiation with high pressure mercury lamp, HIA with an aromatic substituent (**14**) exhibits a reasonable inversion of configuration upon irradiation with LEDs at 278 nm in both DMSO-d_6 and CD_3CN (Table 3.4 entries 5,6; respectively, *Z/E* 0.31 and 0.24) with no significant changes in the aromatic region. The photo-stationary state was reached after 4.5 hours irradiation as shown in the Figure 3.7. In the case of compound **19**, a methylene group between

the phenyl ring and oxime moiety is sufficient to decrease the amount of inversion of configuration from *Z/E* 0.30 to 0.09.

Table 3.4 *E/Z* photoisomerization of selected HIAs at 278 nm.

Entry	RC(NOH)CHO	Solvent	Time (h)	*Z/E* initial	*Z/E* final
1	$(CH_3)_2CH$- (**18**)	DMSO-d_6	2 (24)	Only E	0.07 (0.10)[a]
2	$(CH_3)_2CH$- (**18**)	DMF-d_7	15	Only E	0.10
3	$(CH_3)_2CH$- (**18**)	CD_3CN	13	Only E	0.14 [b]
4	$CH_3(CH_2)_5$- (**17**)	DMSO-d_6	16	Only E	0.05
5	Ph- (**14**)	DMSO-d_6	4.5 (16)	Only E	0.29 (0.31)
6	Ph- (**14**)	CD_3CN	7	Only E	0.24
7	$PhCH_2$- (**19**)	DMSO-d_6	3(5)	Only E	0.09 (0.09)

[a] Traces of CBO

[b] Formation of other peaks between δ=5-7ppm

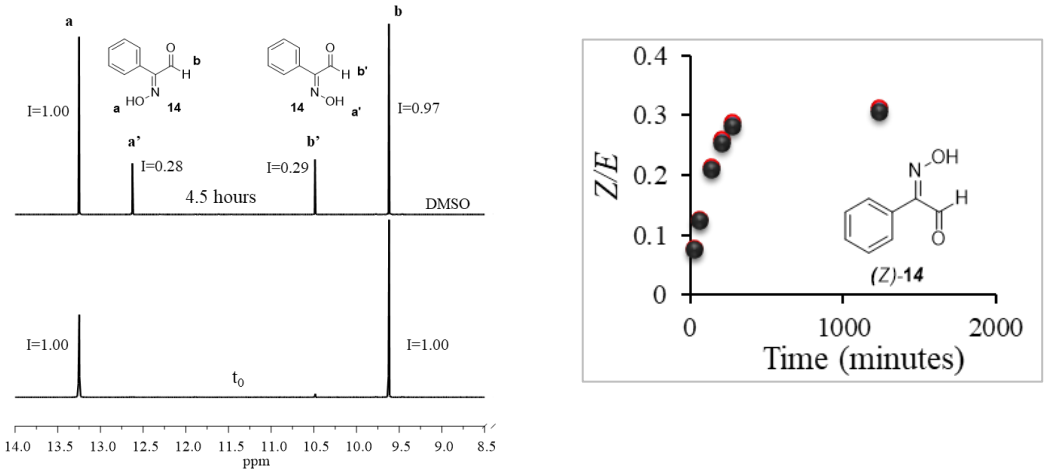

Figure 3.7. Left: expansion of the ^{1}H-NMR spectra (DMSO-d_6, δ: ppm) for the study of *E/Z* isomerism of compounds **14** after 4.5h photostimulation (λ= 278 nm). Full spectra in the Experimental section. Right: Time evolution of the formation of *Z*-**14** upon irradiation at 278 nm, expressed as *Z/E*.

Photoisomerization at λ= 365 nm

The use of LED at 365 nm leads to results substantial different from irradiation at 278 nm. Compounds bearing a hydrogen in γ-position relative to aldehyde moiety (**17**, **18**) gives isomerization to CBO in different yields depending on the alkyl substituent and the solvent employed (Table 3.5). In fact, HIA **18** bearing a secondary alkyl group is completely isomerized to CBO after 16 hours irradiation in DMSO-d_6 (Table 3.5 entry 1). A similar result was obtained in CD_3CN as demonstrated by the presence of diagnostic signals at 4.55 and 4.78 ppm and the complete disappearance of the aldehyde signal (see Experimental section, paragraph 6.4.6) (Table 3.5 entry 3). However, the appearance of other signals between 6 and 10 ppm indicates formation

of noticeable amount of unidentified compounds besides CBO. In contrast, 16 hours irradiation were not sufficient to photo-isomerize completely HIA **18** to CBO in DMF-d_7 (Table 3.5 entry 2) resulting at the end of reaction in the predominance of HIA over CBO. Linear HIA **17** gave more than 70% Norrish-Yang cyclization upon irradiation for 17 hours at 350 nm in DMSO-d_6. This result is in agreement with photoisomerizations with a high pressure mercury lamp, in which HIA bearing a secondary alkyl group gave a larger amount of Norrish-Yang cyclization with respect to HIA with a primary alkyl group. However, the use of LED at 365 nm allows satisfactory yields in DMSO-d_6 with HIA bearing a primary group as well. Compounds that cannot photoisomerize to CBO (**14** and **19**) had negligible *E/Z* inversion with irradiation at 365 nm for 5 hours.

Table 3.5. *E/Z* photoisomerization of selected HIAs at 365 nm.

Entry	**RC(NOH)CHO**	**Solvent**	**Time (h)**	***Z/E* initial**	***Z/E* final**	**CBO/HIA**
1	$(CH_3)_2CH$- (**18**)	DMSO-d_6	16	Only E	Only E	1:<0.05
2	$(CH_3)_2CH$- (**18**)	DMF-d_7	16	Only E	Only E	0.7:1
3	$(CH_3)_2CH$- (**18**)	CD_3CN	16	Only E	-	1:<0.05
4	$CH_3(CH_2)_5$- (**17**)	DMSO-d_6	17	Only E	Only E	1: 0.30
5	Ph- (**14**)	DMSO-d_6	4.5	Only E	<0.05	-
6	$PhCH_2$- (**19**)	DMSO-d_6	5	Only E	<0.05	-

In conclusion, the use of monochromatic LEDs (278 nm and 365 nm) instead of high pressure mercury lamps with maximum of emission at 365 nm gives several advantages. The most important is the possibility to select the type of photoreaction observed. In fact, irradiation with LED 278 nm gives only *E/Z* inversion, while the use of LED at 365 nm promotes the formation of CBO. The extremely low *E/Z* isomerization of **14** with 365 nm with respect to 278 nm suggests the potential to have an orthogonal system. However, none of HIAs considered in this study provides an orthogonal system, since they do not undergo both isomerizations with good efficiency.

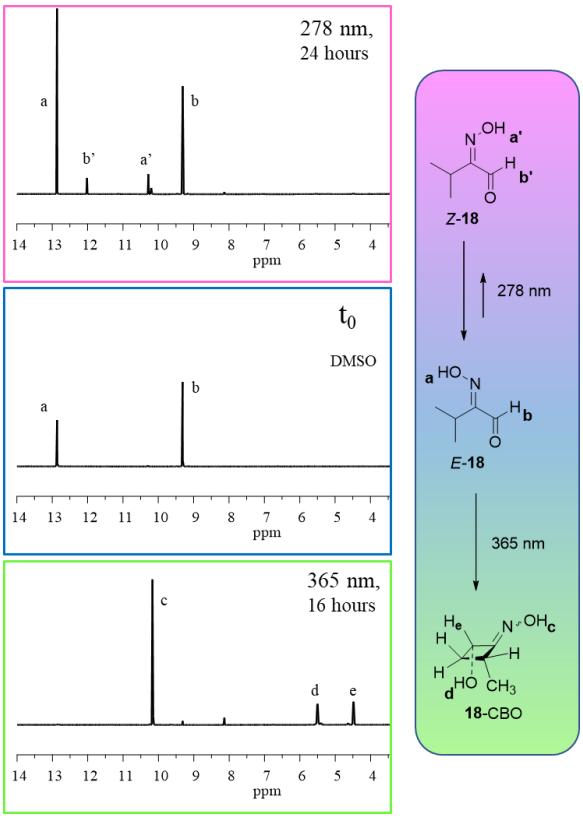

Figure 3.8. Expansion of the ^{1}H-NMR spectra (DMSO-d_6, δ: ppm) for the study of *E/Z* isomerism and Norrish-Yang cyclization of compounds **18**, after, respectively, 24h (λ= 278 nm) and 16h photostimulation (λ= 365 nm).

3.2.3 Thermal back isomerization of 14

As reported in the previous paragraphs, *E/Z* photoisomerization of several HIAs were investigated using both mercury lamp and LEDs in different solvents. In particular, two different photochemical behaviors were found depending on the wavelength of monochromatic light source. Photostimulation at 278 nm gives exclusively *E/Z* interconversion, while illumination at 365 nm results in Norrish-Yang cyclization. Besides the photochemical investigation, a first screening of the thermal back *E/Z* isomerization of HIAs at 40°C was carried out, proving that this process proceeds with a strongly structure-dependent kinetics (Table 3.2).

Most HIAs exhibited only limited *E/Z* photoisomerization (about 10%). Therefore, the kinetics of thermal back *Z*→*E* isomerization was studied only in the case of **14**, which gave about 30% of *Z*-**14** after irradiation at 278 nm in DMSO (Table 3.4). The kinetics of its thermal isomerization was determined at three different temperatures (323 K, 333 K and 343 K) by ^{1}H-NMR. The thermal isomerization rate constants were then obtained by an exponential fit of the *Z*-**14** decay (Figure 3.9) and

the activation energy Ea and Arrhenius prefactor A of the process were estimated using Equation 3.1 and plotting ln(k) versus 1/T (Table 3.6).[126]

$$k = Ae^{-\frac{Ea}{RT}} \qquad \text{Equation 3.1}$$

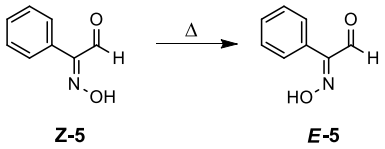

Z-5 ***E*-5**

Scheme 3.3. Thermal back isomerization of **14**.

The estimated activation energy for the thermal *Z*→*E* **14** isomerization (113 kJ/mol) is higher than Ea of C=N double bond of imines (~70 KJ/mol), but lower of the C=C bond of stilbene (175 KJ/mol).[126] Interestingly, the value of the activation energy for HIA **14** *Z* → *E* isomerization obtained from this preliminary study is comparable with that of *cis* → *trans* isomerization of N=N double bond of azobenzenes (~95 kJ/mol),[126] used in light-driven molecular machines.

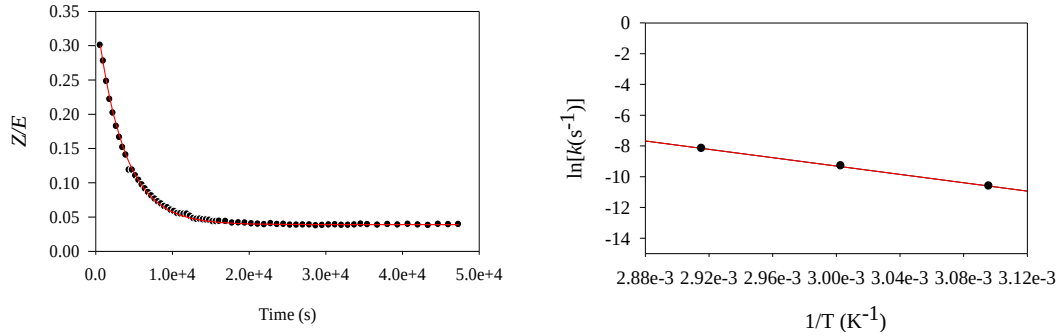

Figure 3.9. Exponential decay of *Z* isomer at 343 K (left) and Arrhenius plot ln(k) versus 1/T constant for *Z*-**14** thermal back isomerization (T= 323, 333 and 343 K) (right).

Table 3.6. Experimental rates of thermal back isomerization of **14** in DMSO at three different temperatures and Arrhenius activation energy Ea and prefactor A.

Temperature (K)	**k (s^{-1})[(a)]**	**Ea (KJ/mol)**	**A (s^{-1})**
323	2.4 x 10^{-5}	113 (27 kcal/mol)	4.2 * 10^13
333	9.1 x 10^{-5}		
343	28 x 10^{-5}		

[(a)] uncertainty 5%

3.3 HIA-BEARING COPOLYMERS

P(HIABMA-*co*-OEGMA$_{475}$) 3:7 in DMSO-d_6 was irradiated in a high pressure mercury lamp (maximum emission at 350 nm) and subjected to ^{1}H-NMR analysis. The spectrum exhibits one peak for the oxime (12.91 ppm) and one for aldehyde proton (9.41 ppm) (Figure 3.10). After 2 hours irradiation at 350 nm, two additional peaks appear at 12.04 and 10.29 ppm. So, the *Z* configuration was populated in small extent (4%). After only one day of thermal equilibration at 40 °C, the *Z* isomer returns to its initial configuration. The extent of photoinversion is comparable to that of monomer HIABMA (paragraph 3.2.1), while thermal back isomerization is much faster. In a recent work Cai and co-workers[82] proved that the *E/Z* population of their copolymers, which encompass a benzylaldoxime side chain, can reach up to 74% *E* to *Z* inversion in the 1:1 copolymer of the photosensitive repeat unit with OEGMA, and that the population is stable for 8 h at 80 °C in DMSO-d_6/D_2O 1:1. Furthermore, the change in *E/Z* population influences the thermal properties of the copolymers. In our case, the limited stability and the little amount of photoinduced *Z* isomer of HIABMA moieties in the copolymer prevented the study of thermal properties in relation to *E/Z* photoisomerism.

When poly(HIABMA-*co*-OEGMA$_{475}$) 3:7 was irradiated for 24 hours, around 30% of HIA groups isomerized to CBO (Figure 3.10). This result is comparable to that of primary HIA **15** irradiated for 22 hours at 350 nm (Table 3.2). However, along with CBO formation, other unidentified signals also appeared. A singlet at 8.13 ppm may be attributed to formic acid derived from decomposition of HIA to nitrile. So far, the three signals of equal intensity around 7 ppm have not yet been identified.

The considerable change on the side chain of copolymer that resulted from Norrish-Yang cyclization may influence the thermal behavior in aqueous solution. For this reason the effect of long time photoisomerization was illustrated in connection with the thermal properties in Chapter 4.

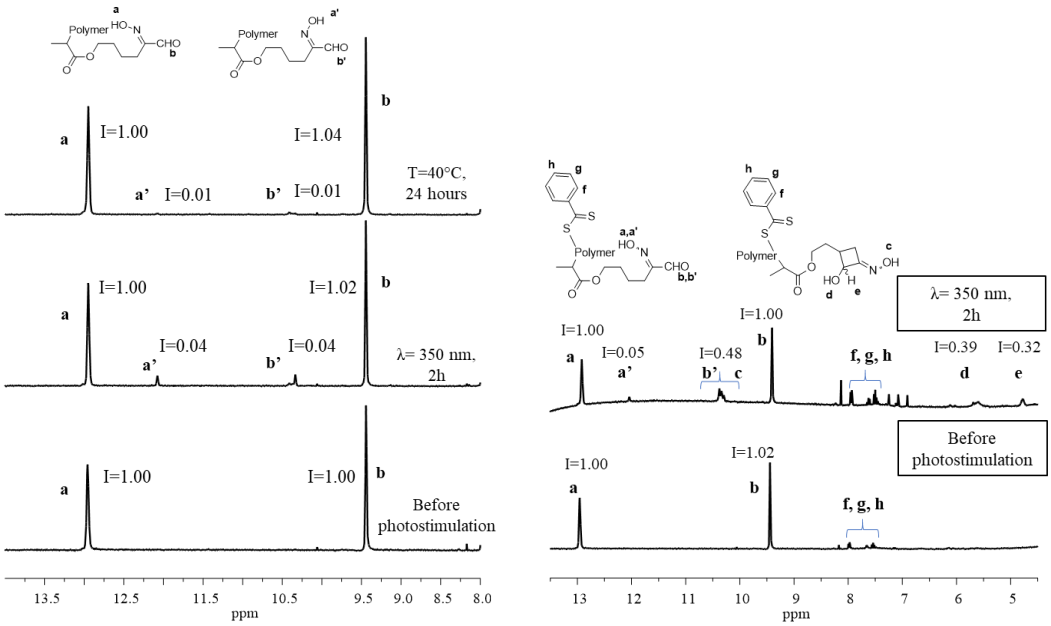

Figure 3.10. Expansion of the ^{1}H-NMR spectra (DMSO-d_6, δ: ppm) for the study of *E/Z* isomerism and Norrish-Yang cyclization of P(HIABMA-*co*-OEGMA$_{475}$) 3:7, after, respectively, 2h (left) and 24h (right) photostimulation at 365 nm. Adapted from Ref.[95] with permission from The Royal Society of Chemistry.

Chapter 4: Thermal behavior in aqueous solution

4.1 INTRODUCTION

Poly[oligo(ethylene glycol)methacrylate]s (POEGMA)s are the most studied thermo-responsive polymers after the well-known poly(N-isopropylacrylamide) (PNIPAM).[127] As other polymers that show a lower critical solution temperature (LCST behavior), some POEGMAs undergo a coil-to-globule transition in aqueous solution upon increasing the temperature. Oligo(ethylene oxide) units in the side chain ensure solubility of the polymer in water thanks to the formation of hydrogen bonds with solvent molecules. As the temperatures is increased, the hydrogen bonds become loose, the polymer chains are partially desolvated and start to aggregate. As a result, the homogeneous solution separates into a concentrated and a dilute phase. In addition, Cloud Point (Tcp) is the transition temperature associated to a specific polymer concentration. This is different from LCST, which is the minimun of the binodal curve of the binary polymer/solvent mixture phase diagram. Besides polymer concentration, there are other factors that determine Tcp, such as molecular weight, the nature of end groups and the amphiphilicity of the polymer.[127] Specifically, OEGMA homopolymers exhibit Tcp depending on the number of oligo(ethylene oxide) units in the side chain[128] and the variation of side chain end-functionality.[129] Furthermore, cloud points can be fine-tuned in a range of 30-60°C by copolymerization of OEGMA of different oligo (ethylene glycol) lengths.[130] An interesting characteristic of POEGMAs that differs from PNIPAM is the absence of significant hysteresis between the heating and cooling cycles.

The role of hydrogen bonding is not only that of providing solvation of polymer chains in water, but also of promoting inter-chain interactions, thus affecting cloud point temperature.[131,132] Cai and coworkers demonstrated that incorporation of several H-bonding units in the side chain of a water-soluble polymer lowers the cloud point in a manner that is dependent on polymer architectures.[133]

When the thermally-responsive polymer is functionalized with chromophores, light comes into play to tune the thermal response.[134] In fact, as a result of exposure to specific wavelengths, a chromophore can change its dipole moment through reversible

cis/trans isomerization, as in the case of azobenzene derivatives,[135] it can switch its polarity as in the spiropyran-merocyanine equilibrium[136] or undergo photocleavage.[137] Moreover, Wu *et al.* prepared oxime-containing amphiphilic copolymers of OEGMA able to pre-organize in compact micelles below the LCST depending on copolymer composition and oxime *E/Z* configuration.[82]

In this chapter, thermal behavior of HIA-containing copolymers is investigated through turbidimetry and Dynamic Light Scattering (DLS) and compared to that of other copolymers bearing either aldehyde or simple oxime groups. In addition, the effect of irradiation of HIA moiety on Tcp is also evaluated. As reported in the previous chapter, the *E/Z* photoisomerization of HIA moiety is negligible in the case of HIA-functionalized polymers, so that if any coupling between photo- and thermal responsivity were to be sought, the photoisomerization of HIA to CBO should be performed.

4.2 RESULTS AND DISCUSSION

Cloud points (defined as 50% Transmittance at a given wavelength) of the synthetized OEGMA copolymers are reported in Table 4.1 as a function of their concentration in water.

Table 4.1. Cloud Points of prepared polymers (Chapter 2).

Entry	Polymer	DP (GPC)	C (mg/ml)	Tcp (°C)
1	$POEGMA_{475}$	28	1.5	>80 [a]
2	P(HIABMA-*co*-$OEGMA_{475}$) 1:9	29	1.5	>80 [a]
3	P(HIABMA-*co*-$OEGMA_{475}$) 3:7	26	1.5	69 [a]
4	P(HIABMA-*co*-$OEGMA_{475}$) 1:1	32	1.0	47 [b]
5	P(OHMA-*co*-$OEGMA_{475}$) 3:7	33	1.5	>80 [a]
6	P(HIHMA-*co*-$OEGMA_{475}$) 3:7	28	2.7	76 [a]
7	P(HIHMA-*co*-$OEGMA_{475}$) 1:1	30	1.0	53 [b]
8	$POEGMA_{300}$	27	1.0	72 [b]
9	P(HIABMA-*co*-$OEGMA_{300}$) 3:7	43	1.0	30 [b]
10	P(HIHMA-*co*-$OEGMA_{300}$) 3:7	36	1.0	35 [b]

50% transmittance at 550 ([a]) or 700 nm ([b]).

$OEGMA_{475}$ homopolymer, as well as P(OHMA-*co*-$OEGMA_{475}$) 3:7, do not show any cloudiness up to 80 °C at 1.5 mg/mL. Similarly, P(HIHMA-*co*-$OEGMA_{475}$) 3:7 solution at 0.5 mg/mL remains clear up to 80 °C, while it shows some turbidity at 1.5 mg/mL after 78°C and a sharp transition between 75-78 °C at 2.7 mg/mL (Figure

4.1 (b)). P(HIABMA-*co*-OEGMA$_{475}$) 1:9 solutions remain clear up to 80 °C (data not shown), while the 3:7 copolymers exhibit concentration-dependent Tcp at lower temperatures (Figure 4.1(a)). Specifically, in the range between 0.5 mg/mL and 2.0 mg/mL, Tcp decreases from 76 °C to 63 °C, while small differences are found between cloud points at 2.0 mg/mL and 7.6 mg/mL (63 vs 61°C). Both P(HIHMA-*co*-OEGMA$_{475}$) 1:1 and P(HIABMA-*co*-OEGMA$_{475}$) 1:1 exhibit lower cloud points than the corresponding 3:7 copolymers (Figure 4.1 (c) and (d)) with only a slight concentration dependence. In particular, HIABMA/OEGMA$_{475}$ 1:1 copolymer has the same turbidity onset at both 1.0 and 5.0 mg/mL. Moreover, sharper transitions result from higher polymer solution concentrations for all synthetized OEGMA$_{475}$ copolymers. In general, the cloud points of HIHMA/OEGMA$_{475}$ copolymers are higher than those of HIABMA/OEGMA$_{475}$ copolymers. This difference is more pronounced with 3:7 ratio where HIHMA copolymer shows a cloud point at 2.7 mg/mL 13°C higher than HIABMA copolymer at 2.0 mg/mL. For 1:1 ratio, we found at most 6°C difference at 1.0 mg/mL.

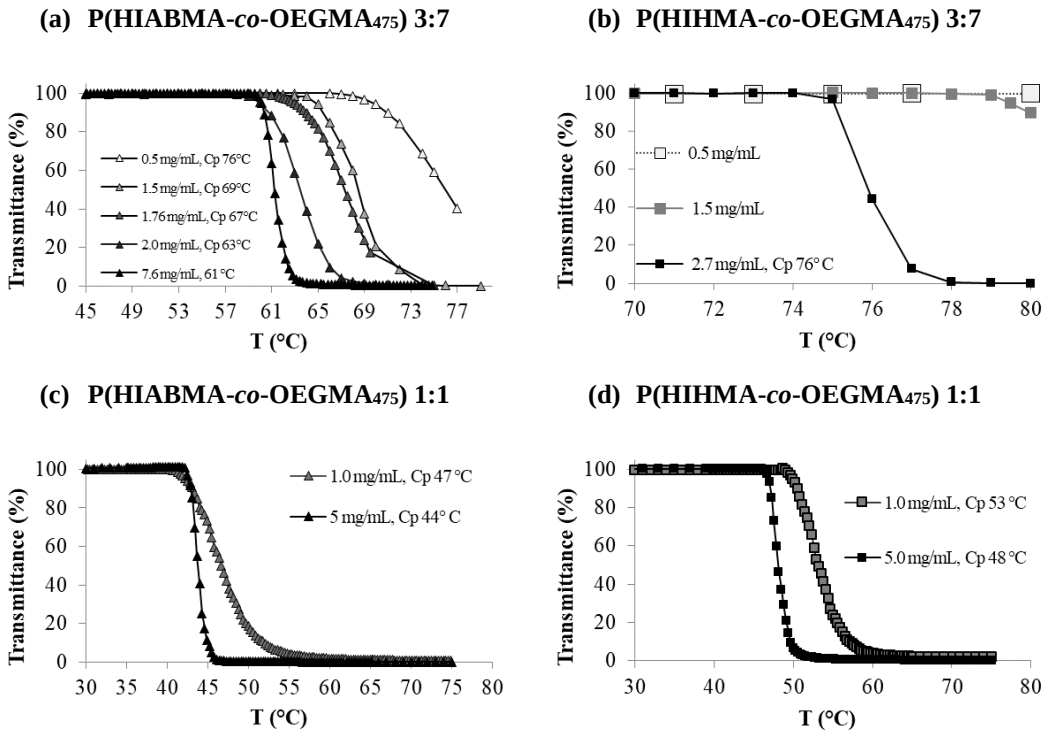

Figure 4.1. Cloud points of HIABMA and HIHMA copolymers with OEGMA$_{475}$ in water determined as 50% transmittance at 550 nm (or 700 nm) up to 80 °C. (a) P(HIABMA-*co*-OEGMA$_{475}$) 3:7 heating scan; (b) P(HIHMA-*co*-OEGMA$_{475}$) 3:7, heating scan; (c) P(HIABMA-*co*-OEGMA$_{475}$) 1:1, heating scan; (d) P(HIHMA-*co*-OEGMA$_{475}$) 1:1, heating scan. Adapted from Ref.[95] with permission from The Royal Society of Chemistry.

Then we checked for hysteresis of phase transition of HIABMA/OEGMA$_{475}$ and HIHMA/OEGMA$_{475}$ 1:1 copolymers for low and high concentrations (Figure 4.2). All curves show no or little hysteresis. In particular, P(HIABMA-*co*-OEGMA$_{475}$) 3:7 and 1:1 show a higher difference between heating and cooling scan for more concentrated solutions, while P(HIHMA-*co*-OEGMA$_{475}$) 1:1 exhibits an opposite behavior.

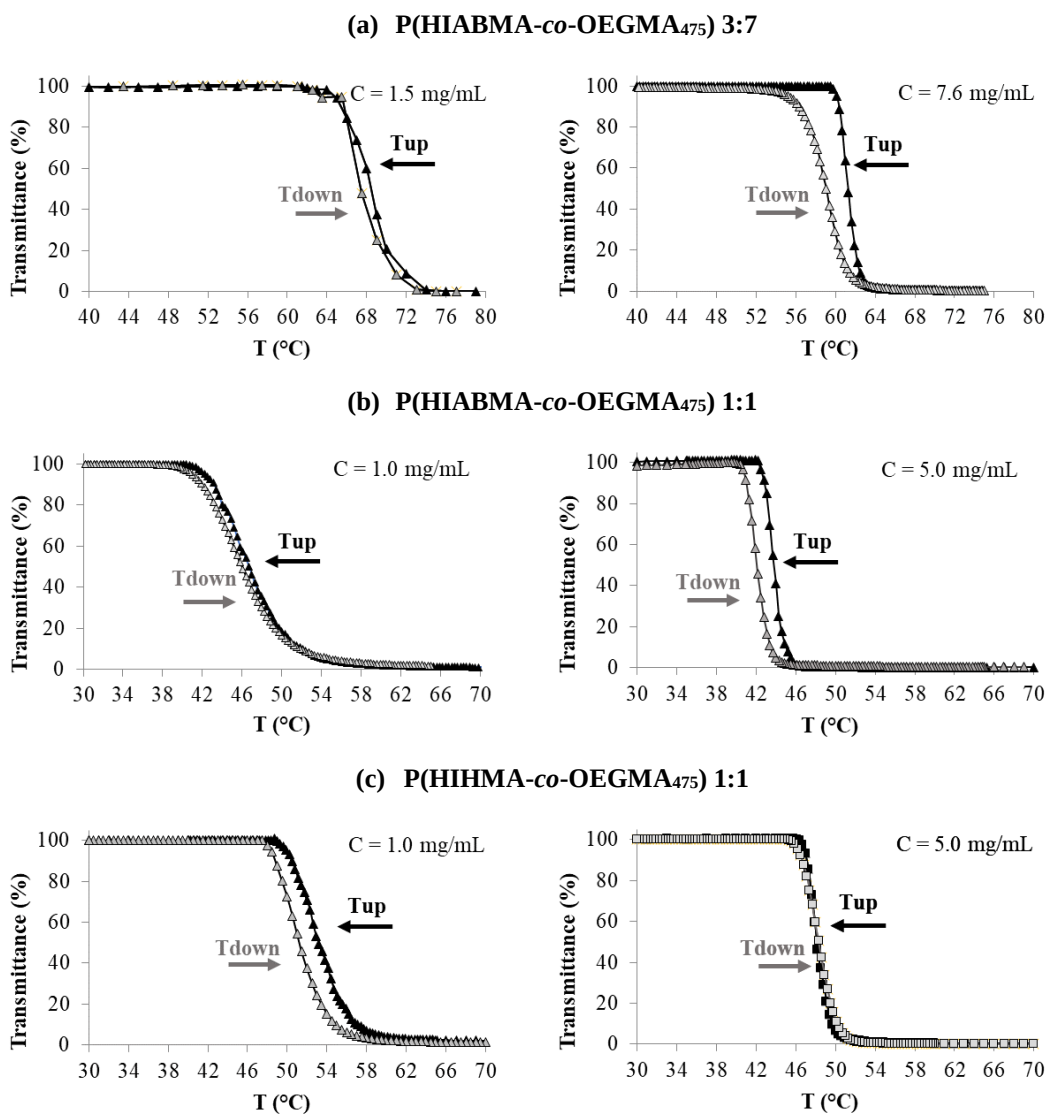

Figure 4.2. Transmittance vs. temperature trace in the heating and cooling scan for (a) P(HIABMA-*co*-OEGMA$_{475}$) 3:7 at 1.5 and 7.6 mg/mL polymer concentration; (b) P(HIABMA-*co*-OEGMA$_{475}$) 1:1 at 1.0 and 5.0 mg/mL polymer concentration; (c) P(HIHMA-*co*-OEGMA$_{475}$) 1:1 at 1.0 and 5.0 mg/mL polymer concentration.

OEGMA$_{300}$ homopolymer has only 4.5 oligo (ethylene glycol) units in the side chain against 7.5 of OEGMA$_{475}$, so that the former is more hydrophobic than the latter. As a consequence, a Tcp of of 71°C is observed at 1.0 mg/mL POEGMA$_{300}$, in contrast with POEGMA$_{475}$. Similarly, OEGMA$_{300}$ copolymers show lower cloud points than

those of $OEGMA_{475}$. Heating and cooling scans of $OEGMA_{300}$ homopolymer and copolymers solutions at 1.0 mg/mL are reported in Figure 4.3. $HIABMA/OEGMA_{300}$ 3:7 shows a slight turbidity already at 20°C, while 50% transmittance is reached at 30°C, resulting in a phase transition more than 20°C broad. $HIHMA/OEGMA_{300}$ 3:7 has a cloud point 6°C higher than that of analogous HIABMA copolymer, while the phase transition takes place in a 10°C interval. Moreover, it is worth noting that heating and cooling scans are close in all $OEGMA_{300}$ polymerization with no more than 2°C of difference, resulting in small hysteresis.

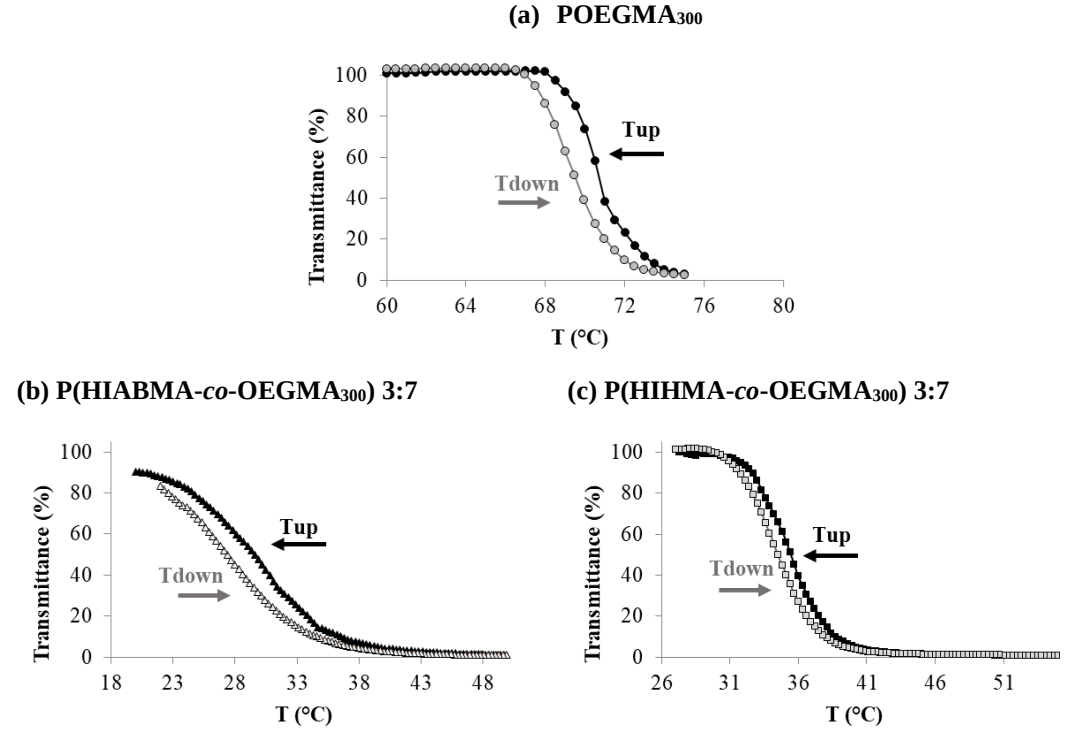

Figure 4.3. Cloud points of homopolymer $OEGMA_{300}$ and its copolymers with HIABMA and HIHMA in water determined as 50% transmittance at 700 nm up to 75°C at 1.0 mg/mL. (a) $POEGMA_{300}$ heating and cooling scan; (b) P(HIABMA-*co*-$OEGMA_{300}$) 3:7, heating and cooling scan; (c) P(HIHMA-*co*-$OEGMA_{300}$) 3:7, heating and cooling scan.

For a more detailed investigation through dynamic light scattering (DLS) measurements, $HIABMA/OEGMA_{475}$ and $HIHMA/OEGMA_{475}$ 1:1 copolymers have been selected. Intensity distributions of particle sizes are reported for temperature below and above cloud points (Figure 4.4). All copolymers are characterized by the presence of both unimolecular chains and small aggregates at 25°C. When the solutions are heated well above cloud point (80°C), aggregates of large dimensions (> 1000 nm) are formed by all polymers. At room temperature and 1 mg/mL concentration, most of P(HIABMA-*co*-$OEGMA_{475}$) 3:7 and 1:1 exist reasonably as unimolecular chains with dimensions below 10 nm, while a small percentage (17%

and 32%, respectively) of aggregates higher than 100 nm is present. The percentage of particles with larger dimensions exhibits only a weak dependence on the copolymer concentration in water. In fact, both 1.0 mg/mL and 5.0 mg/mL solutions have a similar amount of larger aggregates at 25°C. On the contrary, size distributions of P(HIHMA-*co*-OEGMA$_{475}$) 1:1 at room temperature is dependent on solution concentration. The amount of larger aggregates changes from 16% to 52% when the concentration is increased fivefold. In contrast to P(HIABMA-*co*-OEGMA$_{475}$) 1:1 (Figure 4.1 (c)), the presence of larger aggregates which are concentration-dependent may explain the different phase-transition onsets for 1.0 and 5.0 mg/mL solutions (Figure 4.1 (d)).

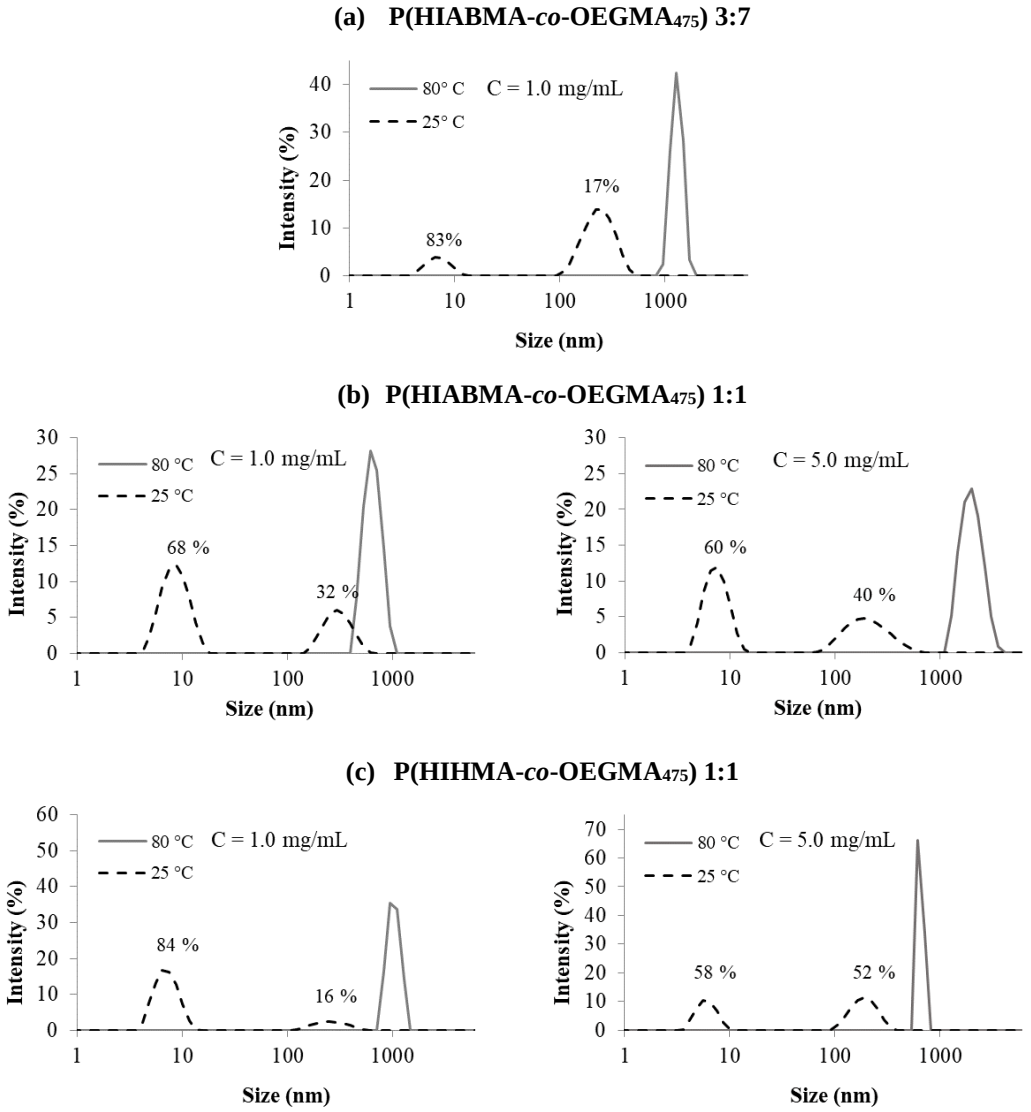

Figure 4.4. DLS measurements of intensity vs. size below (25°C) and above (80°C) cloud points for (a) P(HIABMA-*co*-OEGMA$_{475}$) 3:7 at 1.0 mg/mL; (b) P(HIABMA-*co*-OEGMA$_{475}$) 1:1 at 1.0 and 5.0 mg/mL; (d) P(HIHMA-*co*-OEGMA$_{475}$) 1:1 at 1.0 and 5.0 mg/mL.

Phase transition effect in HIABMA/OEGMA$_{475}$ 1:1 copolymer promoted by light

As discussed in Chapter 3, we have observed two main photoreactions of the HIA group upon irradiation with a high pressure mercury lamp (λ_{max}=350 nm), i.e *E/Z* inversion about the C=N(OH) oxime bond and isomerization to cyclobutanol oxime. We demonstrated that the extent of these two processes depends on several factors, such as irradiation time, type of substituent adjacent to the oxime and steric hindrance close to oxime double bonds. In particular, for HIAs bearing a primary group small amount of *E/Z* inversion is reached after 2 hours of irradiation, whereas 22 hours are sufficient to have about 40% isomerization to CBO. Similar results are obtained for P(HIABMA-*co*-OEGMA$_{475}$) 3:7 in DMSO-d$_6$ (Paragraph 3.4). However, minor photoproducts were detected by ^{1}H-NMR analysis that have not been identified so far.

One of the main differences between HIA and CBO isomers is the presence of a hydroxyl group (hydrogen bond acceptor and donor) in CBO instead of the aldehyde group in HIA (only acceptor). This is expected to give a different hydrogen bond pattern with respect to HIA. Solutions of P(HIABMA-*co*-OEGMA$_{475}$) 1:1 in D_2O or H_2O were irradiated at 350 nm for 22 hours at both 1.0 and 5.0 mg/mL. Samples in D_2O were analyzed by ^{1}H-NMR spectroscopy immediately after photostimulation at different time-points up to 22h. The terminal OC*H*$_3$ of OEGMA was used as the internal standard. Spectra in Figure 4.5 show that the C*H*O (9.4 ppm) peak intensity decreases over time from 1H to 0.25H. A change also occurs in the shape of signals in the 2.8-0 ppm region. These signals comprise polymer backbone protons, the C*H*$_3$ directly attached to the backbone and alkyl protons in the pendent chains that are at least one position away from oxygen atoms. The overall integral of the 2.8-0 ppm region is 11.9H (theor. 12H) before photostimulation and 11.0H after 22h in the photoreactor. Unfortunately, the diagnostic signals for the formation of CBO are not visible in D_2O, since OH protons exchange with deuterated water and C*H*-OH is expected to fall under OCH_2 signals (in the Figure 4.5 marked as **b**). Furthermore, ^{13}C-NMR do not show any diagnostic signals, including aldehyde, oxime and carbons of backbone, probably as a result of limited mobility. As of now we assume, on the basis of our results on the irradiation of P(HIABMA-*co*-OEGMA$_{475}$) 3:7 in DMSO-d$_6$, that the main photoproduct accounting for the loss in aldehyde signal is CBO. However, further proof is being sought to corroborate this inference. Furthermore, a minor signal (<1%) at 8.4 ppm is yet to be identified.

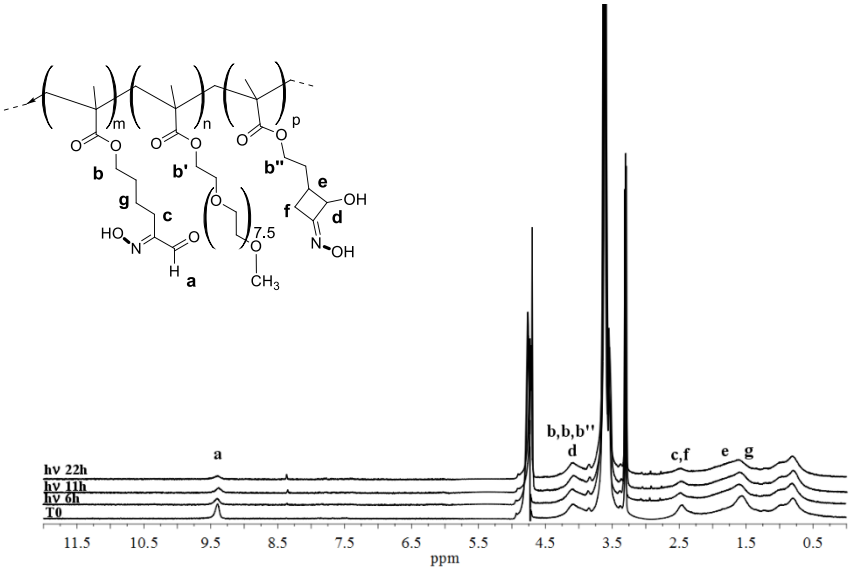

Figure 4.5. ^{1}H-NMR spectra (D_2O) of P(HIABMA-*co*-OEGMA$_{475}$) at different time points of irradiation (λ= 350 nm).

Even though no dramatic structural change is detected directly by NMR, the effect of irradiation on cloud point is remarkable. In fact, phase transition of irradiated P(HIABMA-*co*-OEGMA$_{475}$) 1:1 solution at 5.0 mg/mL polymer concentration increases by 12-13 °C with respect to pristine sample, whereas irradiation completely suppressed the cloud point at 1.0 mg/mL up to 75°C (Table 4.2 and Figure 4.6)

Table 4.2. Temperatures at 90% and 50% transmittance (λ= 700 nm) of aqueous solutions of P(HIABMA-*co*-OEGMA$_{475}$) 1:1 before and after irradiation at λ= 350 nm.

Polymer sample	**T°C (heat/cool)[a] 90% transmittance**	**T°C (heat/cool)[a] 50% transmittance**
5 mg/mL, pristine	42.9/41.0	43.8/42.1
5 mg/mL, photoisomerized	55.4/52.2	56.7/54.2
1 mg/mL, pristine	43.1/42.0	46.0/46.7
1 mg/mL, photoisomerized	Not detected	

[a] Temperatures recorded in the first heating/cooling scans after polymer dissolution in water.

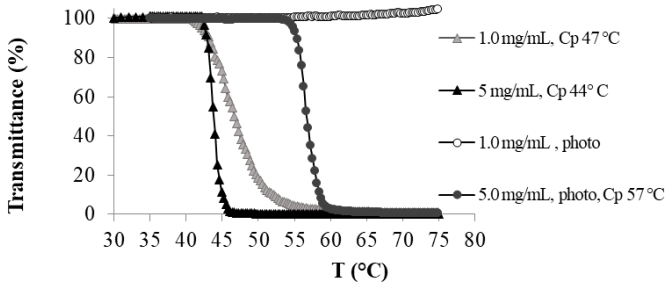

Figure 4.6. Transmittance (λ = 700 nm) vs. Temperature traces of aqueous solutions of P(HIABMA-*co*-OEGMA$_{475}$) 1:1 before and after irradiation at λ = 350 nm. Traces: 5 mg/mL before irradiation, heating (▲) scan; 5 mg/mL after irradiation, heating (●) scan; 1 mg/mL before irradiation heating (▲) scan; 1 mg/mL after irradiation heating (○) scan.

In keeping with these results, ^{1}H-NMR signals of the hydrophobic main chain in P(HIABMA-*co*-OEGMA$_{475}$) 1:1 (Figure 4.7) exhibit a decrease in their intensity as temperature is increased to 323 K, whereas no such decrease is observed with the irradiated sample up to 330 K. This result is consistent with the increase of Tcp of P(HIABMA-*co*-OEGMA$_{475}$) 1:1 solution at 5.0 mg/mL after irradiation.

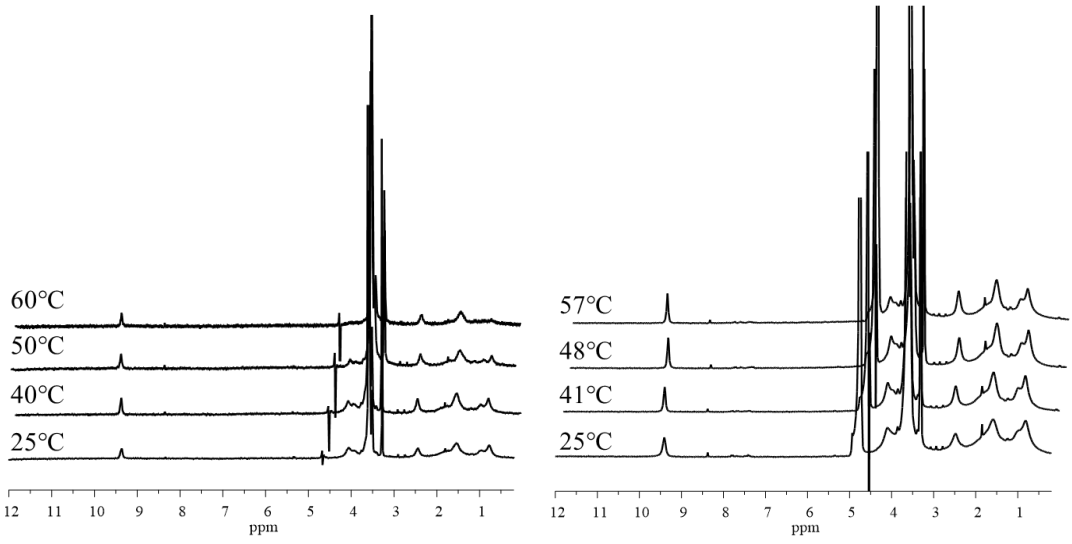

Figure 4.7. Temperature effect on the spectra of polymer solutions before (1 mg/mL) and after (5 mg/mL) photoisomerization for 22h.

The photoisomerized sample (5 mg/mL) was subjected to repeated thermal cycles in the 35 to 75°C range (Figure 4.8) to assess its stability and to highlight any hysteresis effects. We began with a full heat-cool-heat cycle, thereby showing that the first and second heating traces are identical (Figure 4.8 (a)). The sample was then allowed to cool down to only 51°C, i.e. just below the cloud point, prior to heating it once more to 75°C (Figure 4.8 (b)). This time, the transmittance trace upon

temperature increase was slightly off with respect to the corresponding previous curves. This deviation is even more pronounced in the subsequent cooling scan. However, the hysteresis initiated by the partial cooling of the sample down to only 51°C was eliminated by allowing it to equilibrate at room temperature for 24h. In fact, the subsequent heat-cool cycle (35 to 75 to 35°C) overlaps with the initial transmittance vs. temperature trace (Figure 4.6 (c)). We infer from these observations that the chemical structure of the photoisomerized polymer is thermally stable within the time-frame of the experiment and that aggregates formed above the cloud point still exist when the temperature is decreased to just below the Tcp. Re-equilibration then takes place below the Tcp if enough time is allowed.

(a) First and second thermal cycles

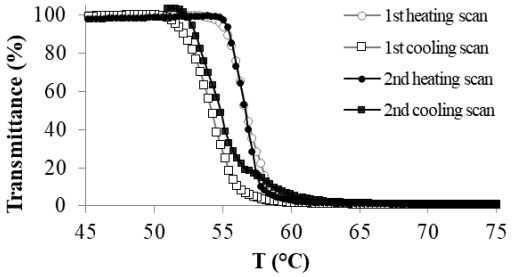

(b) Second and third thermal cycles

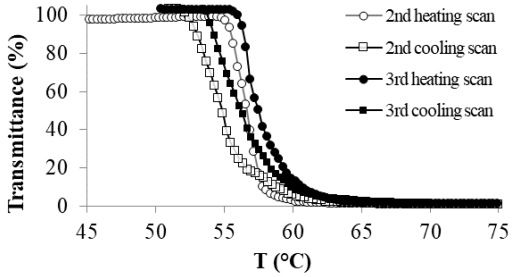

(c)First and fourth thermal cycles (after equilibration for 24 h at 25 °C)

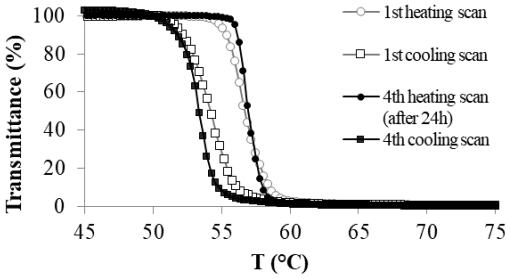

Figure 4.8. Thermal hysteresis of a 5 mg/mL aqueous solution of photoisomerized P(HIABMA-*co*-OEGMA$_{475}$) 1:1 at 1°C min-1 heating/cooling rate. (a) first and second thermal cycles (b) Second and third thermal cycles (c) comparison between first and last thermal cycle (the last thermal cycle was performed after allowing the sample to re-equilibrate at 25°C for 24h).

DLS measurements of intensity as a function of size are reported in Figure 4.9 for P(HIABMA-*co*-OEGMA$_{475}$) 1:1 before and after 22 hours irradiation at 350 nm at different temperatures. Both pre and post-irradiated solutions show a prevalence of particles around 10 nm at 25°C, with a small amount of aggregates having diameters larger than 100 nm (Figure 4.9 (a) and (c)). Between 40°C and 45°C, large aggregates (>100 nm) of the pristine P(HIABMA-*co*-OEGMA$_{475}$) 1:1 form abruptly and continue

to grow as temperature approaches 80°C (Figure 4.9 (a)). Irradiated P(HIABMA-*co*-OEGMA$_{475}$) 1:1 solutions, on the other hand, do not exhibit significant differences in size distribution up to 54°C (Figure 4.9 (c)). Partial aggregation of small particles onsets at 56 °C and becomes complete at 58°C. In the cooling scan of the pristine P(HIABMA-*co*-OEGMA$_{475}$) 1:1(Figure 4.9 (b)), a fair amount of larger aggregates is still present at 40°C, in contrast to the heating scan. Similarly, the cooling scan of irradiated P(HIABMA-*co*-OEGMA$_{475}$) 1:1 (Figure 4.9 (d)) reflects the hysteresis observed in turbidimetry. In fact, at 52°C the presence of aggregates larger than 100 nm are still detectable. In summary, DLS analysis is consistent with turbidimetry and highlights the large difference in cloud point before and after irradiation of P(HIABMA-*co*-OEGMA$_{475}$) 1:1. Indeed, large aggregates are already present at 50°C in an aqueous solution of non-irradiated P(HIABMA-*co*-OEGMA$_{475}$) 1:1, while a predominance of small-sized population (around 10 nm) is still present at 54°C in the irradiated P(HIABMA-*co*-OEGMA$_{475}$) 1:1.

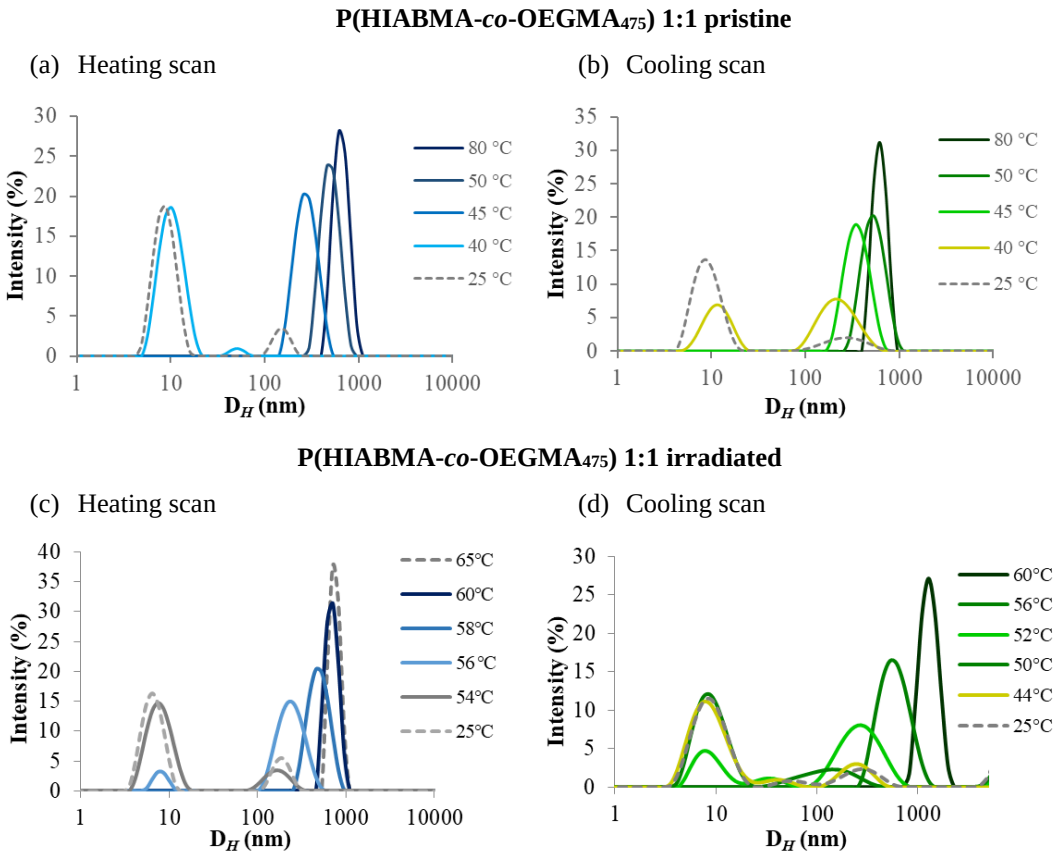

Figure 4.9. DLS measurements of intensity vs. size at different temperatures for pristine P(HIABMA-*co*-OEGMA$_{475}$) 1:1 at 5.0 mg/mL, (a) heating and (b) cooling scan; P(HIABMA-*co*-OEGMA$_{475}$) 1:1 after 22h photostimulation at 5.0 mg/mL, (c) heating and (d) cooling scan.

In conclusion, irradiation of $OEGMA_{475}$ copolymer bearing 50% of HIA group leads to structural changes that result in a remarkable increase of Tcp in aqueous solution. The irradiated polymers are thermally stable upon several heat-cool cycles lasting about 5h. Thermal hysteresis is negligible provided enough equilibration time is allowed well below the Tcp. ^{1}H-NMR data are consistent with turbidimetry and DLS measurements show that both pre and post-irradiated polymers form large aggregates with increasing temperatures according to their cloud points. Even though this remarkable change in LCST behavior of P(HIABMA-*co*-$OEGMA_{475}$) 1:1 may be ascribabed to the isomerization of HIA to CBO, it is not possible so far to demonstrate the formation of this group through NMR analysis. Moreover, we cannot rule out that further photochemical processes be relevant to the thermal properties of copolymers aqueous solutions, since irradiation of P(HIABMA-*co*-$OEGMA_{475}$) 3:7 in DMSO-d_6 showed the formation of other unidentified compounds (Paragraph 3.4).

Chapter 5: Conclusions and future perspectives

In the research group where the project was carried out, the synthesis and characterization of several 2-(hydroxyimino)aldehydes (HIAs) revealed interesting features that make them potential candidates as pKa, light and redox stimuli responsive groups. The present PhD work was aimed at exploring the possibilities offered by the highly versatile HIA group towards obtaining novel multi-stimuli responsive polymers. This goal was pursued through the synthesis and characterization of copolymers of oligo(ethylene glycol) methacrylates (OEGMA) with a methacrylate encompassing the HIA moiety (HIABMA). The resulting HIA-bearing copolymers were expected to combine the thermal response of OEGMA with the potential sensitivity to chemical and physical stimuli of the HIA group. To this end, the multistep synthesis of HIABMA was designed and optimized to good yields (35% overall) and high purity. A suitable method for the controlled radical co-polymerization of HIABMA and OEGMA was then found, i.e. Radical Addition-Fragmentation Chain Transfer (RAFT) polymerization with CPDB as chain transfer agent. This method both afforded random copolymers with different monomers ratio (10% to 50% HIABMA) and a 1:1 diblock copolymer. The outcomes of copolymerization reactions were good to excellent in terms of low Đ (<1.2), high conversions (up to 94%) and linear dependence of M_n *vs*. conversion. Responses to temperature, light and a combination of the two were then investigated on select polymers. It was thus found that P(HIABMA-*co*-OEGMA)s exhibit lower cloud points compared to OEGMA homopolymers and to analogous copolymers encompassing only aldehyde or simple oxime groups. As for the light stimulus, the investigation was at first extended to several small HIAs with different substituents, so as to identify the main photochemical phenomena and their dependence on HIA substituents, solvent and excitation wavelength. It was found that along with classical *E/Z* isomerism of the oxime double bond, Norrish-Yang cyclization to cyclobutanol oxime (CBO) also occurs. The relative amount of these two photochemical processes depends on light source (mercury lamps at 350 nm or LEDs at 278 and 365 nm), substituent adjacent to the oxime, solvent and time of irradiation. With these results in mind, the thermal

behaviour of P(HIABMA-*co*-OEGMA) 1:1 aqueous solutions after photostimulation in the mercury lamp (λmax= 350 nm) was assessed and compared to that of the pristine polymer solution. Indeed, the difference in cloud point induced by light is remarkable, as it amounts to a 13°C increase. ^{1}H-NMR analysis of a P(HIABMA-co-OEGMA) 3:7 photostimulated in DMSO-d_6 confirms the occurrence of Norrish-Yang CBO formation, along with further photochemical processes that are currently under investigation. It is worth noting that the isomerization of HIA to CBO, where an aldehyde group is converted to an alcohol, should result in a different polarity of the polymer and in different hydrogen bonding patterns. Such changes may account for considerable effects on the thermal behaviour after irradiation.

In summary, the research presented in this Thesis covered all aspects of the investigation on a novel stimuli-responsive polymer, from monomer and polymer synthesis and characterization to the effect of sequential application of multiple stimuli. Photochemical and NMR experiments were also carried out for a broader understanding of the photochemical behavior of a versatile functional group that was incorporated for the first time in a polymer structure. These experiments aided the interpretation of the results obtained with the polymers. The coupling of light and thermal stimuli in the polymer performance is thus demonstrated and a preliminary interpretation is provided.

The investigation presented in this Thesis constitutes the starting point for a better understanding of the effect of hydrogen bonding patterns provided by aldehydes, oximes and HIAs on polymer solution behavior. Further stimuli, namely pH and redox, should be explored in future work. The Thesis work also hints at possible structural modifications in the HIA monomer that should be pursued in the near future to fine-tune the responsivity of the resulting polymers.

Chapter 6: Experimental section

6.1 CHEMICALS AND INSTRUMENTS

6.1.1 Materials

All products were purchased from Sigma-Aldrich, except sulfur trioxide pyridine complex (SO_3-Pyr) from TCI Chemicals Europe and Sodium Nitrite ACS reagent, hydroxylamine hydrochloride ACS reagent from Carlo Erba Reagents S.r.l., Italy. 2-Cyanopropan-2-yl dithiobenzoate (CPDB) chain transfer agent was purchased from STREM Chemicals, Inc., BISCHHEIM, France. All solvents were purchased from Sigma-Aldrich except dimethylformamide from VWR International, Milan, Italy. Water for cloud point determinations was MilliQ-grade. Chloroform-*d* was from Acros Organics, dimethylsulfoxide-d_6 (DMSO-d_6; glass ampules) was from VWR International.

All products were used as received unless otherwise specified. Tetrahydrofuran (THF) was distilled over sodium under argon atmosphere. Dimethylformamide (DMF) was distilled under reduced pressure (30 mm Hg, 60°C) and stored over 4Å molecular sieves under argon atmosphere. OEGMA was passed through a basic alumina column to remove inhibitor and stored at −20 °C until use. Triethylamine was distilled at ambient pressure before use.

6.1.2 Characterization techniques

All ^{1}H-NMR and ^{13}C-NMR spectra were recorded in $CDCl_3$ and/or DMSO-d_6 on a Bruker Avance 300 spectrometer (300 MHz) except HMBC, recorded on a Bruker Avance 400 spectrometer (400 MHz). Chemical shifts are referred to the solvent signal and expressed in parts per million (δ scale); coupling constants are expressed in Hertz (Hz).

GC–MS analyses have been run on a HP 5892 series II GC, equipped with a 5% phenyl silicone 30m × 0.25mm × 25μm capillary column and coupled to a HP 5972 MSD instrument operating at 70 eV.

ATR FT-IR spectra were recorded using a Thermo Scientific Nicolet iS10 spectrometer equipped with a triglycine sulfate detector (DTGS), and acquired with Omnic vers. 8.1.10 software. The spectra were the result of 32 scans with a spectral

resolution of 4 cm^{-1}. A Smart iTR ATR accessory provided with a diamond ATR crystal was used. An ATR correction algorithm and automatic atmospheric suppression were applied to all spectra.

UV-vis spectra were recorded with a Hewlett Packard 8452 diode array spectrophotometer equipped with an external water bath circulator (Julabo Labortechnik, GmbH) for temperature control (± 0.1 °C), using quartz cuvettes with 1 cm optical path.

Turbidity measurements were performed on a Cary 300 UV-vis double beam spectrophotometer equipped with an external water bath circulator (Julabo Labortechnik, GmbH) for temperature control (± 0.1 °C), using quartz cuvettes with 1 cm optical path.

GPC analyses were performed on a Hewlett Packard Series 1050 HPLC system equipped with a 1047A RI detector and a TSK gel alpha-4000 GPC column (Tosoh, Japan), using DMF with LiBr 0.1% (w/w) as the mobile phase. The system was coupled to Clarity software version 6.2 (DataApex, Prague, The Czech Republic) for signal processing. Molecular weights are relative to monodisperse PEO standards (Agilent).

DLS data were obtained with a NanoZetaSizer (Malvern) equipped with a 5 mW HeNe laser ($\lambda = 632.8$ nm) within a thermostated cell. In this apparatus, the light scattered by the sample is collected at an angle of 173°. Samples (1 or 5 mg/mL) were filtered with 0.45 mm filters (Durapore, Millipore, USA) before mesurements. A 0.1°C/min scanning rate was used both in heating and cooling experiments.

For the work carried out at Regensburg University (Germany): All ^{1}H-NMR and ^{13}C-NMR were recorded in CD_3CN, DMF-d_7 and/or DMSO-d_6 on a Bruker Avance III 600 spectrometer (600 MHz) or on a Bruker Avance 400 spectrometer (400 MHz). Chemical shifts are referred to the solvent signal and expressed in parts per million (δ scale); coupling constants are expressed in Hertz (Hz).

6.2 SYNTHESIS OF MONOMERS

6.2.1 Synthesis of 6-hydroxyhexyl 2-methylprop-2-enoate (1a)[102]

Under N_2 atmosphere, to an ice-cold solution of 1,6-hexanediol (2.00 g, 16.9 mmol) in anhydrous THF (20 mL) were added successively Et_3N (1.17 mL, 8.46 mmol), DMAP (0.206 mg, 1.69 mmol), and methacrylic anhydride (1.26 mL, 8.46 mmol).The mixture was stirred at 0° C for 1 h. MeOH (2.7 mL) was added, and stirring was

maintained for 10 minutes. After solvents evaporation under reduced pressure, the crude mixture was diluted with ethyl acetate (25 mL) and washed with HCl 1 M, saturated $NaHCO_3$, and brine. The organic phase was dried over Na_2SO_4, filtered, and the solvents evaporated under reduced pressure. 1.052 g of a mixture of ester **1a** and the dimethacrylate by-product (**1b**) was obtained and used in the next step without further purification. Pure **1a** was obtained for characterization through silica gel chromatography with a hexane/ethyl acetate gradient. The dimethacrylate byproduct was also isolated, and it accounted for 14% (mol/mol) of the mixture. **1a** yield: 59% (5 mmol).

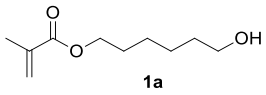

1a

^{1}H-NMR (DMSO-d_6) δ (ppm): 6.00-6.01 (m, 1H, C=C*H*$_2$), 5.65-5.66 (m, 1H, C=C*H*$_2$), 4.32-4.36 (t, 1H, CO*H*, J(t)= 5.2 Hz), 4.05-4.10 (t, 2H, C*H*$_2$O(C=O), J(t)= 6.6 Hz), 3.33-3.40 (td, 2H, C*H*$_2$OH, J(d)= 5.2 Hz, J(t)= 6.2 Hz), 1.87 (m, 3H, C(C=O)C*H*$_3$), 1.57-1.62 (m, 2H, C*H*$_2$CH$_2$O(C=O)), 1.29-1.43 (m, 6H, C*H*$_2$).

^{13}C-NMR ($CDCl_3$) δ (ppm): 167.72 (*C*=O), 136.63 (*C*C=O), 125.37 (C=*C*H$_2$), 64.74 (*C*H$_2$OC=O), 62.86 (*C*H$_2$OH), 32.66, 28.66, 25.86, 25.46, 18.41 (C(C=O)*C*H$_3$).

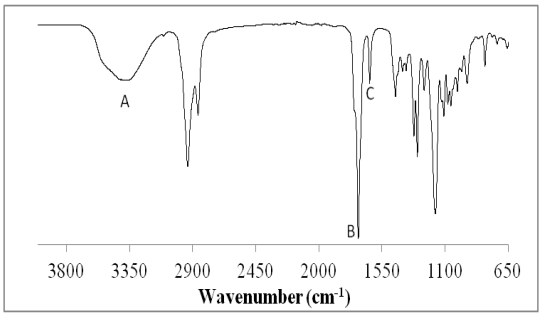

Figure 6.1. FTIR of HHMA: A. O-H stretch, 3367 cm-1; B. Methacrylate C=O stretch, 1718 cm^{-1}; C. C=C stretch, 1637 cm^{-1}

6.2.2 Synthesis of 6-oxohexyl 2-methylprop-2-enoate (OHMA, 2)[103]

Under N_2 atmosphere, to the mixture crude obtained in 6.2.1 (990 mg, 4.6 mmol of **1a**) in dichloromethane (32 mL) was added TEA (2.7 mL, 19.6 mmol), followed, after cooling in an ice bath, by a solution of SO_3-Pyr complex (2.110 g, 13.7 mmol) in DMSO (13.3 mL). The mixture was stirred at room temperature for 24 h. The crude mixture was washed with NH_4Cl (sat), $NaHCO_3$ (sat) and H_2O. The solvent was removed by rotary evaporation, and the mixture was re-dissolved with Et_2O (30 mL), then washed with brine and H_2O. The organic phase was dried over Na_2SO_4, filtered, and the solvents evaporated. The residue was purified by silica gel chromatography

with a hexane/ethyl acetate gradient to afford OHMA (**2**) (835 mg, 4.5 mmol, 98% yield).

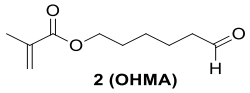

2 (OHMA)

^{1}H-NMR ($CDCl_3$) δ (ppm):9.77-9.78 (t, 1H, C*H*O, J(t)= 1.6 Hz), 6.09 (m, 1H, C=CH_2), 5.54-5.55 (m, 1H, C=CH_2), 4.17-4.13 (t, 2H, CH_2O(C=O), J(t)= 6.6 Hz), 2.43-2.49 (dt, 2H, CH_2CHO, J(t)= 7.2 Hz, J(d)= 1.6 Hz), 1.94 (m, 3H, C(C=O)CH_3), 1.63-1.75 (m, 4H, CH_2), 1.38-1.47 (m, 2H, CH_2).

^{13}C-NMR ($CDCl_3$) δ (ppm): 202.47 (*C*HO); 167.66 (*C*=O), 136.58 (*C*C=O), 125.44 (C=*C*H_2), 64.46 (*C*H_2OC=O), 43.82 (*C*H_2CHO), 28.51, 25.70, 21.17, 18.42 (C(C=O)*C*H_3).

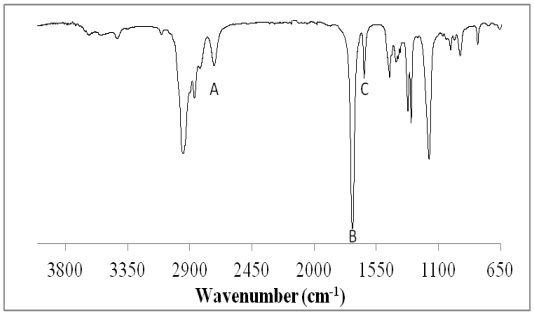

Figure 6.2**.** FTIR of OHMA: A. C(O)-H stretch, 2724 cm^{-1}; B. C=O stretch, methacrylate and unconjugated aldehyde, 1723 cm^{-1}; C. C=C stretch, 1638 cm^{-1}

6.2.3 Synthesis of 6-(hydroxyimino)hexyl 2-methylprop-2-enoate (HIHMA, 3)[138]

To a solution of aldehyde **2** (350 mg, 1.90 mmol) in dichloromethane (8 mL) $NH_2OH{\cdot}HCl$ (284 mg, 3.90 mmol) and Et_3N (1.110 mL, 8 mmol) were added. After stirring for 3.5 hours at room temperature, 5 mL saturated $NaHCO_3$ was added and vigorous stirring was maintained for 1 hour. The mixture was extracted with ethyl acetate, the organic phase was washed with NH_4Cl and brine, then dried over Na_2SO_4, filtered and the solvents evaporated. The residue was dissolved in hexane/ethyl acetate 1:1 and filtered on silica gel to afford HIHMA (**3**) quantitatively.

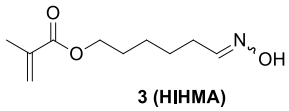

3 (HIHMA)

^{1}H-NMR (DMSO-d_6) δ (ppm): 10.73 (s, 0.5 H, O*H*, *Z* isomer); 10.36 (s, 0.5 H, O*H*, *E* isomer); 7.26-7.32 (t, 0.5 H, C*H*=NOH , *E* isomer, J(t)= 5.9 Hz); 6.61-6.65 (t, 0.5 H, C*H*=NOH, *Z* isomer, J(t)= 5.4 Hz); 6.01 (m, 1H, C=CH_2) ; 5.64-5.67 (m, 1H, C=CH_2); 4.05-4.12 (t, 2H, CH_2O(C=O) , J(t)= 6.5 Hz); 2.22-2.29 (dt, 1H, CH_2C(NOH), *Z* isomer, J(t)= 7.2 Hz, J(d)= 5.5 Hz); 2.05-2.11 (m, 1H, CH_2C(NOH), *E* isomer, J(t)= 7.0 Hz, J(d)= 6.0 Hz); 1.86 (m, 3H, C(C=O)CH_3); 1.30-1.65 (m, 4H, CH_2).

^{13}C-NMR (DMSO-d_6) δ (ppm): 166.45 (*C*=O), 135.99 (*C*C=O), 125.34 (C=*C*H_2), 64.13 (*C*H_2OC=O), 28.67, 27.39, 25.05, 24.86, 17.84 (C(C=O)*C*H_3).

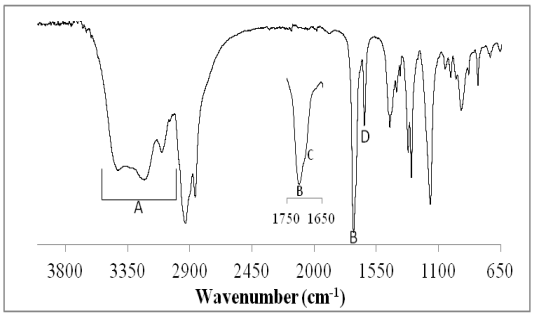

Figure 6.3. FTIR of HIHMA: A. C(O)-H stretch, 3423-3101 cm^{-1}; B. C=O stretch, methacrylate 1714 cm^{-1}; C. C=N(OH) stretch, shoulder at ≈1690 cm^{-1}; D. C=C stretch, 1637 cm^{-1}

6.2.4 Synthesis of 5-(hydroxyimino)-6-oxohexyl 2-methylprop-2-enoate (HIABMA, 1)[85]

Following strictly this order, p-TSA (171 mg, 0.9 mmol), DMF (7 mL), H_2O (162 μL, 9 mmol), pyrrolidine (75 μL, 0.9 mmol), aldehyde **2** (829 mg, 4.5 mmol) were mixed. The mixture was cooled at 0 °C for 5 minutes, then $NaNO_2$ (311 mg, 4.5 mmol) and $FeCl_3$ (730 mg, 4.5 mmol) were added in small aliquots. The mixture was stirred at room temperature for 24 h. Ethyl acetate (7 mL) and NH_4Cl sat (6 mL) were added and stirring was maintained for 30 minutes. The crude mixture was extracted twice more with ethyl acetate. The combined extracts were washed with brine, dried over Na_2SO_4, filtered, and the solvents evaporated. The residue was purified by silica gel chromatography (hexane/ethyl acetate gradient) to afford HIABMA (**1**) (575 mg, 2.7 mmol, 60%).

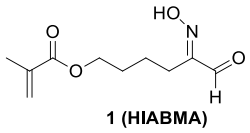

1 (HIABMA)

^{1}H-NMR (DMSO-d_6) δ (ppm): 12.92 (s, 1H, NO*H*, *E* isomer) 9.40 (s 1H, C*H*O, *E* isomer), 5.99 (m, 1H, C=CH_2); 5.65-5.66 (m, 1H, C=CH_2); 4.05-4.09 (t, 2H, CH_2O(C=O), J(t)= 6.2 Hz); 2.35-2.40 (t, 2H, CH_2CHO, J(t)= 7.3 Hz); 1.86 (m, 3H, C(C=O)CH_3); 1.41-1.65 (m, 4H, CH_2).

^{13}C-NMR (DMSO-d_6) δ (ppm): 192.25 (*C*HO); 167.16 (*C*=O), 159.71 (*C*=NOH); 136.31 (*C*C=O), 125.81 (C=*C*H_2), 64.13(*C*H_2OC=O), 28.45, 21.91, 20.99, 18.42 (C(C=O)*C*H_3).

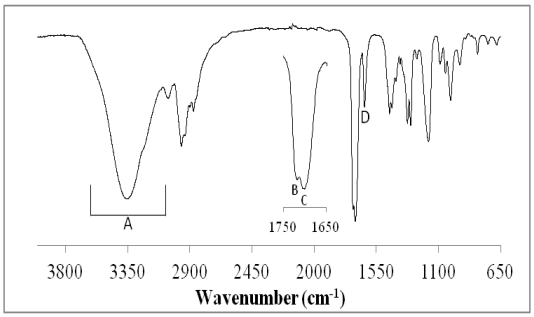

Figure 6.4. FTIR of HIAHMA: A. C(O)-H stretch, 3553-3053 cm^{-1}; B. C=O stretch, methacrylate 1718 cm^{-1}; C. C=N(OH) and C=O conjugated aldehyde stretch, 1704-1700 cm^{-1}; D. C=C stretch, 1634 cm^{-1}

UV-visible spectroscopy

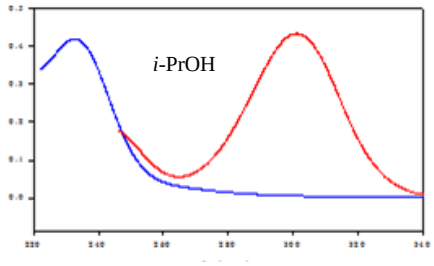

[**1**]= 2.5 10^{-5} M
[**1**]/[Me_4NOH]= [1.3 10^{-5} M]/ [4.5 10^{-5} M]

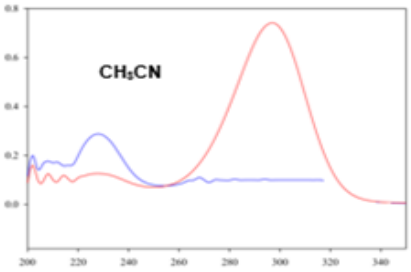

[**1**]= 1.6 10^{-5} M
[**1**]/[Me_4NOH]= 1/4

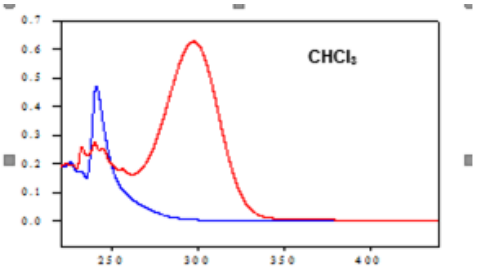

[**1**]= 2.5 10^{-5} M
[**1**]/[Me_4NOH]= [2.2 10^{-5} M]/ [7.5 10^{-5} M]

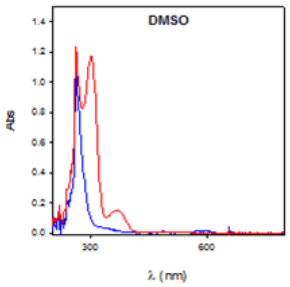

[**1**]= 1.2 10^{-3} M
[**1**]/[Me_4NOH]= 1/2

6.2.5 Synthesis of 4-((tert-butyldimethylsilyl)oxy)-2-methylbutan-2-ol (5)[139]

At room temperature, under N_2, 3-methyl-1,3-butanediol (520 mg, 5 mmol) was added to a solution of DMAP (25 mg, 0.2 mmol) in anhydrous diethyl ether (13 mL). The resulting solution was cooled to 0°C and then, under N_2, triethylamine (1.5 mL, 12 mmol) and tert-butyldimethylsilyl chloride (1.55 g, 10 mmol) were added. The reaction mixture was stirred for 18 hours and the disappearance of diol was followed by GC-MS analysis. The crude mixture was used in the next step without purification, while an aliquot was withdrawn for ^{1}H-NMR analysis.

^{1}H-NMR spectrum showed that tert-butyldimethylsilyl chloride had reached only with primary alcohol.

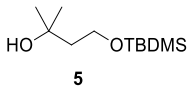

5

^{1}H-NMR (DMSO-d_6), δ (ppm): 4.71 (s, 1H, $C(CH_3)_2OH$); 3.69 (t, 2H, CH_2OSi, J(t)= 7.4 Hz); 1.59 (t, 2H, CH_2CH_2OSi, J(t)= 7.3 Hz); 0.85 (s, 9H, $SiC(CH_3)_3$); 0.84 (s, 6H, $C(CH_3)_2$); 0.02 (s, 6H, $SiCH_3$)

6.2.6 Synthesis of 4-hydroxy-2-methylbutan-2-yl 2-methylprop-2-enoate (7a)[102]

Under N_2 atmosphere, to crude reaction mixture of **5** (5 mmol) in anhydrous diethyl ether (20 mL) were added successively Et_3N (2.775 mL, 20 mmol), DMAP (30.5 mg, 0.25 mmol), and methacrylic chloride (1.955 mL, 20 mmol) at 0°C. The mixture was stirred for 3 days and the disappearance of **5** was followed by GC-MS analysis. MeOH

(1 mL) was added and stirring was maintained for 10 minutes to eliminate the excess of methacrylic chloride. The crude mixture was filtrated and diluted with anhydrous diethyl ether (50 mL) and washed with NH_4Cl (sat) and brine. The organic phase was dried over Na_2SO_4 and filtered.

A solution of tetrabutylammonium fluoride (TBAF)[140] in THF (15 mL (15 mmol) of 1M) was added dropwise to a solution of crude reaction mixture of **6** at 0°C. The reaction mixture was stirred at 0°C until the complete disappearance of **6** followed by GC analysis. The gradual appearance of two new peaks in GC analysis during the deprotection of product **6** and the following ^{1}H-NMR analysis showed the formation of the undesired product **7b** beside **7a** through transesterification. The reaction was stopped adding 15 mL of water, and the crude mixture was extracted twice with AcOEt and the reunited organic phase was washed twice with brine. The organic phase was dried over Na_2SO_4, filtered, and the solvents evaporated. The residue was purified by silica gel chromatography with a hexane/ethyl acetate gradient to afford **7a** (300 mg, 1.75 mmol, 35% yield) and **7b** (259 mg, 1.51 mmol, 30% yield).

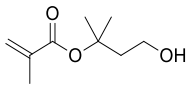

7a

^{1}H-NMR ($CDCl_3$), δ (ppm): 5.98 (s, 1H, C=CH_2); 5.49 (m, 1H, C=CH_2); 3.79 (t, 2H, CH_2OH, J(t)= 6.8 Hz); 2.07 (t, 2H, CH_2CH$_2$OH, J(t)= 6.8 Hz); 1.89 (m, 3H, C(C=O)CH_3); 1.53 (s, 6H, C(CH_3)$_2$).

^{13}C-NMR ($CDCl_3$), δ (ppm): 166.8 (*C*=O); 137.8 (*C*C=O); 124.8 (C=*C*H$_2$); 82.0 (*C*(CH$_3$)$_2$); 59.1 (*C*H$_2$OH); 43.6 (*C*H$_2$CH$_2$OH); 26.5 (C(*C*H$_3$)$_2$; 18.5 (C(C=O)CH$_3$).

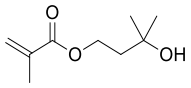

7b

^{1}H-NMR ($CDCl_3$), δ (ppm): 6.09 (s, 1H, C=CH_2); 5.55 (m, 1H, C=CH_2); 4.31 (t, 2H, CH_2O(C=O), J(t)= 7.0 Hz); 1.93 (m, 3H, C(C=O)CH_3); 1.88 (t, 2H, CH_2CH$_2$O, J(t)= 7.0 Hz); 1.75 (broad, 1H, CH$_2$O*H*) 1.26 (s, 6H, C(CH_3)$_2$).

^{13}C-NMR ($CDCl_3$), δ (ppm): 167.6 (*C*=O); 136.4 (*C*C=O); 125.7 (C=*C*H$_2$); 70.21 (*C*(CH$_3$)$_2$); 61.8 (*C*H$_2$O(C=O)); 41.7 (*C*H$_2$CH$_2$O); 29.8 (C(*C*H$_3$)$_2$; 18.5 (C(C=O)CH$_3$).

6.2.7 Synthesis of 2-methyl-4-oxobutan-2-yl 2-methylprop-2-enoate (8)

Parikh-Doering[103]

Under N_2 atmosphere, to the mixture of **7a** and **7b** (120 mg, 60 of **7a**) in dichloromethane (3 mL) was added TEA (350 μL, 2.52 mmol), followed, after cooling in an ice bath, by a solution of SO_3-Pyr complex (280 mg, 1.72 mmol) in DMSO (1.9 mL). The mixture was stirred at room temperature for 20 h. The crude mixture was washed with NH_4Cl (sat), $NaHCO_3$ (sat) and H_2O. The solvent was removed by rotary evaporation, and the mixture was re-dissolved with DCM (5 mL), then washed with

brine and H_2O. The organic phase was dried over Na_2SO_4, filtered, and the solvents evaporated. ^{1}H-NMR analysis of the crude mixture showed no formation of aldehyde **8**, while signal at 3.79 ppm (C*H*$_2$OH) was completely disappeared. From the new signals at 4.13 ppm and 3.10 ppm one could hypothesize that the reaction stopped with the formation of adduct with DMSO.[141]

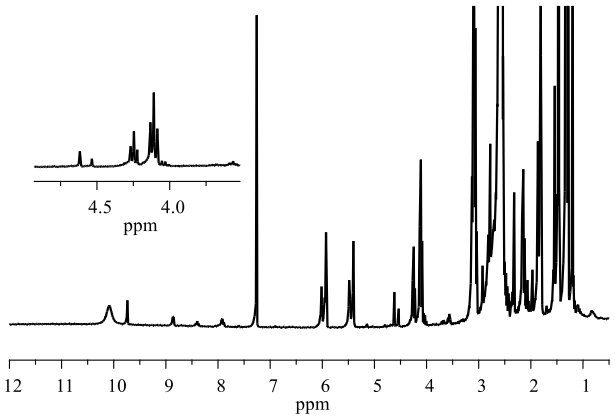

Figure 6.5. ^{1}H-NMR spectrum of crude mixture of Parikh-Doering of **7a** (in presence of **7b**).

TEMPO/BAIB oxidation[142]

To a mixture 1:1 of **7a** and **7b** (18 mg, 0.1 mmol of **7a**) in dichloromethane (0.5 mL) was added TEMPO (8 mg, 0.05 mol) and, in small portion, BAIB (125 mg, 0.38 mmol). The mixture was stirred at room temperature for 3h. The crude mixture was washed with NH_4Cl (sat), $NaHCO_3$ (sat) and H_2O. The organic phase was dried over Na_2SO_4, filtered, and the solvents evaporated. ^{1}H-NMR analysis of the crude mixture showed no formation of aldehyde **8**, while signal at 3.79 ppm (C*H*$_2$OH) was completely disappeared.

PCC oxidation[143]

To a mixture 1:1 of **7a** and **7b** (37 mg, 0.2 mmol of **7a**) in dichloromethane (0.5 mL) was added pyridinium chlorochromate (PCC, 62 mg, 0.29 mmol). The mixture was stirred at room temperature for 3 h and the disappearance of **7a** was followed by GC-MS. Then, the crude mixture was filtered through celite and the solvent evaporated. The residue was purified by silica gel chromatography with a hexane/ethyl acetate 20/1. The product **8** was volatile and was lost during rotatory evaporation of solvent.

6.2.8 Synthesis of 3,3-dimethylpentane-1,5-diol (10)[144]

Under N_2 atmosphere, to the solution of $LiAlH_4$ in THF (1 M, 20 mL) was added Et_2O (10 mL). The reaction mixture was cooled to 0°C and a solution of 3,3-dimethyl

glutaric acid (1.60 g, 10 mmol) in THF (5 mL) and Et_2O (5 mL) was added dropwise. Then, the solution was maintained at reflux for 75 minutes. Successively, a solution of NaOH in H_2O (3 M, 20 mL) was added at room temperature. After 5 minutes, AcOEt (50 mL) and brine (25 mL) were added and stirring was maintained for 30 minutes. The crude mixture was extracted twice more with ethyl acetate. The combined extracts were dried over Na_2SO_4, filtered, and the solvents evaporated. The product **10** was obtained in quantitative yield. (1.290 g, 9.9 mmol).

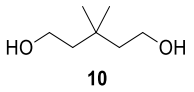

10

^{1}H-NMR ($CDCl_3$), δ (ppm): 3.70 (t, 4H, C*H*$_2$OH, J(t)= 7.0 Hz); 1.55 (t, 4H, C*H*$_2$CH$_2$OH, J(t)= 6.8 Hz); 1.75 (broad, 2H, CH$_2$O*H*); 0.92 (s, 6H, C(C*H*$_3$)$_2$).

6.2.9 Synthesis of 5-hydroxy-3,3-dimethylpentyl 2-methylprop-2-enoate (11a)[102]

Under N_2 atmosphere, to an ice-cold solution of **10** (1.290 g, 9,9 mmol) in anhydrous THF (7 mL) were added successively Et_3N (0.7 mL, 5 mmol), DMAP (12 mg, 10 mmol), and methacrylic anhydride (0.7 mL, 5 mmol). The mixture was stirred at 0° C for 1 h. MeOH (2 mL) was added, and stirring was maintained for 10 minutes. After solvents evaporation under reduced pressure, the crude mixture was diluted with ethyl acetate (8 mL) and washed with HCl 1 M, saturated $NaHCO_3$, and brine. The organic phase was dried over Na_2SO_4, filtered, and the solvents evaporated under reduced. The residue was purified by silica gel chromatography with a hexane/ethyl acetate gradient to afford **11a** (470 mg, 2.35 mmol, 47% yield) and **11b** (267 mg, 1 mmol, 20% yield).

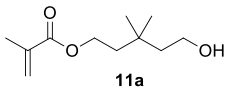

11a

^{1}H-NMR ($CDCl_3$), δ (ppm): 6.07(s, 1H, C=C*H*$_2$); 5.54 (m, 1H, C=C*H*$_2$); 4.20 (t, 2H, C*H*$_2$O(C=O), J(t)= 7.2 Hz); 3.71 (t, 2H, C*H*$_2$OH, J(t)= 7.6 Hz); 1.93 (m, 3H, C(C=O)C*H*$_3$); 1.65-1.51 (m, 4H, C*H*$_2$CH$_2$O,); 0.96 (s, 6H, C(C*H*$_3$)$_2$).

^{13}C-NMR ($CDCl_3$), δ (ppm): 167.7 (*C*=O); 136.5 (*C*C=O); 125.1(C=*C*H$_2$); 62.0 (*C*H$_2$OC=O); 59.7 (*C*H$_2$OH); 44.7; 40.13; 31.78; 27.8 (C(*C*H$_3$)$_2$; 18.5 (C(C=O)CH$_3$).

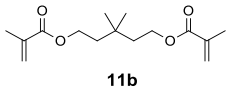

11b

^{1}H-NMR ($CDCl_3$), δ (ppm): 6.07(s, 2H, C=C*H*$_2$); 5.54 (m, 2H, C=C*H*$_2$); 4.21 (t, 4H, C*H*$_2$O(C=O), J(t)= 7.3 Hz); 1.93 (m, 6H, C(C=O)C*H*$_3$); 1.66 (t, 4H, C*H*$_2$CH$_2$O, J(t)= 7.3 Hz); 0.99 (s, 6H, C(C*H*$_3$)$_2$).

6.2.10 Synthesis of 3,3-dimethyl-5-oxopentyl 2-methylprop-2-enoate (12)[103]

Under N_2 atmosphere, to **11a** (470 mg, 2.35 mmol) in dichloromethane (16.5 mL) was added TEA (1.41 mL, 9.4 mmol), followed, after cooling in an ice bath, by a solution of SO_3-Pyr complex (1.146 g, 7.05 mmol) in DMSO (7 mL). The mixture was stirred at room temperature for 18 h. The crude mixture was washed with NH_4Cl (sat),

$NaHCO_3$ (sat) and H_2O. The solvent was removed by rotary evaporation, and the mixture was re-dissolved with Et_2O (30 mL), then washed with brine and H_2O. The organic phase was dried over Na_2SO_4, filtered, and the solvents evaporated. The residue was purified by silica gel chromatography with a hexane/ethyl acetate gradient to afford **12** (290 mg, 1.46 mmol, 62% yield).

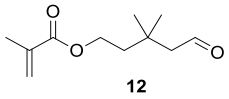

12

^{1}H-NMR ($CDCl_3$), δ (ppm): 9.84 (t, 1H, (C=O)*H*, J(t)= 2.8 Hz); 6.07(s, 1H, C=C*H*$_2$); 5.55 (m, 1H, C=C*H*$_2$); 4.23 (t, 2H, C*H*$_2$O(C=O), J(t)=7.0 Hz); 2.34 (d, 2H, C*H*$_2$(C=O)H, J(d)= 2.8 Hz); 1.92 (m, 3H, C(C=O)C*H*$_3$); 1.77 (t, 2H, C*H*$_2$CH$_2$O, J(t)= 7.0 Hz); 1.12 (s, 6H, C(C*H*$_3$)$_2$).

^{13}C-NMR ($CDCl_3$), δ (ppm): 202.9 ((C=O)*H*); 167.5 (*C*=O); 136.4 (*C*C=O); 125.7(C=*C*H$_2$); 61.5 (*C*H$_2$OC=O); 54.9; 40.3; 32.8; 27.8 (C(*C*H$_3$)$_2$; 18.5 (C(C=O)CH$_3$).

6.2.11 Synthesis of 4-(hydroxyimino)-3,3-dimethyl-5-oxopentyl 2-methylprop-2-enoate (13)[85]

Following strictly this order, p-TSA (56 mg, 0.325 mmol), DMF (2.88 mL), H_2O (52.7 μL, 2.98 mmol), pyrrolidine (24.6 μL, 0.3 mmol), aldehyde **12** (290 mg, 1.46 mmol) were mixed. The mixture was cooled at 0 °C for 5 minutes, then $NaNO_2$ (102.3 mg, 1.5 mmol) and $FeCl_3$ (238 mg, 1.5 mmol) were added in small aliquots. The mixture was stirred at room temperature for 24 h. Ethyl acetate (2.5 mL) and NH_4Cl sat (2 mL) were added and stirring was maintained for 30 minutes. The crude mixture was extracted twice more with ethyl acetate. The combined extracts were washed with brine, dried over Na_2SO_4, filtered, and the solvents evaporated. The residue was purified by silica gel chromatography (hexane/ethyl acetate gradient) to afford **13** (86 mg, 0.37 mmol, 26%). ^{1}H-NMR spectrum of **13** reveals the presence of other unidentified products.

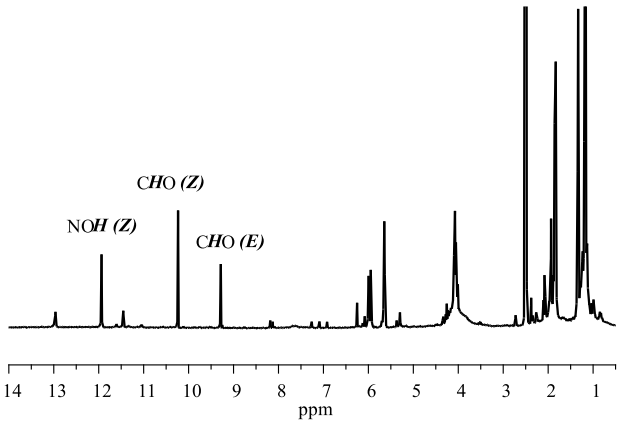

Figure 6.6. Compound **13** after silica gel chromatography.

6.3 POLYMERIZATION REACTIONS

6.3.1 Random copolymerization

The monomers (OEGMA or mixtures of OEGMA and OHMA, HIHMA, or HIABMA, 3 mmol total), CPDB (8.75 mg, 0.04 mmol), AIBN (1.64 mg, 0.01 mmol) and DMF (2.5 mL) were charged in a 20 mL schlenk. The schlenk was capped with a rubber septum and the solution was purged with nitrogen gas for 30 min. Then the mixture was heated to the desired temperature and maintained under vigorous magnetic stirring for 6–9 hours. During the polymerization, samples of 250 mg were taken at fixed time intervals under a nitrogen stream for the kinetic studies. For final workup, the reaction was quenched with air, and the polymer was phase-separated in an excess of diethyl ether at room temperature. The supernatant was removed and the oily residue was washed three more times with fresh diethyl ether. The ether solutions were kept for NMR analysis of unreacted monomers. The product was then dried under high vacuum at room temperature for 24 h, with the exception of OHMA copolymers, which tend to degrade under vacuum, yielding an insoluble residue. These were dried under a nitrogen stream. Monomer ratio in the final product was also determined as part of polymer characterization by ^{1}H-NMR in DMSO-d_6 or $CDCl_3$ after reaction workup.
All homopolymerizations and copolymerizations (monomers ratio 3:7) were carried out at least twice and only small differences were observed (within ± 5%). Examples of polymerizations reproducibility are reported in Figure 6.7.

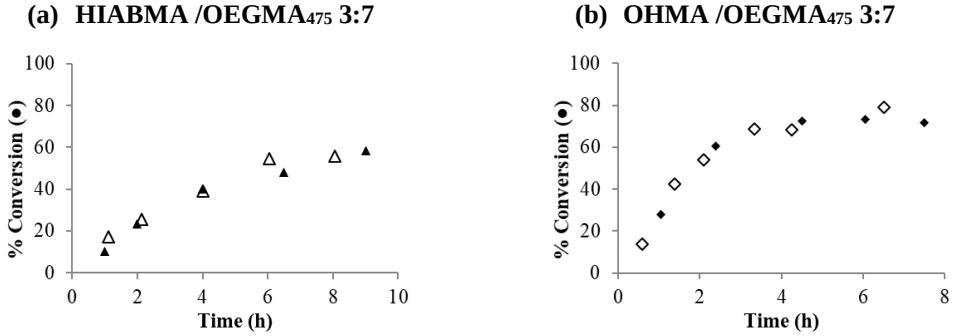

Figure 6.7. Examples of polymerization reproducibility: Conversion *vs.* time for $OEGMA_{475}$ copolymerization with HIABMA (a) and OHMA (b) at 70% (mol/mol) OEGMA reaction feed. Empty and filled symbols refer to different experiments of the same polymerization.

6.3.2 Block polymerization

OEGMA (4 mmol total), CPDB (11.65 mg, 0.053 mmol), AIBN (1.64 mg, 0.013 mmol) and DMF (6.15 mL) were charged in a 20 mL schlenk. The schlenk was capped

with a rubber septum and the solution was purged with nitrogen gas for 30 min. Then the mixture was heated to 72°C and maintained under vigorous magnetic stirring for 3 hours (Monomer conversion: 45%). For final workup, the reaction was quenched with air, and the polymer was phase-separated in an excess of diethyl ether at room temperature. The supernatant was removed and the oily residue was washed three more times with fresh diethyl ether. The product was then dried under high vacuum at room temperature for 24 h. $POEGMA_{500}$ was obtained with 32% yield (616 mg) and M_n (GPC) 11.00 kDa.

Chain extension[145]

The underestimation of GPC molecular weight for brushed-based polymer was taken into account for chain extension reaction.[110] HIABMA (308 mg, 1.446 mol) or $OEGMA_{500}$ (723 mg, 1.446 mmol), macroCTA (311 mg, 0.01446 mmol), AIBN (1.18 mg, 0.0072 mmol) and DMF (1.8 mL) were charged in a 20 mL schlenk. Then the mixture was heated to the desired temperature and maintained under vigorous magnetic stirring for 6 hours. During the polymerization, samples of 250 mg were taken at fixed time intervals under a nitrogen stream for the kinetic studies. Monomer conversions are determined by ^{1}H-NMR analysis. For final workup, the reaction was quenched with air, and the polymer was phase-separated in an excess of diethyl ether at room temperature. The supernatant was removed and the oily residue was washed three more times with fresh diethyl ether. The product was then dried under high vacuum at room temperature for 24 h. Monomer ratio in the final product was also determined as part of polymer characterization by ^{1}H-NMR in $CDCl_3$ after reaction workup.

6.3.3 Monomer conversions

Conversions were determined by ^{1}H-NMR in $CDCl_3$ and/or GPC according to eqn (6.1). Correlation of GPC conversions vs. NMR values is shown in Chapter 2 for P(HIABMA-*co*-$OEGMA_{475}$) 3 :7.

$$\text{Conv } (\%) = 100 * \frac{(I_0 - I_t)}{I_0} \qquad \text{Equation 6.1}$$

In ^{1}H-NMR measurements, I_0 and I_t were the integrals of vinyl signals, normalized to a convenient proton signal. In GPC measurements, I_0 and I_t were obtained as follows: a carefully weighed, homogeneous reaction crude aliquot (about 10–30 mg) was diluted with a weighed amount of DMF for GPC analysis; I_0 and I_t were the areas at

reaction time 0 and t of the peak of the co-eluted monomers, normalized to the sample weight.

6.3.4 Calculation of monomer incorporation

The ratio of the incorporated monomers at different timepoints during the copolymerization reactions was indirectly quantitated through equation (6.2) by determining the % depletion of each monomer in the reaction crudes by ^{1}H-NMR.

$$R_t = \frac{S_0^{OEGMA} - S_t^{OEGMA}}{S_0^{M} - S_t^{M}} \qquad \text{Equation 6.2}$$

In equation (6.2), *S* is the integral of vinyl signals of *cis* protons to the methacrylates ester group ($\boldsymbol{S_{0,t}^{OEGMA}}$: 6.12 ppm, $\boldsymbol{S_{0,t}^{M}}$: 6.08-6.09 ppm for all other monomers), using a convenient proton signal as the internal standard.

Example of monomer incorporation and conversion determined by ^{1}H-NMR

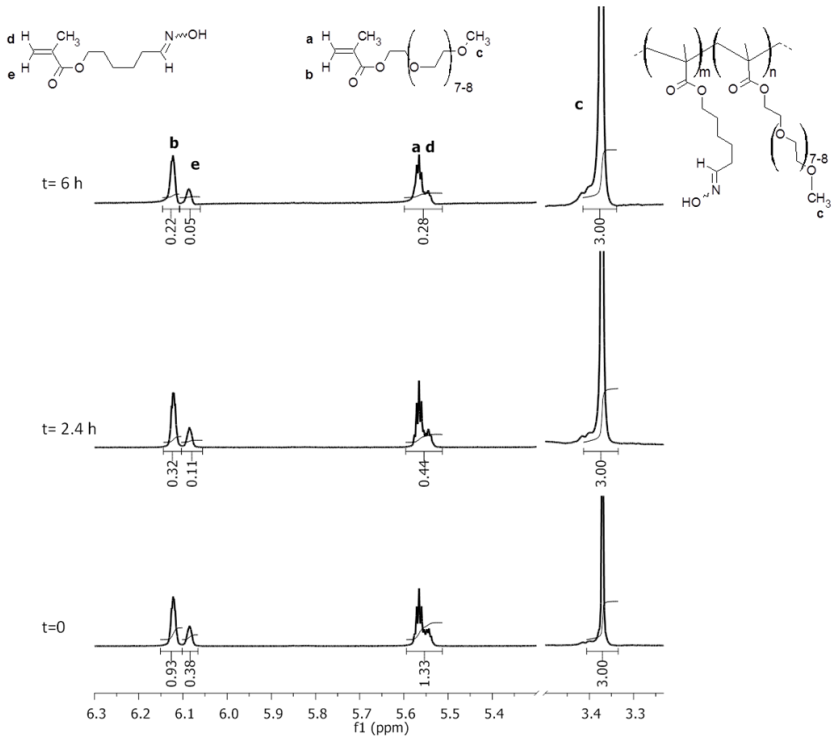

The OCH_3 signal of $OEGMA_{475}$ (3.37 ppm, $CDCl_3$) is the sum of monomer and polymer OCH_3 intensities and, therefore, can be used as internal standard.

- Ratio (R_t) of incorporated monomers at time:

$$R_t = \frac{S_0^{OEGMA} - S_t^{OEGMA}}{S_0^{M} - S_t^{M}}, \text{ where } S_{0,t}^{OEGMA} = \frac{I(6.12\text{ ppm})}{I(3.37\text{ ppm})/3} \text{ and } S_{0,t}^{HIHMA} = \frac{I(6.06\text{ ppm})}{I(3.37\text{ ppm})/3}$$

- Overall monomers conversion (eq. 6.1)

$$Conv\% = 100 \times \frac{(I_0 - I_t)}{I_0}\text{, where } I_{0,t} = \frac{I(5.57-5.54\text{ ppm})}{I(3.37\text{ ppm})/3}$$

6.3.5 FTIR spectra of OEGMA$_{475}$ copolymers

P(OHMA-*co*-OEGMA$_{475}$) 3:7	
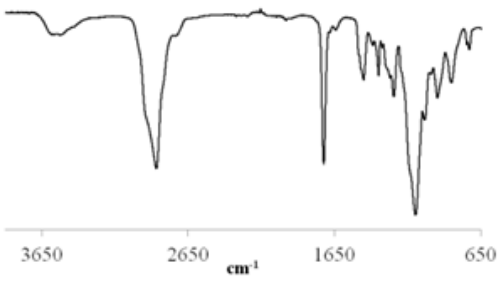	FTIR: C=O stretch methacrylate and unconjugated aldehyde, 1722 cm^{-1}
P(HIHMA-*co*-OEGMA$_{475}$)	
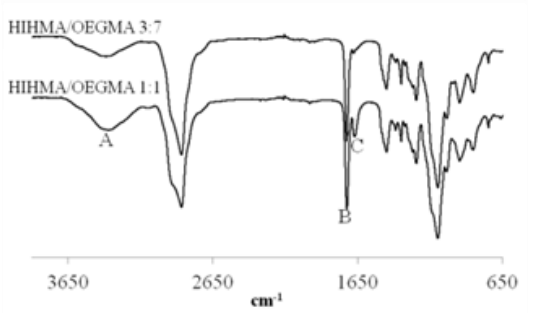	FTIR: A. NO-H stretch, 3380 cm^{-1}; B. C=O stretch, 1726 cm^{-1}; C. C=N stretch 1677-1671 cm^{-1}.
P(HIABMA-*co*-OEGMA$_{475}$)	
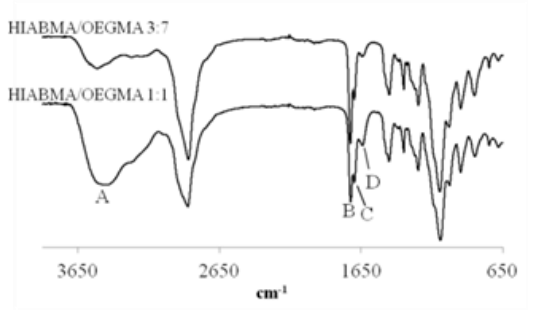	FTIR: A. NO-H stretch, 3460-3518 cm^{-1}; B. C=O ester stretch, 1722-1726 cm^{-1}; C. C=O aldehyde stretch, 1698-1697 cm^{-1}; D. C=N stretch 1638-1640 cm^{-1}.

6.4 PHOTOCHEMICAL BEHAVIOR OF HIAs

6.4.1 Synthesis of HIAs

Compounds **4**, **15** and **16** were already available in the laboratory, whereas **14**, **17**, **18** and **19** were prepared directly from phenyl acetaldehyde, octanal, isovaleraldehyde

and 3-phenylpropionaldehyde, respectively, through α-oximation reaction described in section 6.2.4.[88] Compound **1** was prepared as described in paragraph 6.2.

Yields and characterization of compounds 14, 17, 18 and 19

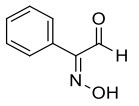

14

Yield: 86%

^{1}H-NMR (DMSO-d_6) δ (ppm): 13.2 (s, 1H, NO*H*); 9.6 (s, 1H, C*H*O); 7.44-7.40 (m, 5H, C*H* $_{arom.}$).

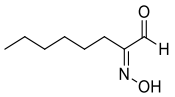

17

Yield: 47%

^{1}H-NMR (DMSO-d_6) δ, (ppm): 12.9 (s, 1H, NO*H*); 9.4 (s, 1H, C*H*O); 2.3 (t, 2H, CH_2, J(t)=7.14 Hz); 1.4 (m, 2H, CH_2); 1.2 (m, 6H, CH_2); 0.8 (m, 3H, CH_3).
^{13}C-NMR (DMSO-d_6 δ, (ppm): 191.9 (*C*HO); 159.4 (*C*=NOH); 30.9; 28.7; 24.9; 21.9; 21.3; 13.9.

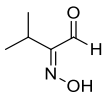

18

Yield: 55%

^{1}H-NMR (DMSO-d_6) δ (ppm): 12.9 (s, 1H, NO*H*); 9.3 (s, 1H, C*H*O); 3.2 (sept., 1H, C*H*, J(s)=7.0 Hz); 1.12 (s, 6H, CH_3, J=7.14 Hz).
^{13}C-NMR (DMSO-d_6 δ, (ppm): 192.0(*C*HO); 162.2 (*C*=NOH); 23.2; 17.2.

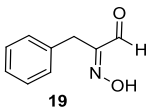

19

Yield: 63%

^{1}H-NMR (DMSO-d_6) δ (ppm): 13.1 (s, 1H, NO*H*); 9.5 (s, 1H, C*H*O); 7.26-7.16 (m, 5H, C*H* arom.); 3.71 (s, 2H, CH_2).
^{13}C-NMR (DMSO-d_6) δ (ppm): 192.7 (*C*HO); 158.9 (*C*=NOH); 137.1 (Ph. C_{ipso}); 129.5 (Ph, C_{orto}); 129.4 (Ph, C_{meta}); 127.2 (Ph, C_{para}); 28.2 (*C*H_2).

6.4.2 Photoisomerization with high pressure mercury lamps at 350 nm.

5-10 mg of HIA **1**, **14**, **15** and **16** or P(HIABMA-*co*-OEGMA$_{475}$) 3:7 were weighed in an NMR tube, 0.6 mL dry DMSO-d_6 (ampoules) was rapidly added and purged with argon. Finally, the tube was flame-sealed. The sample was allowed to equilibrate at 40°C for 24h, and ^{1}H-NMR analysis was run before irradiation in a Rayonet RPR-100 photoreactor equipped with 16 lamps emitting in the 350 nm region (Pyrex filtered, lamps details in Figure 6.7, pink curve). The sample was kept in a glass cooling sleeve to avoid excessive heating. After irradiation, the sample was placed in a thermostat at 40°C in the dark for thermal equilibration. Both photoisomerization, and thermal relaxation were monitored by ^{1}H-NMR at suitable timepoints.

6.4.3 Photoisomerization with LED at 278 nm or 365 nm

In a glovebox, 5-10 mg of HIA **14**, **17**, **18** or **19** was weighed in an NMR tube and 0.6 mL dry DMSO-d_6, CD_3CN or DMF-d_7 was added. The sample was allowed to equilibrate at room temperature for 24h, and ^{1}H-NMR analysis was run before irradiation with LED. The LED employed were purchase from LUMITRONIX:365

nm, 100 mW: Nichia SMD LED UV NVSU233A with PCB; 278 nm, 2 mW: LG Innotek LED UV-C 3535 series. Photoisomerization was monitored by ^{1}H-NMR at suitable timepoints.

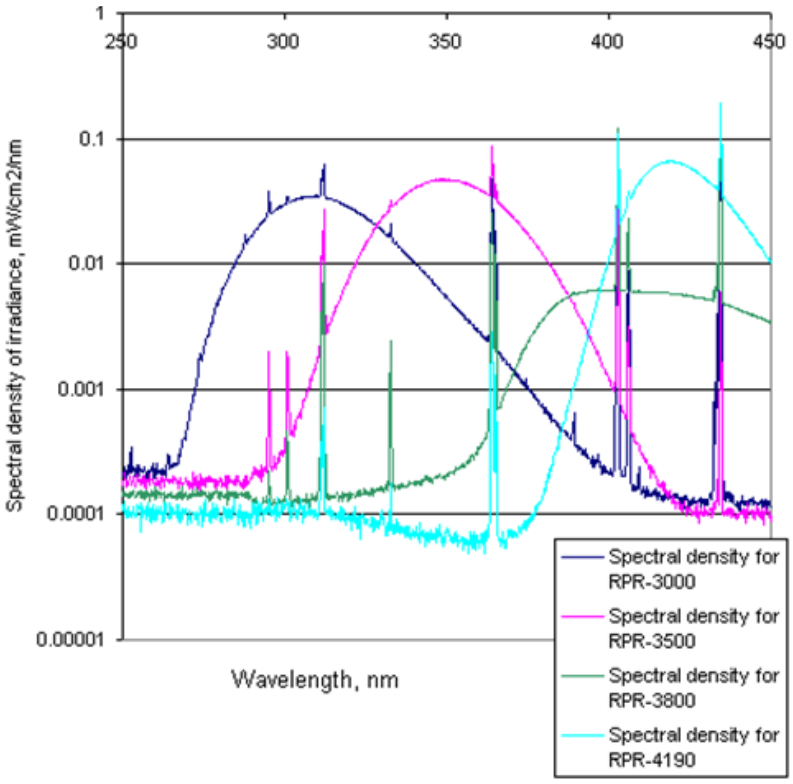

Figure 6.8. Spectral distribution of irradiance density for UV mercury lamps.

6.4.4 Results of photoisomerizations with high pressure mercury lamps at 350 nm.

Photoisomerization of 15

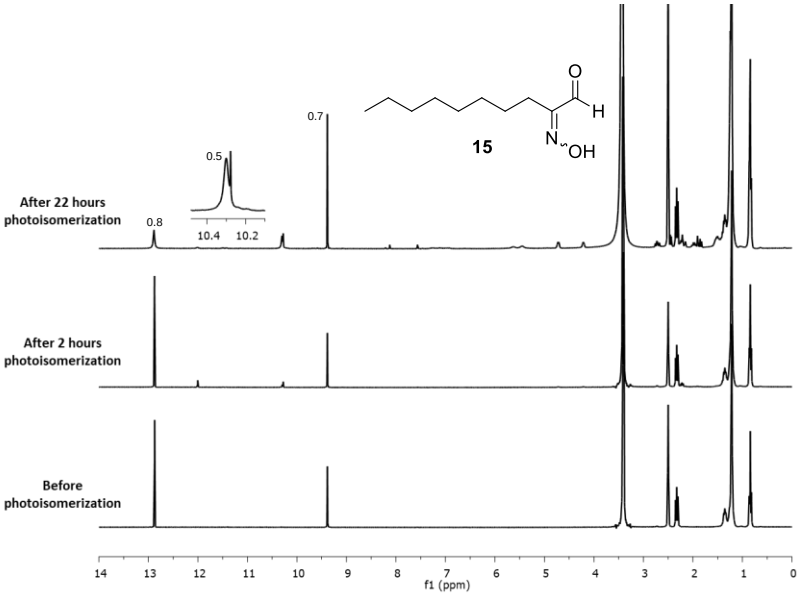

Photoisomerization of 16

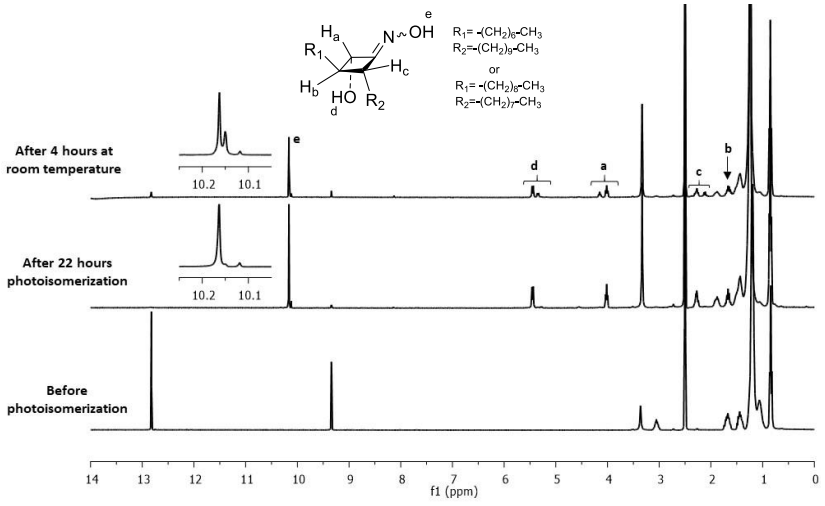

^{1}H-NMR with D_2O exchange

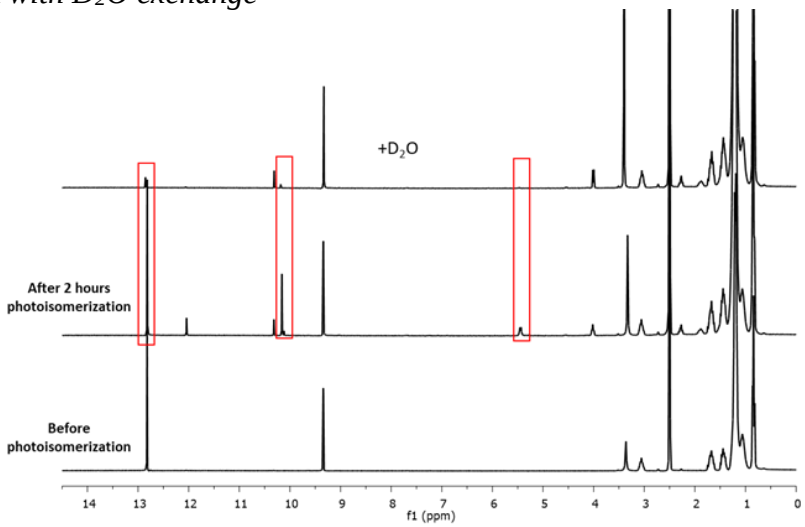

DEPT

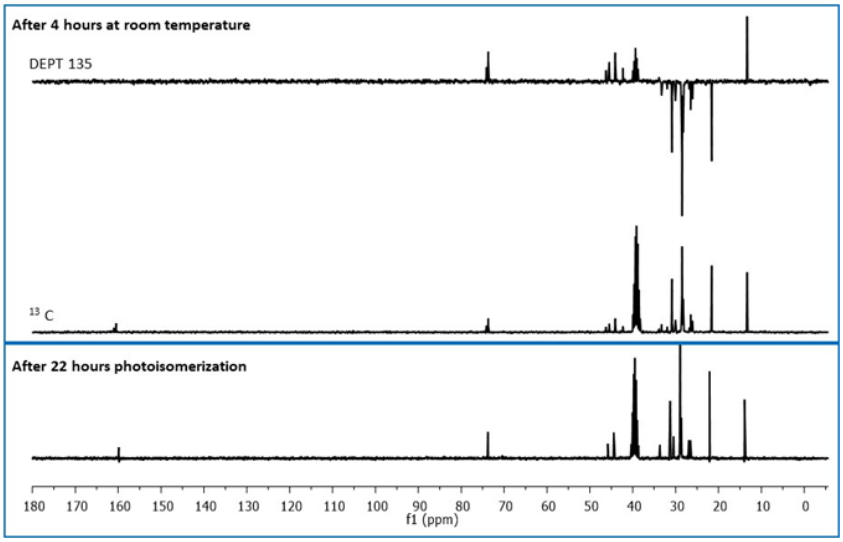

2D spectra of the product derived from Norrish-Yang cyclization of 16

All the 2D spectra of the product derived from photoisomerization of **16** are recorded in DMSO-d_6 after photoisomerization for 22 hours (λ=350 nm) and thermal equilibration for 4 hours.

COSY

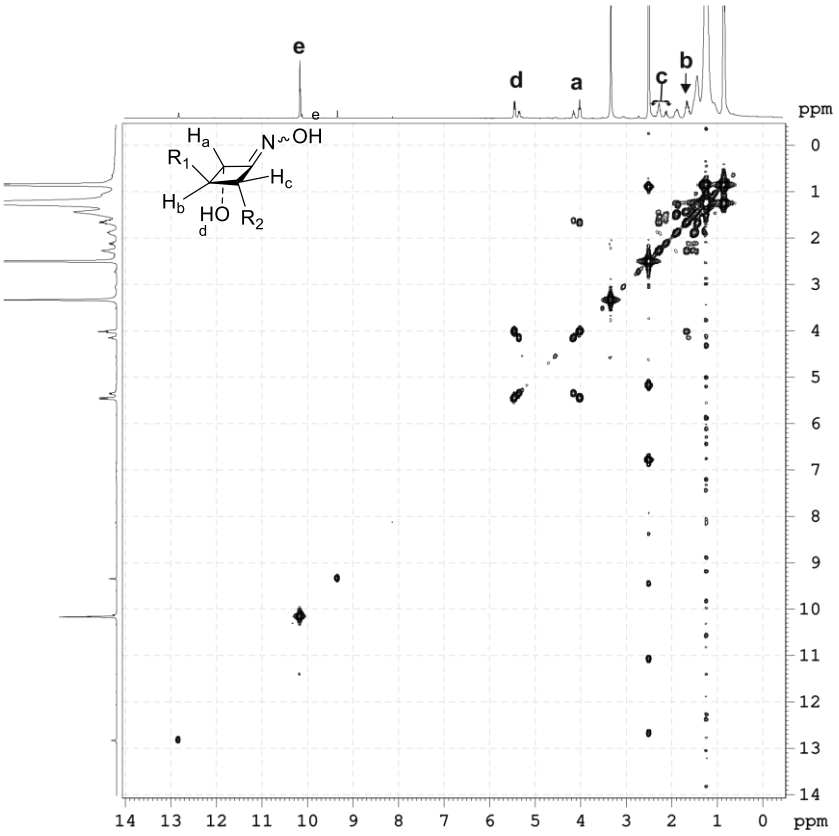
e
d
a
c
b
ppm
Ha
R1
N~OH
Hc
Hb
HO
d
R2
14 13 12 11 10 9 8 7 6 5 4 3 2 1 0 ppm

NOESY

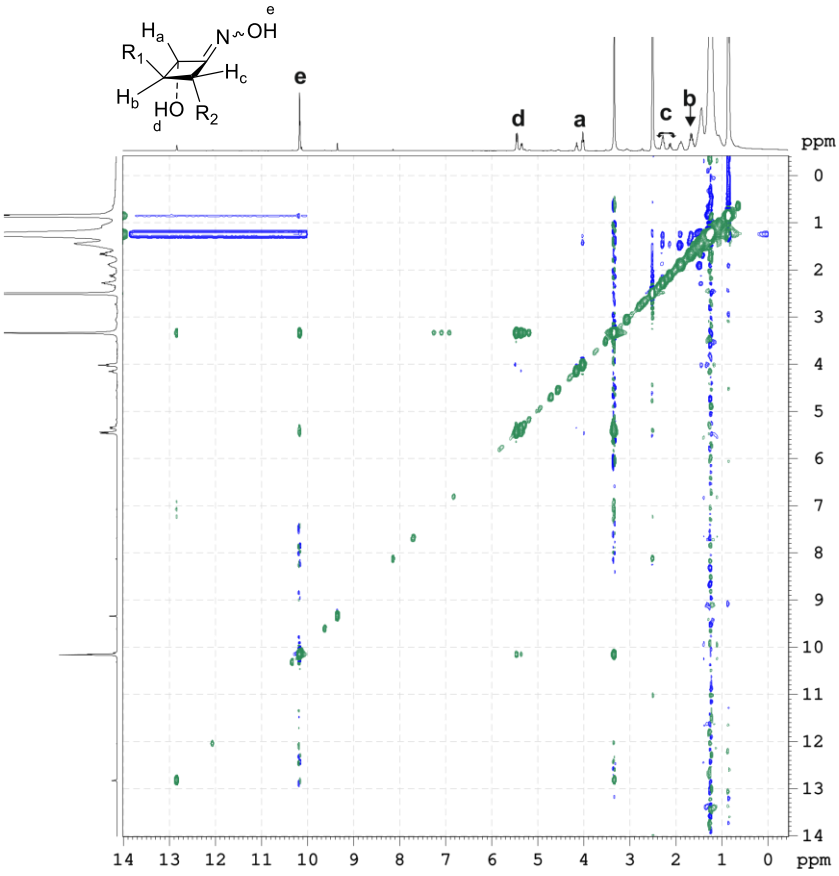
e
Ha
R1
N~OH
Hc
Hb
HO
d
R2
e
d
a
c
b
ppm
14 13 12 11 10 9 8 7 6 5 4 3 2 1 0 ppm

HSQC

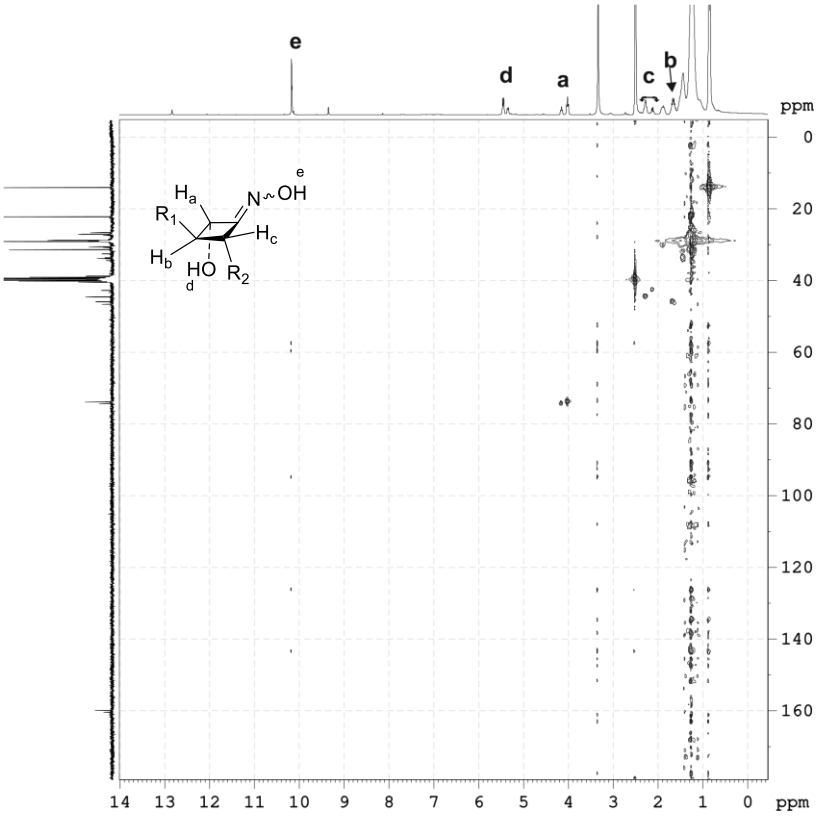
e
d
a
c
b
ppm
0
20
40
60
80
100
120
140
160
14 13 12 11 10 9 8 7 6 5 4 3 2 1 0 ppm
Ha
R1
N
OH
e
Hc
Hb
HO
d
R2

HMBC

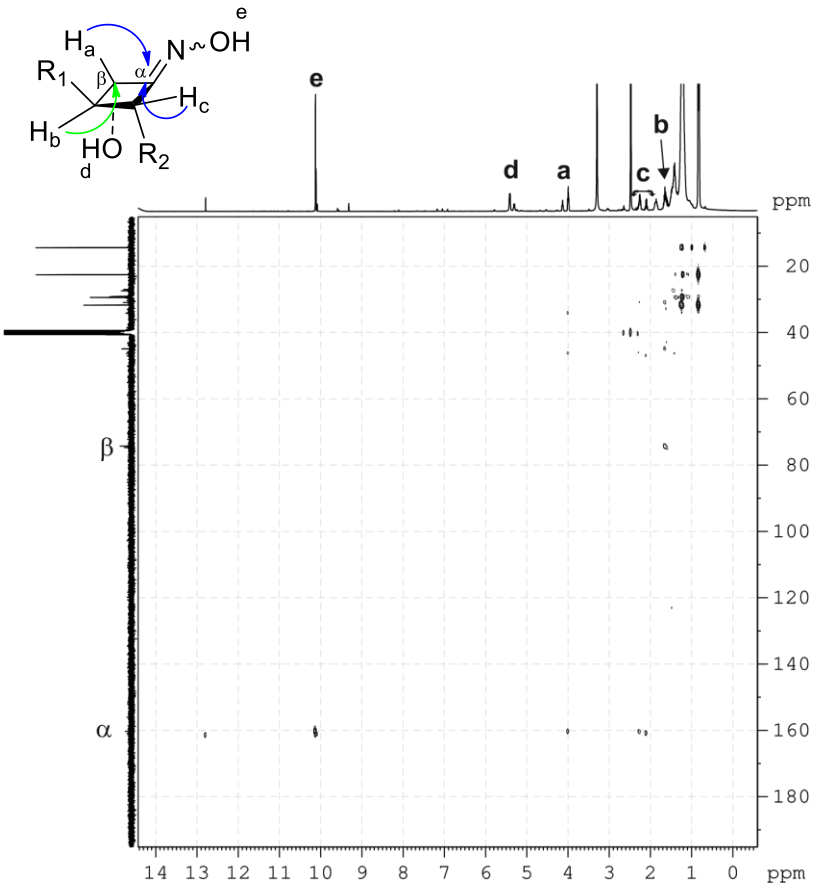
Ha
R1
β
α
N
OH
e
Hc
Hb
HO
d
R2
e
d
a
c
b
ppm
20
40
60
β
80
100
120
140
α
160
180
14 13 12 11 10 9 8 7 6 5 4 3 2 1 0 ppm

Photoisomerization of 4

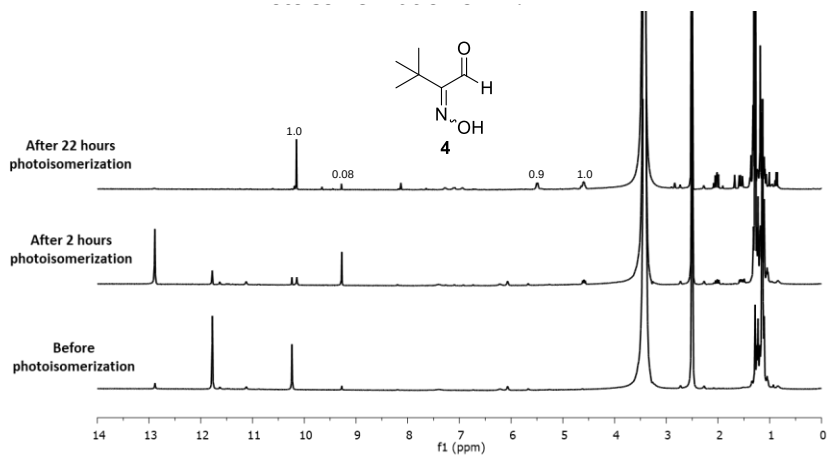

Photoisomerization of 1

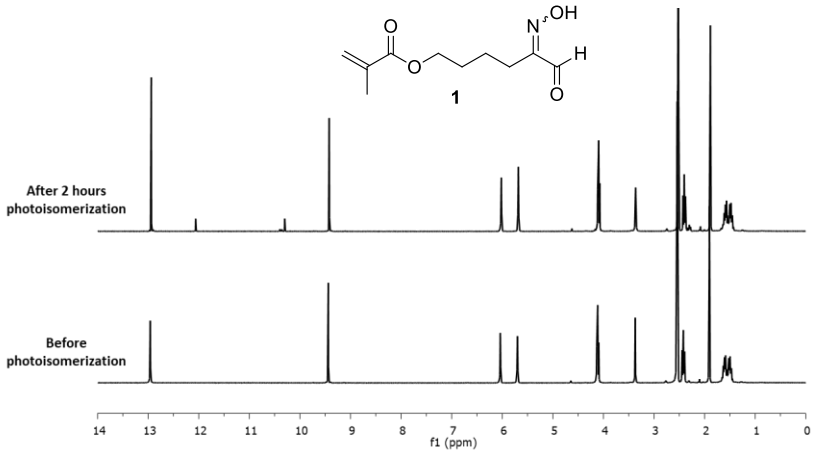

Photoisomerization of 14

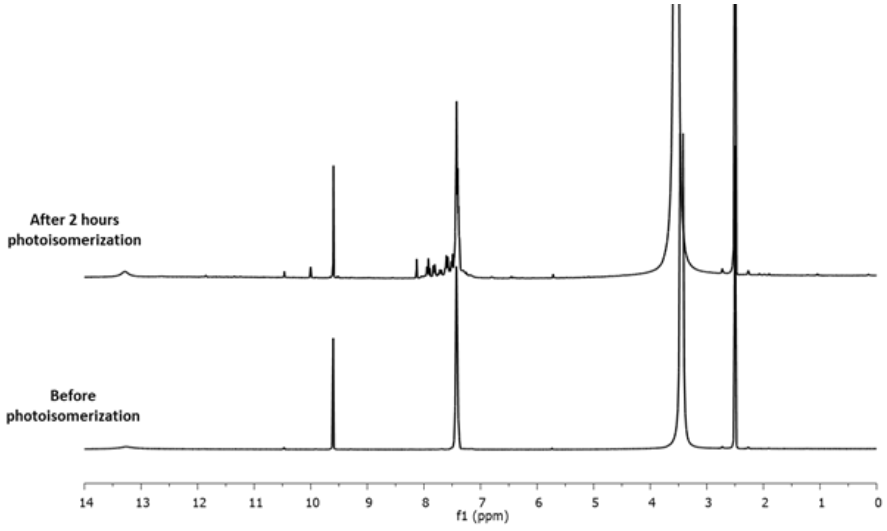

6.4.5 Results of photoisomerizations with 278 nm (LED)

Photoisomerization of 18

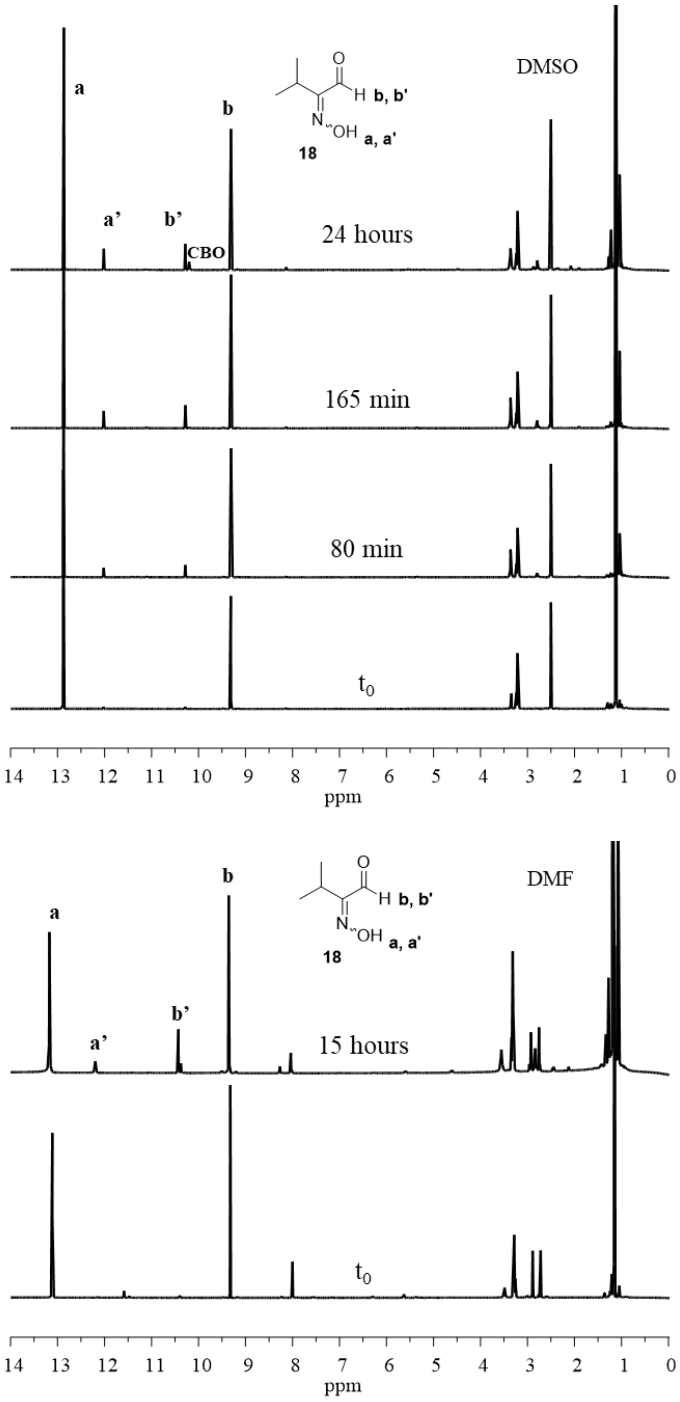

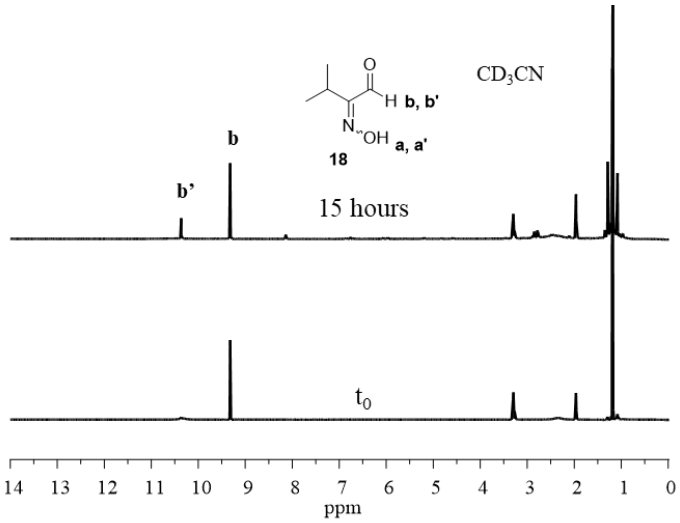

Photoisomerization of 17

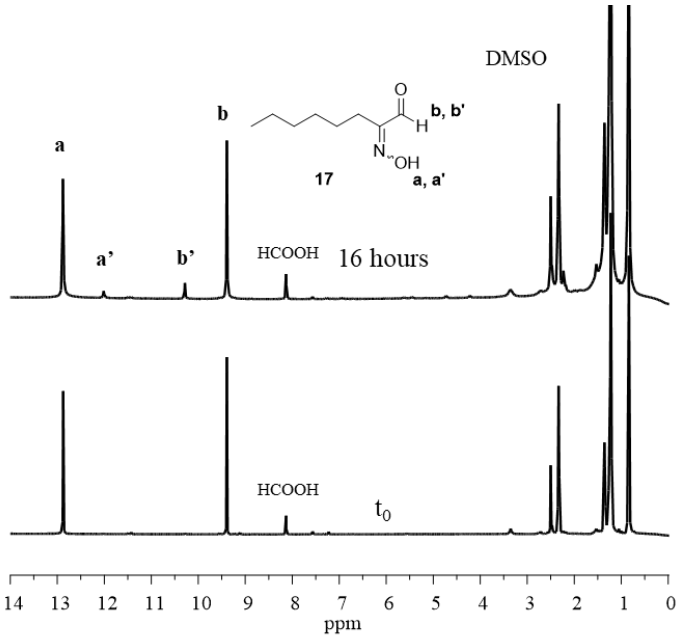

Photoisomerization of 14

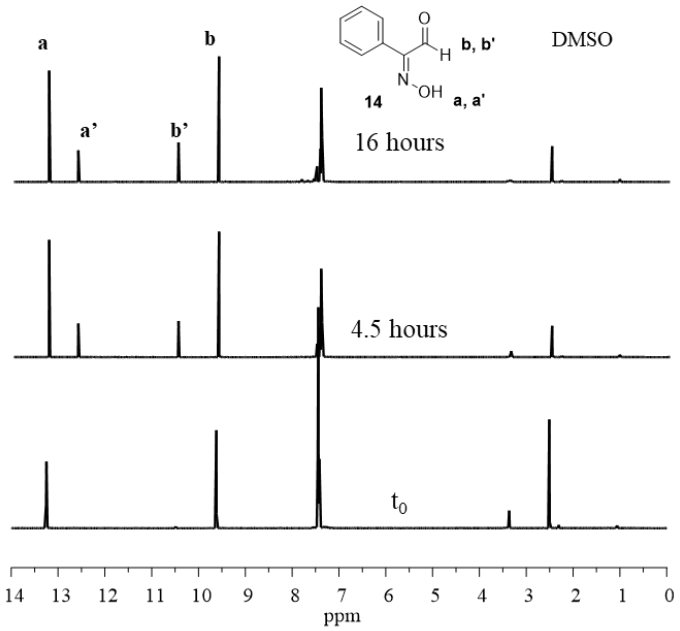

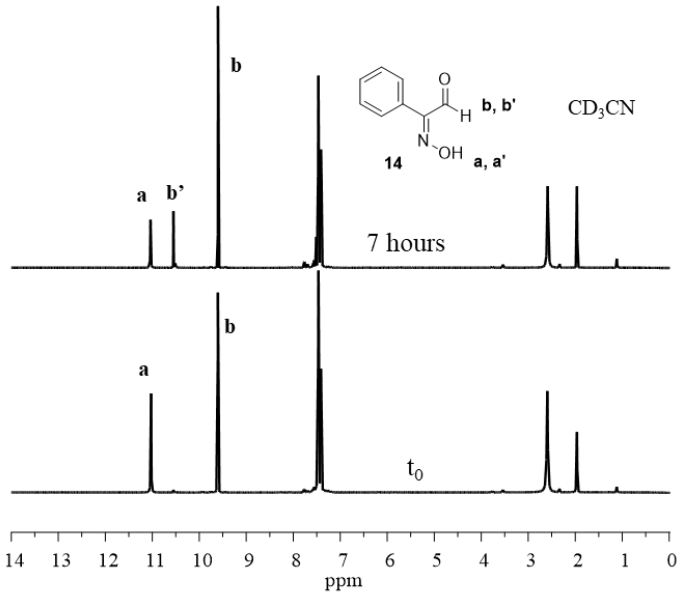

Photoisomerization of 19

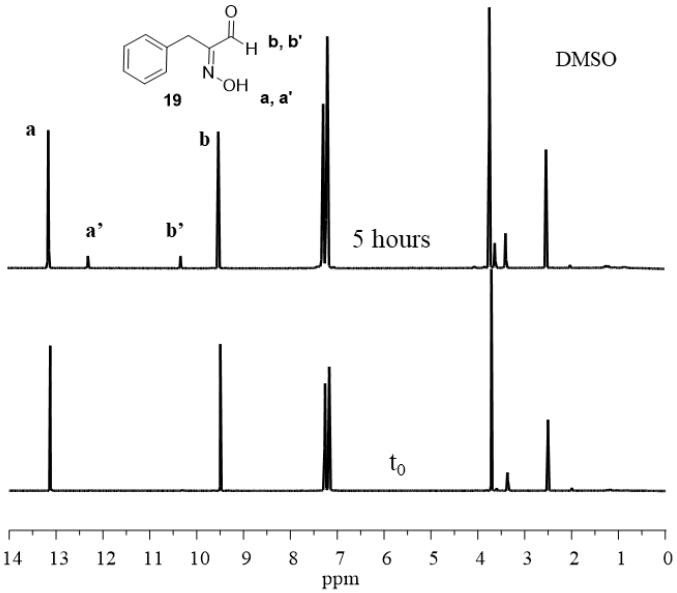

6.4.6 Results of photoisomerizations with 365 nm (LED)

Photoisomerization of 18

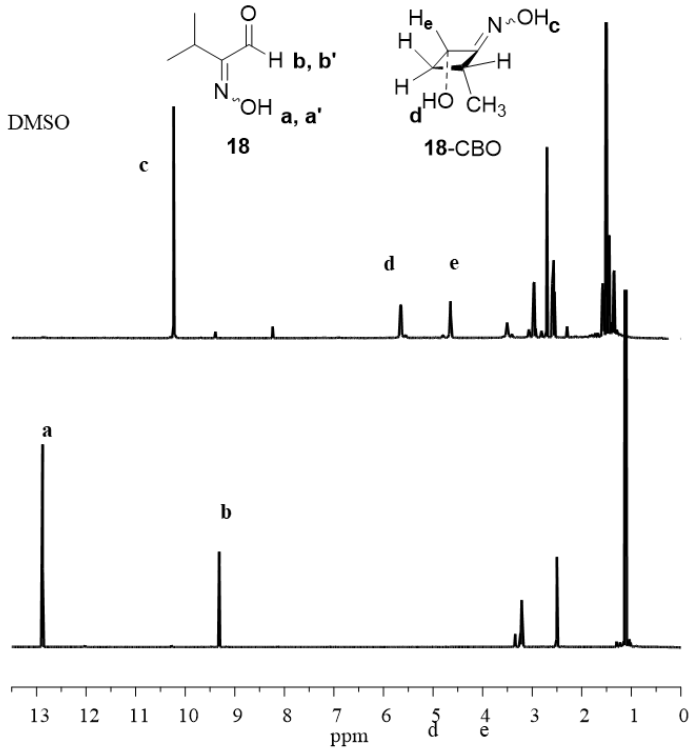

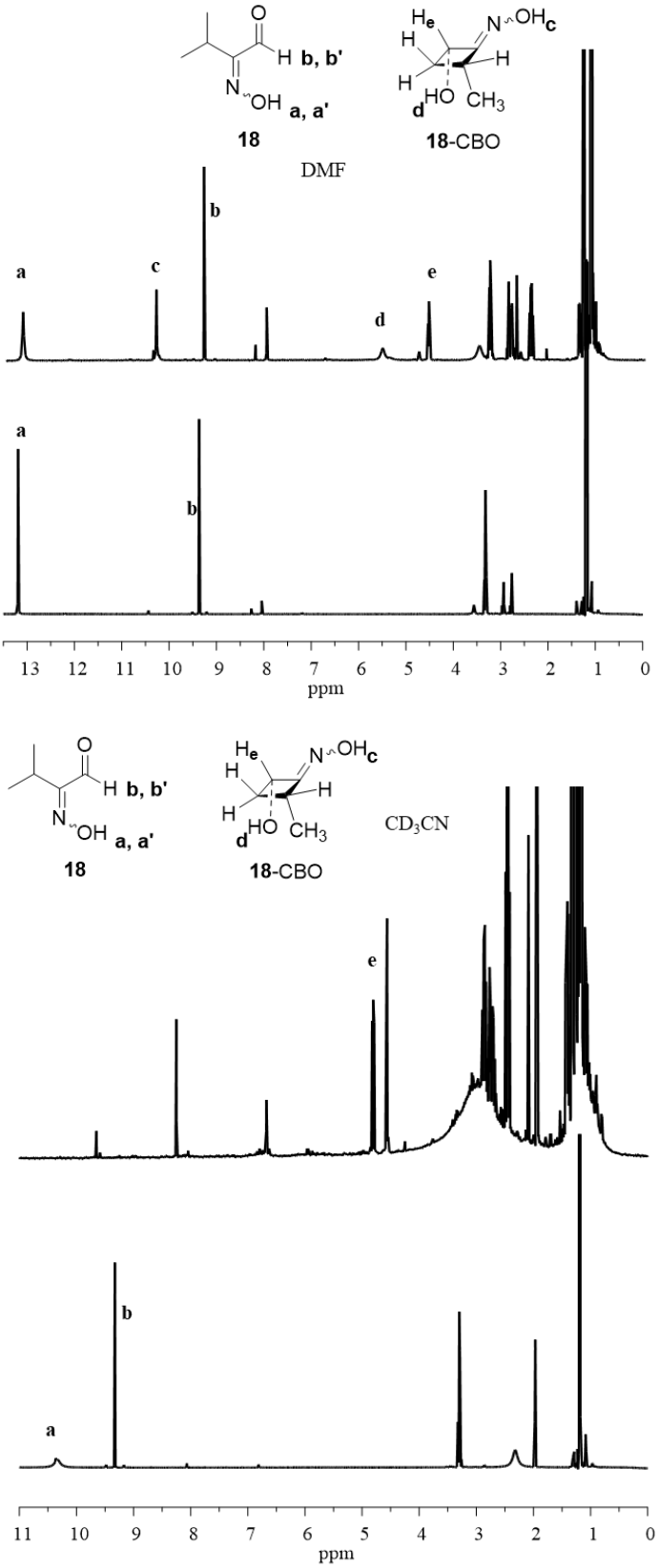
18
18-CBO
DMF
a
b
c
d
e
13 12 11 10 9 8 7 6 5 4 3 2 1 0
ppm
18
18-CBO
CD3CN
11 10 9 8 7 6 5 4 3 2 1 0
ppm

Photoisomerization of 17

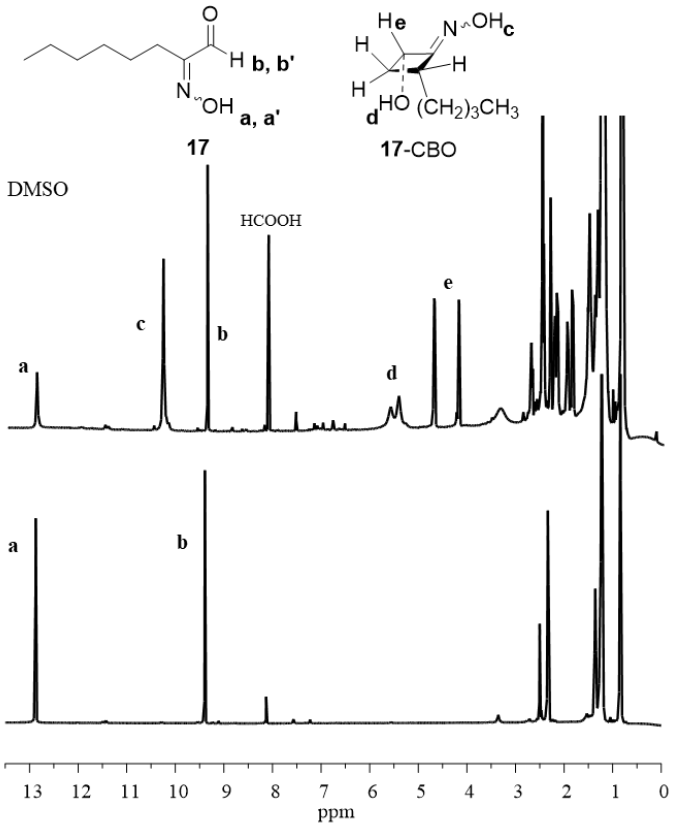

Photoisomerization of 14

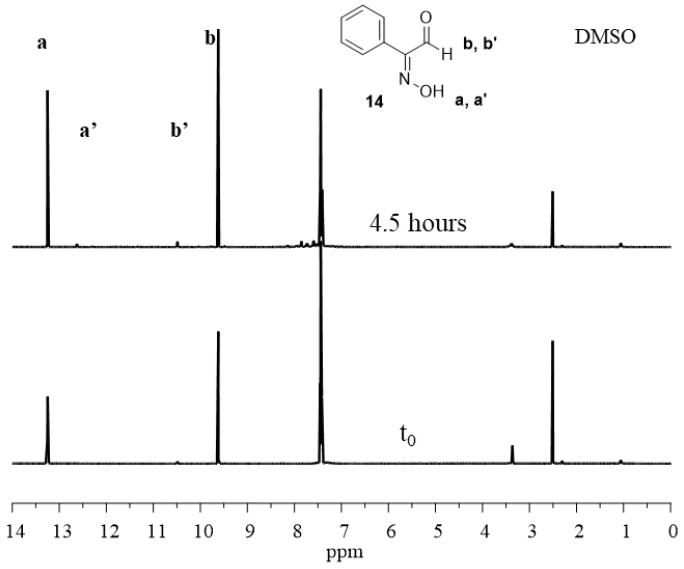

Photoisomerization of 19

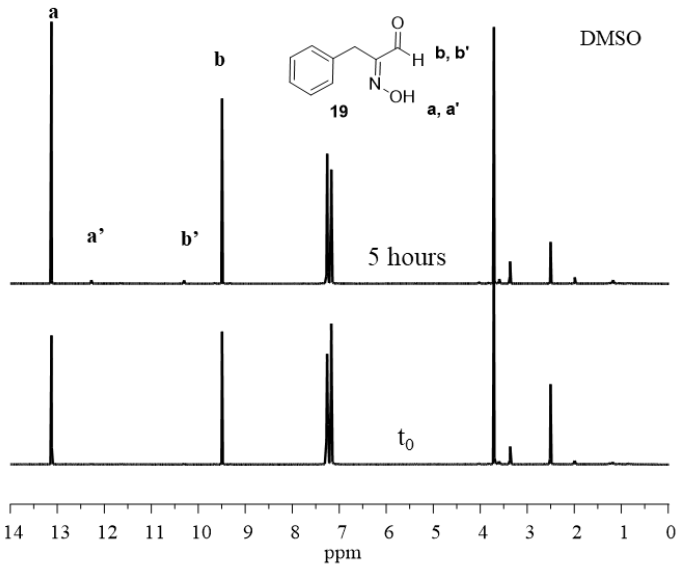

6.4.7 Thermal back isomerization of 14[126]

The photochemical and thermal isomerization of **14** was measured by ^{1}H-NMR analysis with a 600 MHz Bruker spectrometer. Experimental procedure: ^{1}H-NMR spectrum of **14** (C= 0.044 M) was recorded before irradiation at 25 °C. Then, **5** was irradiated using a UV LED of 278 nm (2 mW power output) for 14 hours at room temperature directly in the NMR tube. The *Z/E* ratio passed from 0 to 0.30 after irradiation, as shown by ^{1}H-NMR spectrum recorded at 25 °C. Since the thermal back isomerization of HIAs is very slow at room temperature (see paragraph 3.2), the time passed from turning off the light to record the spectrum after illumination (15 minutes) is irrelevant in the thermal back isomerization process. Finally, compound **14** was heated to the target temperature (323, 333 or 343K) and ^{1}H-NMR spectra was continuously recorded through time to monitor the decay of *Z* isomer to *E* and to determine the *Z*->*E* rate constant *k*. This is obtained by a mono-exponential fit of the decay of Z isomer through time at the target temperature. (Figure 6.7) The Arrhenius activation energy Ea and prefactor A could be estimated from Arrhenius Equation by plotting ln(k) versus 1/T.

$$k = A\mathrm{e}^{-Ea/RT}$$

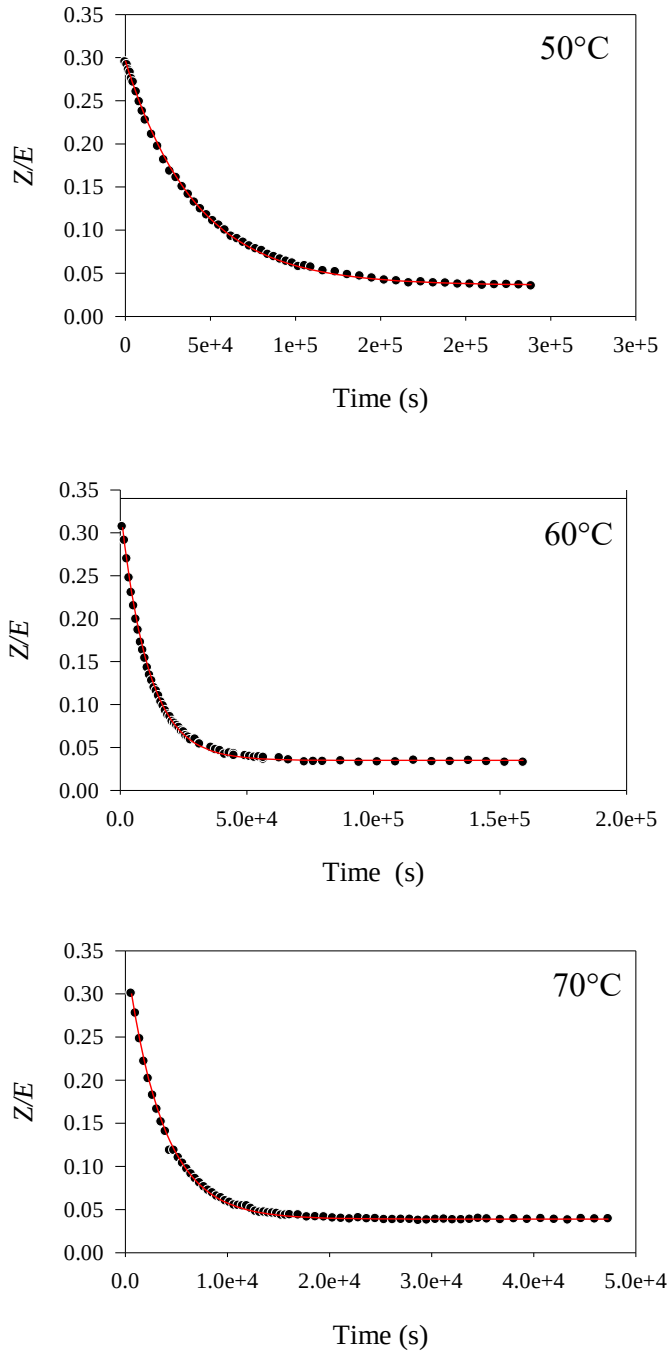

Figure 6.9. Exponential decay of *Z*-**5** at three different temperatures.

Bibliography

(1) Wolfgang, O. An Introduction to Theoretical and Applied Colloid Chemistry; the World of Neglected Dimensions, 1917

(2) Mülhaupt, R. Hermann Staudinger and the Origin of Macromolecular Chemistry. *Angew. Chemie Int. Ed.* **2004**, *43* (9), 1054–1063.

(3) Guragain, S.; Bastakoti, B. P.; Malgras, V.; Nakashima, K.; Yamauchi, Y. Multi-Stimuli-Responsive Polymeric Materials. *Chem. – A Eur. J.*, **2015**, *21* (38), 13164–13174.

(4) Herbert, K. M.; Schrettl, S.; Rowan, S. J.; Weder, C. 50th Anniversary Perspective: Solid-State Multistimuli, Multiresponsive Polymeric Materials. *Macromolecules* **2017**, *50* (22), 8845–8870.

(5) Schattling, P.; Jochum, F. D.; Theato, P. Multi-Stimuli Responsive Polymers – the All-in-One Talents. *Polym. Chem.* **2014**, *5* (1), 25–36.

(6) Pasparakis, G.; Vamvakaki, M. Multiresponsive Polymers: Nano-Sized Assemblies, Stimuli-Sensitive Gels and Smart Surfaces. *Polym. Chem.* **2011**, *2* (6), 1234.

(7) Cao, Z.-Q.; Wang, G.-J. Multi-Stimuli-Responsive Polymer Materials: Particles, Films, and Bulk Gels. *Chem. Rec.*, **2016**, *16* (3), 1398–1435.

(8) Liu, Y.; Li, Y.; Yang, G.; Zheng, X.; Zhou, S. Multi-Stimulus-Responsive Shape-Memory Polymer Nanocomposite Network Cross-Linked by Cellulose Nanocrystals. *ACS Appl. Mater. Interfaces* **2015**, *7* (7), 4118–4126.

(9) Aghabegi Moghanjoughi, A.; Khoshnevis, D.; Zarrabi, A. A Concise Review on Smart Polymers for Controlled Drug Release. *Drug Deliv. Transl. Res.* **2016**, *6* (3), 333–340.

(10) Zhu, J.; Niu, Y.; Li, Y.; Gong, Y.; Shi, H.; Huo, Q.; Liu, Y.; Xu, Q. Stimuli-Responsive Delivery Vehicles Based on Mesoporous Silica Nanoparticles: Recent Advances and Challenges. *J. Mater. Chem. B* **2017**, *5* (7), 1339–1352.

(11) Bauri, K.; Nandi, M.; De, P. Amino Acid-Derived Stimuli-Responsive Polymers and Their Applications. *Polym. Chem.* **2018**, *9* (11), 1257–1287.

(12) Pilate, F.; Toncheva, A.; Dubois, P.; Raquez, J.-M. Shape-Memory Polymers for Multiple Applications in the Materials World. *Eur. Polym. J.* **2016**, *80*, 268–294.

(13) Chen, L.; Wang, X.; Lu, W.; Wu, X.; Li, J. Molecular Imprinting: Perspectives and Applications. *Chem. Soc. Rev.* **2016**, *45* (8), 2137–2211.

(14) Lorenzo, R. A.; Carro, A. M.; Concheiro, A.; Alvarez-Lorenzo, C. Stimuli-Responsive Materials in Analytical Separation. *Anal. Bioanal. Chem.* **2015**, *407* (17), 4927–4948.

(15) Zhang, K.; Monteiro, M. J.; Jia, Z. Stable Organic Radical Polymers: Synthesis and Applications. *Polym. Chem.* **2016**, *7* (36), 5589–5614.

(16) Zhang, Q.; Weber, C.; Schubert, U. S.; Hoogenboom, R. Thermoresponsive Polymers with Lower Critical Solution Temperature: From Fundamental Aspects and Measuring Techniques to Recommended Turbidimetry Conditions. *Mater. Horizons* **2017**, *4* (2), 109–116.

(17) Weber, C.; Hoogenboom, R.; Schubert, U. S. Temperature Responsive Bio-Compatible Polymers Based on Poly(Ethylene Oxide) and Poly(2-Oxazoline)S. *Prog. Polym. Sci.* **2012**, *37* (5), 686–714.

(18) Ilčíková, M.; Tkáč, J.; Kasák, P. Switchable Materials Containing Polyzwitterion Moieties. *Polymers (Basel).* **2015**, *7* (11), 2344–2370.

(19) El'tsov, A. V. *Organic Photochromes*; Springer US, 1990.

(20) Yokoyama, Y. Molecular Switches with Photochromic Fulgides. In *Molecular Switches*; Wiley-VCH Verlag GmbH: Weinheim, FRG; 2011, pp 107–121.

(21) Langer, M.; Mueller, J. O.; Goldmann, A. S.; Schacher, F. H.; Barner-Kowollik, C. α,ω-Reactive Building Blocks Based on a Dual Functional RAFT Agent for Thermal and Light-Induced Ligation. *ACS Macro Lett.* **2016**, *5* (5), 597–601.

(22) Telitel, S.; Blasco, E.; Bangert, L. D.; Schacher, F. H.; Goldmann, A. S.; Barner-Kowollik, C. Photo-Reversible Bonding and Cleavage of Block Copolymers. *Polym. Chem.* **2017**, *8* (27), 4038–4042.

(23) Dai, S.; Ravi, P.; Tam, K. C. PH-Responsive Polymers: Synthesis, Properties and Applications. *Soft Matter* **2008**, *4* (3), 435.

(24) Liu, H.; Lin, S.; Feng, Y.; Theato, P. CO_2 -Responsive Polymer Materials. *Polym. Chem.* **2017**, *8* (1), 12–23.

(25) Roy, D.; Cambre, J. N.; Sumerlin, B. S. Triply-Responsive Boronic Acid Block Copolymers: Solution Self-Assembly Induced by Changes in Temperature, PH, or Sugar Concentration. *Chem. Commun.* **2009**, *16*, 2106.

(26) Wan, W.-M.; Cheng, F.; Jäkle, F. A Borinic Acid Polymer with Fluoride Ion-

and Thermo-Responsive Properties That Are Tunable over a Wide Temperature Range. *Angew. Chem. Int. Ed. Engl.* **2014**, *53* (34), 8934–8938.

(27) Ritter, H.; Sadowski, O.; Tepper, E. Influence of Cyclodextrin Molecules on the Synthesis and the Thermoresponsive Solution Behavior of N-Isopropylacrylamide Copolymers with Adamantyl Groups in the Side-Chains. *Angew. Chemie Int. Ed.* **2003**, *42* (27), 3171–3173.

(28) Jochum, F. D.; Forst, F. R.; Theato, P. PNIPAM Copolymers Containing Light-Responsive Chromophores: A Method Toward Molecular Logic Gates. *Macromol. Rapid Commun.* **2010**, *31* (16), 1456–1461.

(29) Fu, H.; Policarpio, D. M.; Batteas, J. D.; Bergbreiter, D. E. Redox-Controlled 'Smart' Polyacrylamide Solubility. *Polym. Chem.* **2010**, *1* (5), 631.

(30) Uchiyama, S.; Kawai, N.; De Silva, A. P.; Iwai, K. Fluorescent Polymeric AND Logic Gate with Temperature and PH as Inputs. **2004**, *126* (10), 3032-3033.

(31) Patil, S. S.; Misra, R. D. K. The Significance of Macromolecular Architecture in Governing Structure-Property Relationship for Biomaterial Applications: An Overview. *Mater. Technol.* **2018**, *33* (5), 364–386.

(32) Wang, D.; Jin, Y.; Zhu, X.; Yan, D. Synthesis and Applications of Stimuli-Responsive Hyperbranched Polymers. *Prog. Polym. Sci.* **2017**, *64*, 114–153.

(33) Mathers, R. T.; Magenau, A. J. D.; Schröder, K.; Matyjaszewski, K. Overview of Controlled/Living Polymerization Methods of Vinyl Monomers. In *Monitoring Polymerization Reactions*; John Wiley & Sons: Hoboken, NJ, 2014; pp 29–44.

(34) Penczek, S.; Moad, G. Glossary of Terms Related to Kinetics, Thermodynamics, and Mechanisms of Polymerization (IUPAC Recommendations 2008). *Pure Appl. Chem.* **2008**, *80* (10), 2163–2193.

(35) Quirk, R. P.; Lee, B. Experimental Criteria for Living Polymerizations. *Polym. Int.* **1992**, *27* (4), 359–367.

(36) SZWARC, M. 'Living' Polymers. *Nature* **1956**, *178* (4543), 1168–1169.

(37) Grubbs, R. H. Olefin Metathesis. *Tetrahedron* **2004**, *60* (34), 7117–7140.

(38) Mathers, R. T. Overview of Ring-Opening Metathesis Polymerizations (ROMP) and Acyclic Diene Metathesis (ADMET) Polymerizations with Selected Ruthenium and Molybdenum Complexes. In *Handbook of Transition Metal Polymerization Catalysts*; John Wiley & Sons, Inc.: Hoboken, NJ, USA,

2018; pp 631–659.

(39) Chen, Y.; Abdellatif, M. M.; Nomura, K. Olefin Metathesis Polymerization: Some Recent Developments in the Precise Polymerizations for Synthesis of Advanced Materials (by ROMP, ADMET). *Tetrahedron* **2018**, *74* (6), 619–643.

(40) Chen, Y.; Fuchise, K.; Satoh, T.; Kakuchi, T. Group Transfer Polymerization of Acrylic Monomers. In *Anionic Polymerization*; Springer Japan: Tokyo, 2015; pp 451–494.

(41) Fuchise, K.; Chen, Y.; Satoh, T.; Kakuchi, T. Recent Progress in Organocatalytic Group Transfer Polymerization. *Polym. Chem.* **2013**, *4* (16), 4278.

(42) Huang, Z.; Qin, B.; Chen, L.; Xu, J.-F.; Faul, C. F. J.; Zhang, X. Supramolecular Polymerization from Controllable Fabrication to Living Polymerization. *Macromol. Rapid Commun.* **2017**, *38* (17), 1700312.

(43) Andrzejewska, E. Free Radical Photopolymerization of Multifunctional Monomers. In *Three-Dimensional Microfabrication Using Two-photon Polymerization*; Elsevier, 2016; pp 62–81.

(44) *Controlled/Living Radical Polymerization*; Matyjaszewski, K., Ed.; ACS Symposium Series; American Chemical Society: Washington, DC, 2000; Vol. 768.

(45) Charleux, B.; Delaittre, G.; Rieger, J.; D'Agosto, F. Polymerization-Induced Self-Assembly: From Soluble Macromolecules to Block Copolymer Nano-Objects in One Step. *Macromolecules* **2012**, *45* (17), 6753–6765.

(46) Pan, X.; Tasdelen, M. A.; Laun, J.; Junkers, T.; Yagci, Y.; Matyjaszewski, K. Photomediated Controlled Radical Polymerization. *Progress in Polymer Science*. **2016**, *62*, 73-125.

(47) Flores, J. D.; Abel, B. A.; Smith, D.; McCormick, C. L. Stimuli-Responsive Polymers Via Controlled Radical Polymerization. In *Monitoring Polymerization Reactions*; John Wiley & Sons: Hoboken, NJ, 2014; pp 45–58.

(48) Fischer, H. The Persistent Radical Effect: A Principle for Selective Radical Reactions and Living Radical Polymerizations. *Chem. Rev.* **2001**, *101* (12), 3581–3610.

(49) *Nitroxide Mediated Polymerization*; Gigmes, D., Ed.; Polymer Chemistry Series; Royal Society of Chemistry: Cambridge, 2015.

(50) Nicolas, J.; Guillaneuf, Y.; Lefay, C.; Bertin, D.; Gigmes, D.; Charleux, B. Nitroxide-Mediated Polymerization. *Prog. Polym. Sci.* **2013**, *38* (1), 63–235.

(51) Chmielarz, P.; Fantin, M.; Park, S.; Isse, A. A.; Gennaro, A.; Magenau, A. J. D.; Sobkowiak, A.; Matyjaszewski, K. Electrochemically Mediated Atom Transfer Radical Polymerization (e ATRP). *Prog. Polym. Sci.* **2017**, *69*, 47–78.

(52) Pan, X.; Fantin, M.; Yuan, F.; Matyjaszewski, K. Externally Controlled Atom Transfer Radical Polymerization. *Chem. Soc. Rev.* **2018**, *47* (14), 5457–5490.

(53) Matyjaszewski, K. Controlled Radical Polymerization: State-of-the-Art in 2014. In *Controlled Radical Polymerization: Mechanisms*, 2015; pp 1–17.

(54) Anastasaki, A.; Nikolaou, V.; Nurumbetov, G.; Wilson, P.; Kempe, K.; Quinn, J. F.; Davis, T. P.; Whittaker, M. R.; Haddleton, D. M. Cu(0)-Mediated Living Radical Polymerization: A Versatile Tool for Materials Synthesis. *Chem. Rev.* **2016**, *116* (3), 835–877.

(55) Theriot, J. C.; McCarthy, B. G.; Lim, C.-H.; Miyake, G. M. Organocatalyzed Atom Transfer Radical Polymerization: Perspectives on Catalyst Design and Performance. *Macromol. Rapid Commun.* **2017**, *38* (13), 1700040.

(56) Yilmaz, G.; Yagci, Y. Photoinduced Metal-Free Atom Transfer Radical Polymerizations: State-of-the-Art, Mechanistic Aspects and Applications. *Polym. Chem.* **2018**, *9* (14), 1757–1762.

(57) Perrier, S. *50th Anniversary Perspective* : RAFT Polymerization—A User Guide. *Macromolecules* **2017**, *50* (19), 7433–7447.

(58) Moad, G. RAFT Polymerization to Form Stimuli-Responsive Polymers. *Polym. Chem.* **2017**, *8* (1), 177–219.

(59) Keddie, D. J.; Moad, G.; Rizzardo, E.; Thang, S. H. RAFT Agent Design and Synthesis. *Macromolecules* **2012**, *45* (13), 5321–5342.

(60) Moad, G.; Keddie, D.; Guerrero-Sanchez, C.; Rizzardo, E.; Thang, S. H. Advances in Switchable RAFT Polymerization. *Macromol. Symp.* **2015**, *350* (1), 34–42.

(61) Hill, M. R.; Carmean, R. N.; Sumerlin, B. S. Expanding the Scope of RAFT Polymerization: Recent Advances and New Horizons. *Macromolecules* **2015**, *48* (16), 5459–5469.

(62) Canning, S. L.; Smith, G. N.; Armes, S. P. A Critical Appraisal of RAFT-Mediated Polymerization-Induced Self-Assembly. *Macromolecules* **2016**, *49*

(6), 1985–2001.

(63) Hornung, C. H.; Nguyen, X.; Kyi, S.; Chiefari, J.; Saubern, S. Synthesis of RAFT Block Copolymers in a Multi-Stage Continuous Flow Process Inside a Tubular Reactor. *Aust. J. Chem.* **2013**, *66* (2), 192.

(64) Hornung, C. H.; Von Känel, K.; Martinez-Botella, I.; Espiritu, M.; Nguyen, X.; Postma, A.; Saubern, S.; Chiefari, J.; Thang, S. H. Continuous Flow Aminolysis of RAFT Polymers Using Multistep Processing and Inline Analysis. *Macromolecules* **2014**, *47* (23), 8203-8213.

(65) Xu, J.; Jung, K.; Atme, A.; Shanmugam, S.; Boyer, C. A Robust and Versatile Photoinduced Living Polymerization of Conjugated and Unconjugated Monomers and Its Oxygen Tolerance. *J. Am. Chem. Soc.* **2014**, *136* (14), 5508–5519.

(66) Abele, E.; Abele, R. Recent Advances in the Synthesis of Heterocycles from Oximes. *Curr. Org. Synth.* **2014**, *11* (3), 403–428.

(67) Ashani, Y.; Silman, I. The Chemistry of Hydroxylamines, Oximes and Hydroxamic Acids, Ed. Z. Rappoport and JF Liebman. **2008**.

(68) Bolotin, D. S.; Bokach, N. A.; Kukushkin, V. Y. Coordination Chemistry and Metal-Involving Reactions of Amidoximes: Relevance to the Chemistry of Oximes and Oxime Ligands. *Coord. Chem. Rev.* **2016**, *313*, 62–93.

(69) Singh, N.; Karpichev, Y.; Tiwari, A. K.; Kuca, K.; Ghosh, K. K. Oxime Functionality in Surfactant Self-Assembly: An Overview on Combating Toxicity of Organophosphates. *J. Mol. Liq.* **2015**, *208*, 237–252.

(70) Gordillo, M. A.; Soto-Monsalve, M.; Carmona-Vargas, C. C.; Gutiérrez, G.; D'vries, R. F.; Lehn, J.-M.; Chaur, M. N. Photochemical and Electrochemical Triggered Bis(Hydrazone) Switch. *Chem. - A Eur. J.* **2017**, *23* (59), 14872–14882.

(71) Fast, D. E.; Lauer, A.; Menzel, J. P.; Kelterer, A. M.; Gescheidt, G.; Barner-Kowollik, C. Wavelength-Dependent Photochemistry of Oxime Ester Photoinitiators. *Macromolecules* **2017**, *50* (5), 1815-1823.

(72) Ma, X.; Gu, R.; Yu, L.; Han, W.; Li, J.; Li, X.; Wang, T. Conjugated Phenothiazine Oxime Esters as Free Radical Photoinitiators. *Polym. Chem.* **2017**, *8* (39), 6134–6142.

(73) Sun, X.; Jin, M.; Wu, X.; Pan, H.; Wan, D.; Pu, H. Bis-Substituted Thiophene-Containing Oxime Sulfonates Photoacid Generators for Cationic

Polymerization under UV-Visible LED Irradiation. *J. Polym. Sci. Part A Polym. Chem.* **2018**, *56* (7), 776–782.

(74) Mukherjee, S.; Hill, M. R.; Sumerlin, B. S. Self-Healing Hydrogels Containing Reversible Oxime Crosslinks. *Soft Matter* **2015**, *11* (30), 6152–6161.

(75) Kuhl, N.; Abend, M.; Bode, S.; Schubert, U. S.; Hager, M. D. Oxime Crosslinked Polymer Networks: Is Every Reversible Covalent Bond Suitable to Create Self-Healing Polymers? *J. Appl. Polym. Sci.* **2016**, *133* (44).

(76) Collins, J.; Xiao, Z.; Müllner, M.; Connal, L. A. The Emergence of Oxime Click Chemistry and Its Utility in Polymer Science. *Polym. Chem.* **2016**, *7* (23), 3812–3826.

(77) Kölmel, D. K.; Kool, E. T. Oximes and Hydrazones in Bioconjugation: Mechanism and Catalysis. *Chemical Reviews*. **2017**, *117* (15), 10358-10376.

(78) Ganivada, M. N.; Kumar, P.; Kanjilal, P.; Dinda, H.; Sarma, J. Das; Shunmugam, R. Polycarbonate-Based Biodegradable Copolymers for Stimuli Responsive Targeted Drug Delivery. *Polym. Chem.* **2016**, 7, 4237-4245.

(79) Jin, Y.; Song, L.; Su, Y.; Zhu, L.; Pang, Y.; Qiu, F.; Tong, G.; Yan, D.; Zhu, B.; Zhu, X. Oxime Linkage: A Robust Tool for the Design of PH-Sensitive Polymeric Drug Carriers. *Biomacromolecules* **2011**, *12* (10), 3460–3468.

(80) Liu, W.-X.; Zhang, C.; Zhang, H.; Zhao, N.; Yu, Z.-X.; Xu, J. Oxime-Based and Catalyst-Free Dynamic Covalent Polyurethanes. *J. Am. Chem. Soc.* **2017**, *139* (25), 8678–8684.

(81) Metz, N.; Theato, P. Controlled Synthesis of Poly(Acetone Oxime Acrylate) as a New Reactive Polymer: Stimuli-Responsive Reactive Copolymers. *Eur. Polym. J.* **2007,** *43* (4), 1202-1209.

(82) Wu, F.; Tang, X.; Guo, L.; Yang, K.; Cai, Y. Switching Preorganization and Thermoresponsive Behavior of a Water-Soluble Polymer via Light-Tunable Hydrogen Bonding. *Soft Matter* **2013**, *9*, 4036-4044.

(83) Guo, L.; Ding, Y.; Han, J.; Xu, N.; Lu, X.; Cai, Y. Reconstruction of Block Copolymer Micelles to Long-Range Ordered Dense Nanopatterns Via Light-Tunable Hydrogen-Bonding Association. *Macromol. Rapid Commun.* **2015**, *36* (16), 1505–1510.

(84) Balamurugan, A.; Lee, H. Aldoxime-Derived Water-Soluble Polymer for the Multiple Analyte Sensing: Consecutive and Selective Detection of Hg^{2+}, Ag

$^{+}$, ClO^{-}, and Cysteine in Aqueous Media. *Macromolecules* **2015**, *48* (12), 3934–3940.

(85) Gentili, P.; Pedetti, S. A Remarkably Simple α-Oximation of Aldehydes via Organo-SOMO Catalysis. *Chem. Commun.* **2012**, *48* (43), 5358.

(86) Kool, E. T.; Crisalli, P.; Chan, K. M. Fast Alpha Nucleophiles: Structures That Undergo Rapid Hydrazone/Oxime Formation at Neutral PH. *Org. Lett.* **2014**, *16* (5), 1454–1457.

(87) Kalia, J.; Raines, R. T. Advances in Bioconjugation. *Curr. Org. Chem.* **2010**, *14* (2), 138–147.

(88) Gentili, P.; Nardi, M.; Antignano, I.; Cambise, P.; D'Abramo, M.; D'Acunzo, F.; Pinna, A.; Ussia, E. 2-(Hydroxyimino)Aldehydes: Photo- and Physicochemical Properties of a Versatile Functional Group for Monomer Design. *Chem. - A Eur. J.* **2018**, *24* (30), 7683-7694.

(89) Friis, E. P.; Andersen, J. E. T.; Madsen, L. L.; Bonander, N.; Møller, P.; Ulstrup, J. Dynamics of Pseudomonas Aeruginosa Azurin and Its Cys3Ser Mutant at Single-Crystal Gold Surfaces Investigated by Cyclic Voltammetry and Atomic Force Microscopy. *Electrochim. Acta* **1998**, *43* (9), 1114–1122.

(90) Yasuda, M. Dissociation Constants of Some Carboxylic Acids in Mixed Aqueous Solvents. *Bull. Chem. Soc. Jpn.* **1959**, *32* (5), 429–432.

(91) Buys, T. S. V.; Cerfontain, H.; Geenevasen, J. A. J.; Stunnenberg, F. Photochemistry of α-Oxo Oximes. Part 9. The γ-Hydrogen Abstraction in α-Oxo Oxime Ethers. *Recl. des Trav. Chim. des Pays-Bas* **2010**, *105* (6), 188–194.

(92) Infantes, L.; Motherwell, S. Prediction of H-Bonding Motifs for Pyrazoles and Oximes Using the Cambridge Structural Database. In *Science of Crystal Structures: Highlights in Crystallography*; 2015.

(93) Hill, M. R.; Mukherjee, S.; Costanzo, P. J.; Sumerlin, B. S. Modular Oxime Functionalization of Well-Defined Alkoxyamine-Containing Polymers. *Polym. Chem.* **2012**, *3*, 1758-1762.

(94) Barner-Kowollik, C.; Du Prez, F. E.; Espeel, P.; Hawker, C. J.; Junkers, T.; Schlaad, H.; Van Camp, W. "Clicking" Polymers or Just Efficient Linking: What Is the Difference? *Angew. Chemie Int. Ed.* **2011**, *50* (1), 60–62.

(95) Nardi, M.; D'Acunzo, F.; Clemente, M.; Proietti, G.; Gentili, P. A First Study on Copolymers of a Methacrylate Containing the 2-(Hydroxyimino)Aldehyde

Group and OEGMA. RAFT Polymerization and Assessment of Thermal and Photoresponsive Polymer Behavior. *Polym. Chem.* **2017**, *8*, 4233-4245.

(96) Pratt, D.A.; Blake, J. A.; Mulder, P.; Walton, J. C.; Korth, H.-G.; Ingold, K. U. O−H Bond Dissociation Enthalpies in Oximes: Order Restored. *J. Am. Chem. Soc.* **2004**, *126* (34),10667-10675.

(97) Miyabe, H.; Shibata, R.; Sangawa, M.; Ushiro, C.; Naito, T. Intermolecular Alkyl Radical Addition to the Carbon-Nitrogen Double Bond of Oxime Ethers and Hydrazones. *Tetrahedron* **1998**, *54* (38), 11431-11444.

(98) Sato, T.; Sato, N.; Seno, M.; Hirano, T. Effect of Glyoxylic Oxime Ether on Radical Polymerization of Styrene. *J. Polym. Sci. Part A Polym. Chem.* **2002**, *40* (16), 2772–2781.

(99) Mann, A.; Gerasimchuk, N.; Silchenko, S. New Non-Aggregating Bivalent Cis-ML2 (M = Pd, Pt; L = Pivaloylcyanoxime). *Inorganica Chim. Acta* **2016**, *440*, 118–128.

(100) Klaus, D. R.; Keene, M.; Silchenko, S.; Berezin, M.; Gerasimchuk, N. 1D Polymeric Platinum Cyanoximate: A Strategy toward Luminescence in the Near-Infrared Region beyond 1000 Nm. *Inorg. Chem.* **2015**, *54* (4), 1890–1900.

(101) Becer, C. R.; Hahn, S.; Fijten, M. W. M.; Thijs, H. M. L.; Hoogenboom, R.; Schubert, U. S. Libraries of Methacrylic Acid and Oligo(Ethylene Glycol) Methacrylate Copolymers with LCST Behavior. *J. Polym. Sci. Part A Polym. Chem.* **2008**, *46* (21), 7138–7147.

(102) Merten, J.; Hennig, A.; Schwab, P.; Fröhlich, R.; Tokalov, S. V.; Gutzeit, H. O.; Metz, P. A Concise Sultone Route to Highly Oxygenated 1,10-Seco-Eudesmanolides – Enantioselective Total Synthesis of the Antileukemic Sesquiterpene Lactones(–)-Eriolanin and (–)-Eriolangin. *European J. Org. Chem.* **2006**, *2006* (5), 1144–1161.

(103) Parikh, J. R.; Doering, W. v. E. Sulfur Trioxide in the Oxidation of Alcohols by Dimethyl Sulfoxide. *J. Am. Chem. Soc.* **1967**, *89* (21), 5505–5507.

(104) D. Roth, H. Light-Induced Chemistry of Oximes and Derivatives. In *PATAI'S Chemistry of Functional Groups*; John Wiley & Sons, Ltd: Chichester, UK, 2010.

(105) Kaatze, U.; Pottel, R.; Schaefer, M. Dielectric Spectrum of Dimethyl Sulfoxide/Water Mixtures as a Function of Composition. *J. Phys. Chem.* **1989**,

93 (14), 5623–5627.

(106) Chong, S.; Fu, Y.; Liu, L.; Guo, Q.-X. O−H Bond Dissociation Enthalpies of Oximes: A Theoretical Assessment and Experimental Implications. **2007**, *111* (50), 13112-13125.

(107) Luo, Y.-R. *Comprehensive Handbook of Chemical Bond Energies*; CRC Press, 2007.

(108) Rúnarsson, Ö. V.; Malainer, C.; Holappa, J.; Sigurdsson, S. T.; Másson, M. Tert-Butyldimethylsilyl O-Protected Chitosan and Chitooligosaccharides: Useful Precursors for N-Modifications in Common Organic Solvents. *Carbohydr. Res.* **2008**, *343* (15), 2576–2582.

(109) Fife, T. H.; Benjamin, B. M. Intramolecular General Base Catalyzed Transesterification: The Cyclization of Ethyl 2-Hydroxymethylbenzoate and Ethyl 2-Hydroxymethyl 4-Nitrobenzoate to Phthalide and 5-Nitrophthalide. *Bioorg. Chem.* **1976**, *5* (1), 37–50.

(110) Pietsch, C.; Fijten, M. W. M.; Lambermont-Thijs, H. M. L.; Hoogenboom, R.; Schubert, U. S. Unexpected Reactivity for the RAFT Copolymerization of Oligo(Ethylene Glycol) Methacrylates. *J. Polym. Sci. Part A Polym. Chem.* **2009**, *47* (11), 2811–2820.

(111) Moad, G.; Barner-Kowollik, C. The Mechanism and Kinetics of the RAFT Process: Overview, Rates, Stabilities, Side Reactions, Product Spectrum and Outstanding Challenges. In *Handbook of RAFT Polymerization*; Wiley-VCH Verlag GmbH & Co. KGaA: Weinheim, Germany; pp 51–104.

(112) Wang, Z.; He, J.; Tao, Y.; Yang, L.; Jiang, H.; Yang, Y. Controlled Chain Branching by RAFT-Based Radical Polymerization **2003**, *36* (20), 7446-7452.

(113) Lowe, A. B.; McCormick, C. L. RAFT Polymerization in Homogeneous Aqueous Media: Initiation Systems, RAFT Agent Stability, Monomers and Polymer Structures. In *Handbook of RAFT Polymerization*; Wiley-VCH Verlag GmbH & Co. KGaA: Weinheim, Germany; pp 235–284.

(114) Xu, J.; He, J.; Fan, D.; Tang, W.; Yang, Y. Thermal Decomposition of Dithioesters and Its Effect on RAFT Polymerization. **2006**, *39* (11), 3753-3759.

(115) Plummer, R.; Goh, Y.-K.; Whittaker, A. K.; Monteiro, M. J. Effect of Impurities in Cumyl Dithiobenzoate on RAFT-Mediated Polymerizations. **2005**, *38* (12), 5352-5355.

(116) Favier, A.; Barner-Kowollik, C.; Davis, T. P.; Stenzel, M. H. A Detailed On-Line FT/NIR And1H NMR Spectroscopic Investigation into Factors Causing Inhibition in Xanthate-Mediated Vinyl Acetate Polymerization. *Macromol. Chem. Phys.* **2004**, *205* (7), 925–936.

(117) Barner-Kowollik, C. *Handbook of RAFT Polymerization*.

(118) Oelgemöller, M.; Hoffmann, N. Studies in Organic and Physical Photochemistry – an Interdisciplinary Approach. *Org. Biomol. Chem.* **2016**, *14* (31), 7392–7442.

(119) Cyman, M.; Wielińska, J.; Myszka, H.; Trzybiński, D.; Sikorski, A.; Nowacki, A.; Liberek, B. Influence of the Oxime and Anomeric Configurations on the Stability of 2-Deoxy-2-Hydroxyimino-d-Hexopyranosides. *J. Mol. Struct.* **2016**, *1125*, 558–569.

(120) Blanco, F.; Alkorta, I.; Elguero, J. Barriers about Double Carbon-Nitrogen Bond in Imine Derivatives (Aldimines, Oximes, Hydrazones, Azines). *Croat. Chem. Acta* **2013**, *82* (1), 173-183.

(121) Stunnenberg, F.; Cerfontain, H.; Rexwinkel, R. B. Spectroscopy and Photochemistry of a Series of Alkyl-Substituted o- and p-Benzoquinones and Their Mono-Oxime O-Methyl Ethers. *Recl. des Trav. Chim. des Pays-Bas* **1992**, *111* (10), 438–447.

(122) Baas, P.; Cerfontain, H. Photochemistry of α-Oxo-Oximes. Part 2. Irradiation of 4-Ethoxyimino-2,6-Dimethylheptan-3-One: A Novel Type II Cyclobutanol Formation. *Tetrahedron Lett.* **1978**, *19* (17), 1501–1504.

(123) Buys, T. S. V.; Cerfontain, H.; Geenevasen, J. A. J.; Stunnenberg, F. Photochemistry of A-oxo Oximes. Part 9. The Γ-hydrogen Abstraction in A-oxo Oxime Ethers. *Recl. des Trav. Chim. des Pays-Bas* **1986**, No. 105, 188.

(124) Pierens, G. K. ^{1}H and ^{13}C NMR Scaling Factors for the Calculation of Chemical Shifts in Commonly Used Solvents Using Density Functional Theory. *J. Comput. Chem.* **2014**, *35* (18), 1388–1394.

(125) Baas, P.; Cerfontain, H. Photochemistry of α-Oxo-Oximes. Part 4. Spectral Properties, Conformations, and Photoisomerization of α-Oxo-Oximes and Their Acetates. *J. Chem. Soc., Perkin Trans. 2* **1979**, *0* (2), 156–162.

(126) Luo, Y.; Utecht, M.; Dokić, J.; Korchak, S.; Vieth, H.-M.; Haag, R.; Saalfrank, P. Luo, Y.; Utecht, M.; Dokić, J.; Korchak, S.; Vieth, H.-M.; Haag, R.; Saalfrank, P. Cis-Trans Isomerisation of Substituted Aromatic Imines: A

Comparative Experimental and Theoretical Study. *ChemPhysChem* **2011**, *12* (12), 2311–2321.

(127) Hoogenboom, R. Temperature-Responsive Polymers: Properties, Synthesis and Applications. In *Smart Polymers and their Applications*; Elsevier, 2014; pp 15–44.

(128) Han, S.; Hagiwara, M.; Ishizone, T. Synthesis of Thermally Sensitive Water-Soluble Polymethacrylates by Living Anionic Polymerizations of Oligo(Ethylene Glycol) Methyl Ether Methacrylates. *Macromolecules* **2003**, *36* (22),8312-8319.

(129) Ishizone, T.; Seki, A.; Hagiwara, M.; Han, S.; Yokoyama, H.; Oyane, A.; Deffieux, A.; Carlotti, S. Anionic Polymerizations of Oligo(Ethylene Glycol) Alkyl Ether Methacrylates: Effect of Side Chain Length and ω-Alkyl Group of Side Chain on Cloud Point in Water. *Macromolecules* **2008**, *41* (8), 2963–2967.

(130) Lutz, J.-F.; Hoth, A. Preparation of Ideal PEG Analogues with a Tunable Thermosensitivity by Controlled Radical Copolymerization of 2-(2-Methoxyethoxy)Ethyl Methacrylate and Oligo(Ethylene Glycol) Methacrylate. *Macromolecules* **2006**, *39* (2), 893-896.

(131) Chen, S.; Wang, K.; Zhang, W. A New Thermoresponsive Polymer of Poly(N-Acryloylsarcosine Methyl Ester) with a Tunable LCST. *Polym. Chem.* **2017**, *8* (20), 3090–3101.

(132) Zhou, K.; Lu, Y.; Li, J.; Shen, L.; Zhang, G.; Xie, Z.; Wu, C. The Coil-to-Globule-to-Coil Transition of Linear Polymer Chains in Dilute Aqueous Solutions: Effect of Intrachain Hydrogen Bonding. *Macromolecules* **2008**, *41* (22), 8927–8931.

(133) Hao, Z.; Li, G.; Yang, K.; Cai, Y. Thermoresponsive Synergistic Hydrogen Bonding Switched by Several Guest Units in a Water-Soluble Polymer. *Macromol. Rapid Commun.* **2013**, *34* (5), 411-416.

(134) Jochum, F. D.; Theato, P. Temperature- and Light-Responsive Smart Polymer Materials. *Chem. Soc. Rev.* **2013**, *42* (17), 7468–7483.

(135) Jochum, F. D.; zur Borg, L.; Roth, P. J.; Theato, P. Thermo- and Light-Responsive Polymers Containing Photoswitchable Azobenzene End Groups. *Macromolecules* **2009**, *42* (20), 7854–7862.

(136) Jin, Q.; Liu, G.; Ji, J. Micelles and Reverse Micelles with a Photo and Thermo

Double-Responsive Block Copolymer. *J. Polym. Sci. Part A Polym. Chem.* **2010**, *48* (13), 2855–2861.

(137) Benoit, C.; Talitha, S.; David, F.; Michel, S.; Anna, S.-J.; Rachel, A.-V.; Patrice, W. Dual Thermo- and Light-Responsive Coumarin-Based Copolymers with Programmable Cloud Points. *Polym. Chem.* **2017**, *8* (31), 4512–4519.

(138) Keita, M.; Vandamme, M.; Paquin, J.-F. Synthesis of Nitriles from Aldoximes and Primary Amides Using XtalFluor-E. *Synthesis (Stuttg).* **2015**, *47* (23), 3758–3766.

(139) Han, J. H.; Kwon, Y. E.; Sohn, J.-H.; Ryu, D. H. A Facile Method for the Rapid and Selective Deprotection of Methoxymethyl (MOM) Ethers. *Tetrahedron* **2010**, *66* (9), 1673–1677.

(140) Li, S.-N.; Fang, L.-L.; Zhong, J.-C.; Shen, J.-J.; Xu, H.; Yang, Y.-Q.; Hou, S.-C.; Bian, Q. Catalytic Asymmetric Synthesis of the Colorado Potato Beetle Pheromone and Its Enantiomer. *Tetrahedron: Asymmetry* **2014**, *25* (8), 591–595.

(141) Torssell, K.; Johansson, N.-G.; Nilsson, Å.; Sandström, J.; Theorell, H.; Blinc, R.; Paušak, S.; Ehrenberg, L.; Dumanović, J. Positive Halogen Compounds. VI. Preparation of Alkoxydimethylsulfonium Salts and Their Role in the Kornblum Oxidation. Revision of the Structure for the Olefin-Bromotrinitromethane Adduct. *Acta Chem. Scand.* **1967**, *21*, 1–14.

(142) De Mico, A.; Margarita, R.; Parlanti, L.; Vescovi, A.; Piancatelli, G. A Versatile and Highly Selective Hypervalent Iodine (III)/2,2,6,6-Tetramethyl-1-Piperidinyloxyl-Mediated Oxidation of Alcohols to Carbonyl Compounds. **1997**, *62* (20), 6974-6977.

(143) Corey, E. J.; Suggs, J. W. Pyridinium Chlorochromate. An Efficient Reagent for Oxidation of Primary and Secondary Alcohols to Carbonyl Compounds. *Tetrahedron Lett.* **1975**, *16* (31), 2647–2650.

(144) Eilbracht, P.; Acker, M.; Totzauer, W. Alkylsubstituierte Cyclopentanone Durch Hydrocarbonylierende Cyclisierung von 1,4-Pentadiensystemen Mit Hilfe von Metallcarbonylen. *Chem. Ber.* **1983**, *116* (1), 238–242.

(145) Topuzogullari, M.; Bulmus, V.; Dalgakiran, E.; Dincer, S. PH- and Temperature-Responsive Amphiphilic Diblock Copolymers of 4-Vinylpyridine and Oligoethyleneglycol Methacrylate Synthesized by RAFT

Polymerization. *Polymer (Guildf).* **2014**, *55* (2), 525–534.

(146) Schaftenaar, G.; Vlieg, E.; Vriend, G. Molden 2.0: Quantum Chemistry Meets Proteins. *J. Comput. Aided. Mol. Des.* **2017**, *31* (9), 789–800.

(147) Frisch, M.; Trucks, G.; Schlegel, H.; Frisch, M. J.; Trucks, G. W.; Schlegel, H. B.; Scuseria, G. E.; Robb, M. A.; Cheeseman, J. R.; Scalmani, G.; et al. Gaussian 09, Revision A.02. January 1, 2009.

(148) Pierens, G. K. ^{1}H and ^{13}C NMR Scaling Factors for the Calculation of Chemical Shifts in Commonly Used Solvents Using Density Functional Theory. *J. Comput. Chem.* **2014**, *35* (18), 1388–1394.

(149) Lodewyk, M. W.; Tantillo, D. J. Prediction of the Structure of Nobilisitine A Using Computed NMR Chemical Shifts. *J. Nat. Prod.* **2011**, *74* (5), 1339–1343.

(150) Lodewyk, M. W.; Soldi, C.; Jones, P. B.; Olmstead, M. M.; Rita, J.; Shaw, J. T.; Tantillo, D. J. The Correct Structure of Aquatolide—Experimental Validation of a Theoretically-Predicted Structural Revision. *J. Am. Chem. Soc.* **2012**, *134* (45), 18550–18553.

(151) Lodewyk, M. W.; Siebert, M. R.; Tantillo, D. J. Computational Prediction of ^{1}H and ^{13}C Chemical Shifts: A Useful Tool for Natural Product, Mechanistic, and Synthetic Organic Chemistry. *Chem. Rev.* **2012**, *112* (3), 1839–1862.

(152) Jain, R.; Bally, T.; Rablen, P. R. Calculating Accurate Proton Chemical Shifts of Organic Molecules with Density Functional Methods and Modest Basis Sets. *J. Org. Chem.* **2009**, *74* (11), 4017–4023.

(153) Rablen, P. R.; Pearlman, S. A.; Finkbiner, J. A Comparison of Density Functional Methods for the Estimation of Proton Chemical Shifts with Chemical Accuracy. *J. Phys. Chem. A* **1999**, *103* (36), 7357-7363.

Appendices

Appendix A

DFT calculation

Computational calculations were performed in Prof. Marco D'Abramo research group by Mrs. Irene Antignano.

The coordinates of the molecules were prepared using Molden[146] software and all the calculations were performed with Gaussian 09 program.[147] For the calculation of the BDE the geometries of the neutral species and of the corresponding radicals were optimized by means of DFT using the B3LYP functional, the 6-311+G(2d,2p) basis set. The enthalpy correction terms have been estimated from the Hessian matrix.

To compare the effect of the substituents, the molecular geometries (here including also the corresponding anions) have been optimized using the same level of theory and including the solvent effect by means of the Polarizable Continuum Model (solvent DMF).

Concerning the NMR parameter estimates, the chemical shifts were computed using the procedure found in Pierens,[148] which provides the best estimate of the experimental values of the chemical shifts;[149–153] that is, the optimizations were performed in vacuo and the shielding tensors were calculated by means of the PCM (solvent DMSO) using the WPO4 functional and the aug-cc-pVdZ basis set.

In all the optimizations described above, the computation of the Hessian matrix excluded the presence of negative frequencies.

Table A. Calculated bond lenghts (Å) and angles (degrees) for HIAs **1** and **4** with their corresponding anions and radicals in DMF[a]. Reproduced from Ref.[87] with permission.

RC(NOH)CHO	r(R-CN)	r(C-CO)	r(C=N)	r(N-O)	r(C=O)	∠RCN	∠RCC	∠CCN	∠CNO
(*Z*)-**4** *syn/anti*	1.53/1.53	1.48/1.50	1.29/1.28	1.37/1.39	1.23/1.21	118.35/117.37	118.66/121.64	123.00/120.99	119.17/115.22
(*Z*)-**4**$^{\bullet-}$ *syn/anti*	1.54/1.53	1.44/1.44	1.33/1.34	1.29/1.30	1.24/1.24	116.84/117.68	117.15/121.98	126.00/120.34	120.51/120.50
(*Z*)-**4**$^{\bullet}$ *syn/anti*	1.52/1.52	1.48/1.48	1.29/1.29	1.22/1.22	1.21/1.21	120.89/120.33	122.41/124.70	116.71/114.95	132.55/135.02
(*E*)-**1** *syn/anti*	1.50/1.50	1.50/1.48	1.28/1.29	1.38/1.38	1.21/1.21	126.28/127.04	118.63/121.23	115.09/111.73	112.86/113.18
(*E*)-**1**$^{\bullet-}$ *syn/anti*	1.51/1.50	1.44/1.43	1.33/1.33	1.29/1.29	1.24/1.24	123.02/124.17	119.58/122.45	117.40/113.38	117.55/117.98
(*E*)-**1**$^{\bullet}$ *syn/anti*	1.51/1.50	1.48/1.47	1.29/1.30	1.21/1.22	1.21/1.22	121.52/122.41	122.40/123.52	116.07/114.07	133.73/133.94

[a] Geometry optimization at the B3LYP/6-311+G(2d,2p) level; effect of DMF solvent by means of the PCM

Appendix B

Publications from this PhD project.

1) D'Acunzo, F., De Santis, S., Masci, G., Nardi, M., Renzi, P., Sobolev, A. P., *"A Remarkably Large Phase-Transition Effect in a Random Copolymer of Oligo(ethylene glycol) Methyl Ether Methacrylate (OEGMA)$_{500}$ Induced by the Photochemistry of the 2-(Hydroxyimino)aldehyde Group."* In preparation

2) P. Gentili, M. Nardi, I. Antignano, P. Cambise, M. D'Abramo, F. D'Acunzo, A. Pinna, E. Ussia *"2-(Hydroxyimino)aldehydes: Photochemical and Physico-Chemical Properties of a versatile functional group for monomer design"* Chemistry, A European Journal, 24, 7683, 2018.

3) M. Nardi, F. D'Acunzo, M. Clemente, G. Proietti, P. Gentili *"A first study on copolymers of a methacrylate containing the 2-(hydroxyimino)aldehyde group and OEGMA. RAFT polymerization and assessment of thermal and photoresponsive polymer behavior"* Polymer Chemistry, 8, 4233, 2017.